Technical Report No. 32-415

Convective Heat Transfer in a Convergent–Divergent Nozzle

(Revision No. 1)

L. H. Back

P. F. Massier

H. L. Gier

JET PROPULSION LABORATORY

CALIFORNIA INSTITUTE OF TECHNOLOGY

PASADENA, CALIFORNIA

February 15, 1965

Technical Report No. 32-415

Convective Heat Transfer in a Convergent–Divergent Nozzle

(Revision No. 1)

L. H. Back

P. F. Massier

H. L. Gier

D. R. Bartz, Chief
Propulsion Research Section

JET PROPULSION LABORATORY
CALIFORNIA INSTITUTE OF TECHNOLOGY
PASADENA, CALIFORNIA

February 15, 1965

Prepared Under Contract No. NAS 7-100
National Aeronautics & Space Administration

CONTENTS

TABLES

FIGURES

FIGURES (Cont'd)

PREFACE

Portions of this paper were originated under studies conducted for the Department of Army Ordnance Corps under Contract No. DA-04-495-Ord-18. Such studies are now conducted for the National Aeronautics and Space Administration under Contract No. NAS 7-100.

ABSTRACT

19684

The results of an experimental investigation of convective heat transfer from turbulent boundary layers accelerated under the influence of large pressure gradients in a cooled convergent–divergent conical nozzle are presented. The investigation covered a range of stagnation pressures from 30 to 250 psia, stagnation temperatures from 1030 to 2000°R, and nozzle-inlet boundary-layer thicknesses between 5 and 25% of the inlet radius. Steady-state heat-transfer rates from air heated by the combustion of methanol were determined locally from measurements using thermocouples embedded in the nozzle wall. The most significant unexpected trend in the results is the reduction in the heat-transfer coefficient, below the variation with stagnation pressure anticipated for a turbulent boundary layer, at stagnation pressures less than about 75 psia. As expected, the results include a maximum in the heat-transfer coefficient upstream of the throat, where the mass flow rate per unit area is largest, and a substantial decrease in heat transfer downstream of the point of flow separation, which occurred in the divergent section of the nozzle at the low stagnation pressures. A reduction of about 10% in the heat-transfer coefficient resulted from an increase in the inlet boundary-layer thickness between the minimum and maximum thicknesses investigated.

Heat-transfer predictions with which the data were compared either incorporate a prediction of the boundary-layer characteristics or are related to pipe flow. At the higher stagnation pressures, predicted values from a modification of Bartz' turbulent boundary-layer analysis are in fair agreement with the data. As a possible explanation of the low heat-transfer rates at the lower stagnation pressures, a parameter is found which is a measure of the importance of flow acceleration in reducing the turbulent transport below that typical of a fully turbulent boundary layer.

AUTHOR

I. INTRODUCTION

Comprehensive studies of convective heat transfer from gases flowing under the influence of comparatively large pressure gradients have been mostly analytical. Laminar flow cases have been solved by boundary-layer theory approaches in which the restrictive assumptions are within the realm of describing actual processes. Turbulent flows, however, are too complex to formulate in such a way that descriptions of the momentum and energy transport processes can be made without the use of considerable empirical information or assumptions which are so drastic that they themselves are essentially the solutions. The present investigation was undertaken in order to provide experimental convective heat-transfer information on turbulent flows subjected to large pressure gradients with boundary layers that are thin in comparison to the cross section of the channels. It was anticipated that these results could be incorporated with turbulent boundary-layer theories to arrive at a meaningful method of predicting convective heat transfer in accelerating flows.

Experimental measurements of heat transfer from gases flowing under the influence of pressure gradients have been made to some extent by other investigators. Data obtained from rocket-engine firings indicate that the local heat fluxes in nozzles (particularly the convergent sections) are sensitive to injection schemes, combustion phenomena, and the proximity of a nozzle to the injector (Ref. 1). Furthermore, superimposed on the convective component is a radiation component, which, together with the other effects, introduces complexities into the gross heat-transfer process. Hence, results of measurements such as these have not been particularly informative about the convective heat-transfer mechanism in accelerating turbulent boundary-layer flows.

Most experimental results of previous investigations of convective heat transfer in a nozzle without injection and combustion effects were obtained either with nozzles of small angles of convergence and divergence or at relatively low stagnation pressures and temperatures. Saunders and Calder's measurements (Ref. 2) were made only in the conical divergent section, with the half-angle of divergence about ½ deg. Ragsdale and Smith (Ref. 3), using superheated steam, made measurements in a nozzle which had small convergent and divergent half-angles of about 1 deg. The stagnation temperature was about 1000°R, and the stagnation pressure ranged from 20 to 35 psia. Baron and Durgin's measurements (Ref. 4) in two-dimensional nozzles were made at a stagnation temperature of 570°R and over a stagnation pressure range of 6 to 30 psia. In preliminary results (Ref. 5), from the system shown in Fig. 1, semilocal values of heat transfer were determined by calorimetry for a few operating conditions. Only for Kolozsi's measurements (Ref. 6) in a 7½-deg half-angle convergent and divergent conical nozzle at a stagnation temperature of about 1200°R were

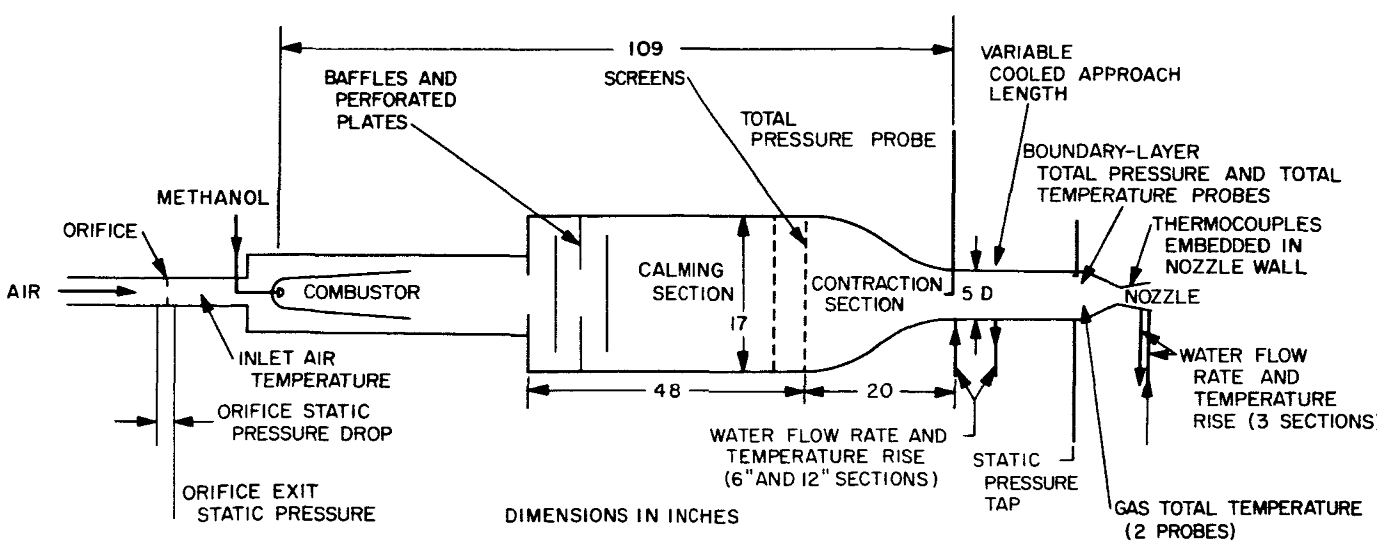

Fig. 1. Flow and instrumentation diagram

data reported at higher stagnation pressures of 225 and 370 psia.

In this investigation, which covered a range of stagnation pressures from 30 to 250 psia and stagnation temperatures from 1030 to 2000°R, compressed air was heated by the internal combustion of methanol and then mixed to obtain uniformity before it entered the nozzle. The mixing and distance of the combustion from the nozzle (Fig. 1) minimized maldistributions, and the ratio of methanol-to-air weight flow rate was small enough, even for the highest stagnation temperature, so that the products of combustion could be treated approximately as air. The nozzle had a throat diameter of 1.803 in., a contraction-area ratio of 7.75 to 1, an expansion-area ratio of 2.68 to 1, a convergent half-angle of 30 deg, and a divergent half-angle of 15 deg. The exit Mach number was about 2.5. Local convective heat-transfer results were obtained by measuring steady-state temperatures with thermocouples embedded in plugs pressed into the water-cooled nozzle wall. The construction and calibration of these plugs are described in Appendix A. Radiation effects were negligible over the stagnation-temperature range. To determine the effect of boundary-layer thickness at the nozzle inlet on heat transfer in the nozzle, the length of the constant-diameter cooled approach section upstream of the nozzle inlet was changed in 6-in. lengths from 0 to 18 in.

In addition to the results given in graphical form in this Report, numerical values which could be used for future correlation and which supply additional information, such as wall and free-stream conditions, are included in Appendix B.

II. INSTRUMENTATION

The system flow and instrumentation diagram is shown in Fig. 1. Stagnation pressure was measured just upstream of the water-cooled approach section, and stagnation temperature was determined by averaging the readings of two shielded thermocouples placed 0.25 in. upstream of the nozzle inlet. These two thermocouples, located 1 in. from the centerline, were spaced 180 deg apart circumferentially and generally read within 2% of each other. To determine the static-pressure distribution along the nozzle, thirty-two static-pressure holes 0.040 in. in diameter were spaced circumferentially and axially in the nozzle wall. These static pressures were measured with mercury manometers.

Boundary-layer traverses were made in the 5.07-in.-diameter cooled approach section at a location 1.25 in. upstream of the nozzle inlet. The stagnation-pressure probe was located 90 deg circumferentially from the stagnation-temperature probe. Details of the probe tips are shown in Fig. 2. The tip design is similar to that of probes used by Livesey (Ref. 7), with which he found a

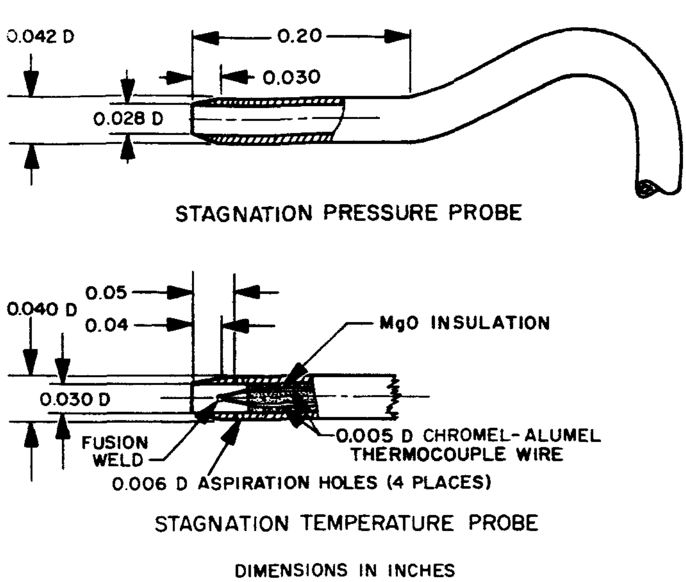

Fig. 2. Tip details of traversing boundary-layer probes

negligible velocity displacement effect of the probe in the wall vicinity. The probes were moved mechanically via a micrometer lead screw, and their location from the wall was determined by a counter and a helipot.

Steady-state wall temperatures and heat fluxes were obtained from thermocouples embedded in cylindrical plugs, a typical one of which is shown in Fig. 3. Three thermocouples were formed along the length of each plug, which was pressed into a hole drilled through the nozzle wall. In Appendix A, the construction and calibration of the plugs are described, including the determination of the distance between thermocouple weld junctions by means of a Kelvin bridge circuit. One thermocouple plug was located at each of twenty-one axial locations, except at $z/L = 0.864$, where there were two. These plugs were also spaced at numerous circumferential locations along the nozzle, as indicated in the table in Fig. 3, such that every third plug was located in a quadrant within 55 deg of successive ones. The nozzle and plugs were fabricated from the same billet of 502-type stainless steel. Available data on the thermal conductivity of this material indicated a small variation with temperature in the attainable wall temperature range. Values of thermal conductivity used in the data reduction were obtained experimentally on material taken from the same billet that was used to fabricate the nozzle. Three longitudinal water-coolant passages cooled the outer surface of the nozzle and plugs. The nozzle installation is shown in Fig. 4.

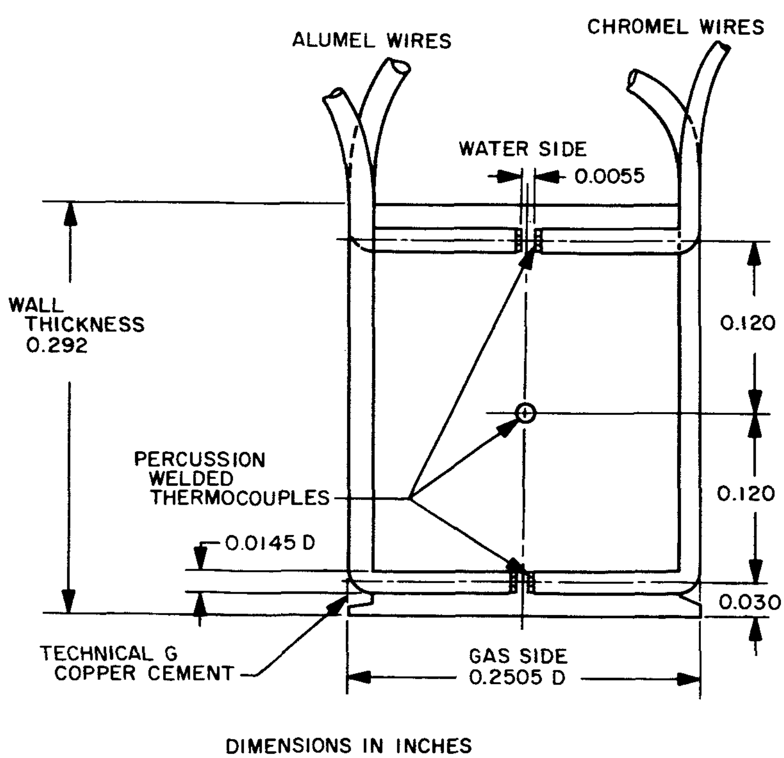

PLUG POSITION[a]			
PLUG No.	z/L	A/A^*	CIRCUMFERENTIAL ANGLE FROM ARBITRARY ZERO deg
I24	0.133	6.39	330
D25	0.204	5.05	30
D34	0.276	3.86	150
I23	0.336	2.98	280
D26	0.385	2.37	80
D35	0.429	1.88	200
I22	0.469	1.48	315
D28	0.512	1.23	45
H37[b]	0.541	1.10	155
I20[c]	0.573	1.02	300
D29	0.603	1.00	60
F42	0.634	1.02	180
I19	0.664	1.08	285
D30	0.693	1.19	75
F43	0.717	1.28	200
I18	0.750	1.41	320
D31	0.782	1.55	40
F45[c]	0.825	1.74	150
I17	0.864	1.94	275
C16	0.864	1.94	320
D33	0.905	2.14	85
F46	0.938	2.41	205

[a] $L = 5.925$ in. and $A^* = 2.552$ in.^{2} at $z/L = 0.603$.

[b] Data from this plug are questionable and have been omitted.

[c] Water side wall thermocouple in this plug has been damaged.

Fig. 3. Thermocouple plug diagram and positions

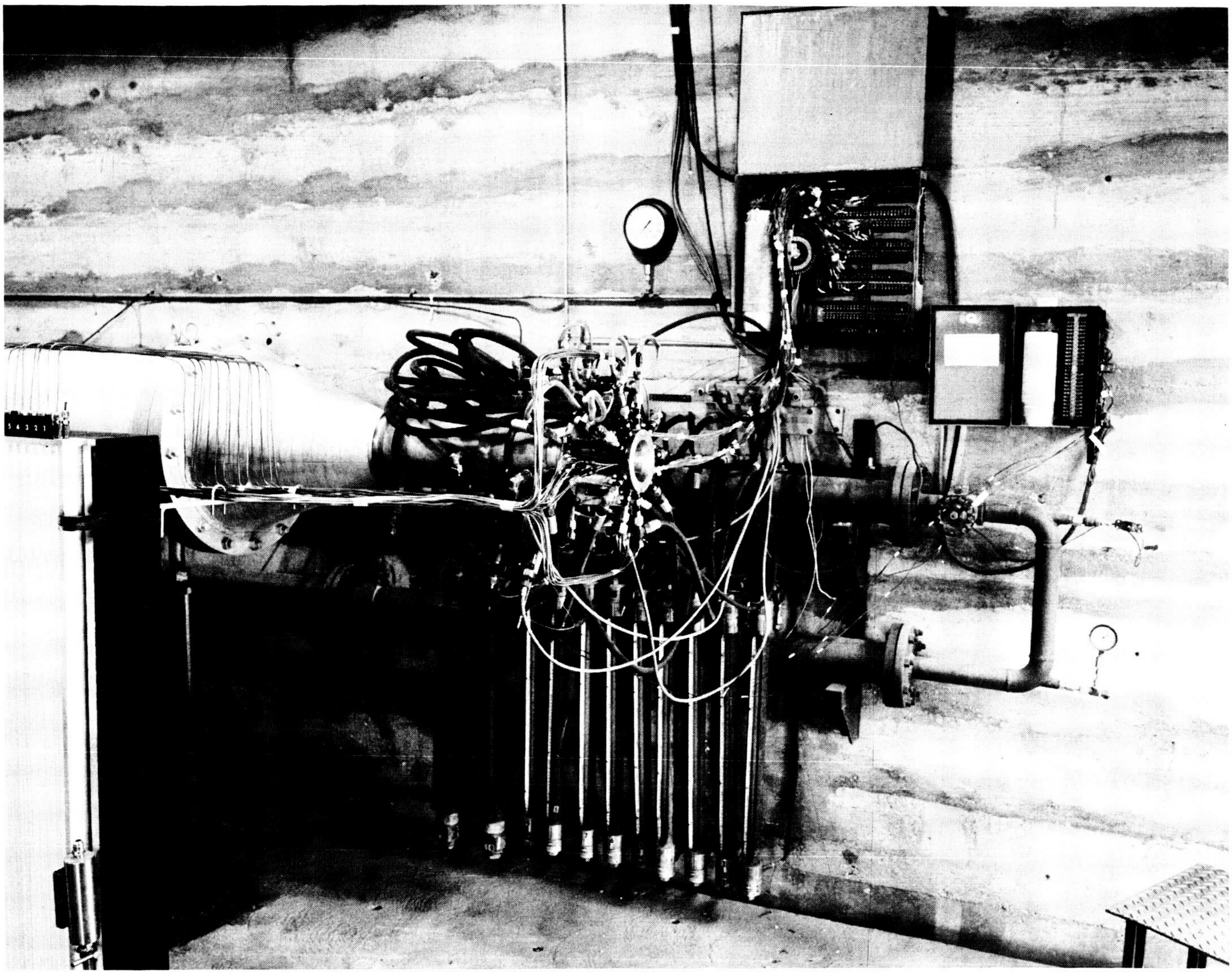

Fig. 4. Nozzle installation

III. HEAT-TRANSFER CALCULATION PROCEDURE

Although temperature gradients existed along the nozzle wall, as indicated by the wall isotherms shown in Fig. 5 for a particular test, these were generally small, and the three thermocouple readings in each plug indicated that only radial heat conduction normal to the wall need be considered. The local heat flux q_w normal to the gas-side wall was computed from

$$q_w = \frac{k\,(T_a - T_b)}{r_a \ln r_b/r_a} \tag{1}$$

For a given plug, the radii r_w (gas-side wall radius), r_a, and r_b are collinear; they are taken perpendicular to the gas-side surface of the nozzle and extend to the centerline; T_a and T_b are internal wall temperatures measured with the thermocouples embedded in the plug. The thermal conductivity k is the arithmetic average of the values at T_a and T_b.

The gas-side wall temperatures determined from the different thermocouple combinations in each plug were generally within 1%. However, in determining the wall heat flux from Eq. (1), there were inconsistencies. If the center thermocouple and the one nearest the gas-side wall were used, the calculated wall heat flux was on the average about 10% higher than with the thermocouples nearest the gas-side and water-side walls. With a combination of the center thermocouple and the one nearest the gas-side wall, the total heat load was found to agree within 5% of that computed from the coolant flow rate and the coolant temperature rise; consequently, these two thermocouples were used to calculate the wall heat flux. The estimated errors resulting from the use of these thermocouples are discussed near the end of Appendix A.

The heat-transfer coefficient was computed by

$$h = \frac{q_w}{T_{aw} - T_w} \tag{2}$$

The adiabatic wall temperature T_{aw} was calculated from a recovery factor assumed equal to the 1/3 power of the stagnation temperature value of the Prandtl number:

$$\frac{T_{aw}}{T_t} = \frac{1 + Pr^{1/3}\,\frac{\gamma - 1}{2}\,M^2}{1 + \frac{\gamma - 1}{2}\,M^2}$$

The Mach number M was determined from the experimental static-to-stagnation pressure ratio p/p_t for isentropic flow (γ = const.) at the corresponding stagnation temperature value of γ for the products of combustion. The adiabatic wall temperatures so calculated differ only slightly from those corresponding to a recovery factor equal to 0.89. This value is based on measurements with air accelerated over a flat plate by a convergent opposite wall (Ref. 8) and by extrapolating wall temperatures to the zero heat-flux condition for air flow through a nozzle (Ref. 4). In both of these investigations, the recovery factor was found to be independent of pressure gradient. Actually, for the large differences between the stagnation and wall temperatures in the present results, the calculated heat-transfer coefficients are insensitive to the assumed recovery-factor dependence.

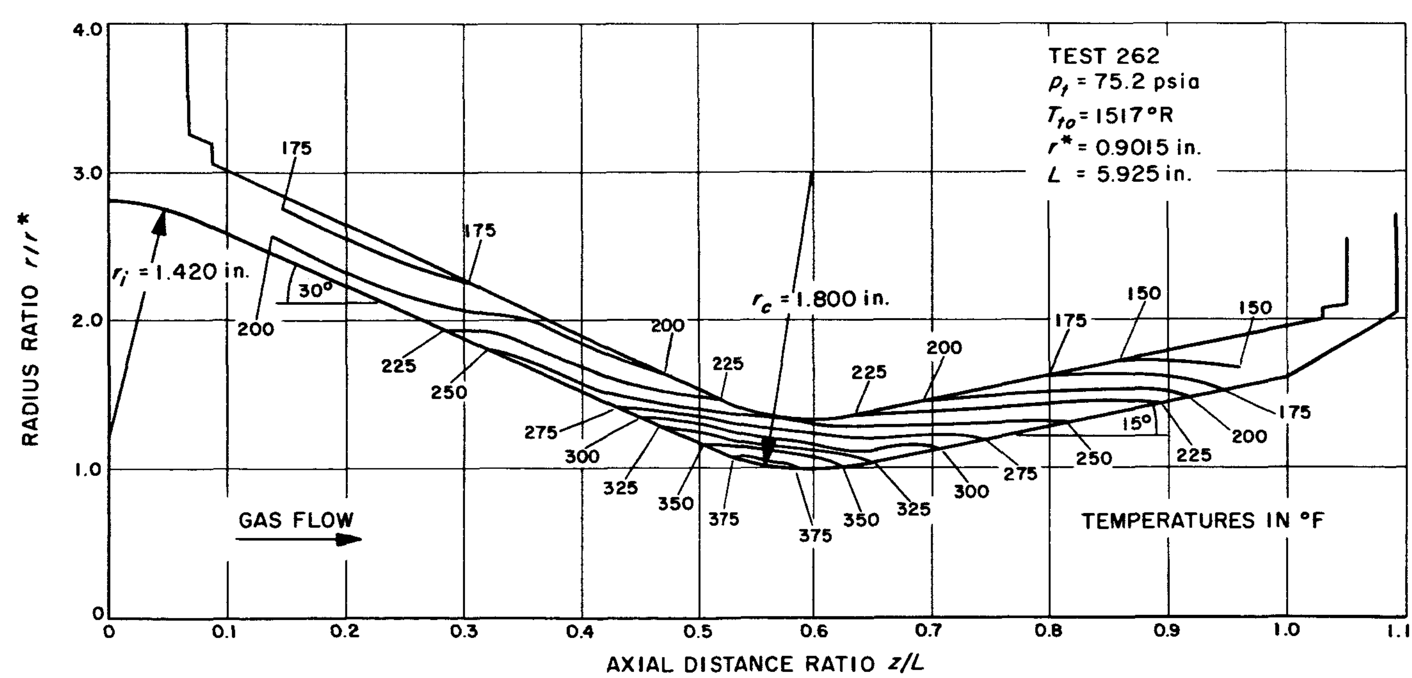

Fig. 5. Nozzle wall isotherms

IV. STATIC PRESSURE AND MASS FLUX DISTRIBUTIONS

The measured static-to-stagnation pressure ratio along the nozzle is shown in Fig. 6 at a stagnation temperature of 1500°R for a range of stagnation pressures from 45 to 150 psia. Measurements at higher stagnation pressures were not possible because of manometer limitations. Except in the nozzle-exit region, where the rapid rise in static pressure at the lower stagnation pressures indicates flow separation, the pressure-ratio distribution is nearly invariant. For computational purposes, it is assumed to be invariant above 150 psia. Deviations of measured pressure distributions from that predicted from one-dimensional isentropic flow are indicated. The deviations result from radial-velocity components caused by the taper and curvature of the nozzle and are as large as 30% just downstream of the throat.

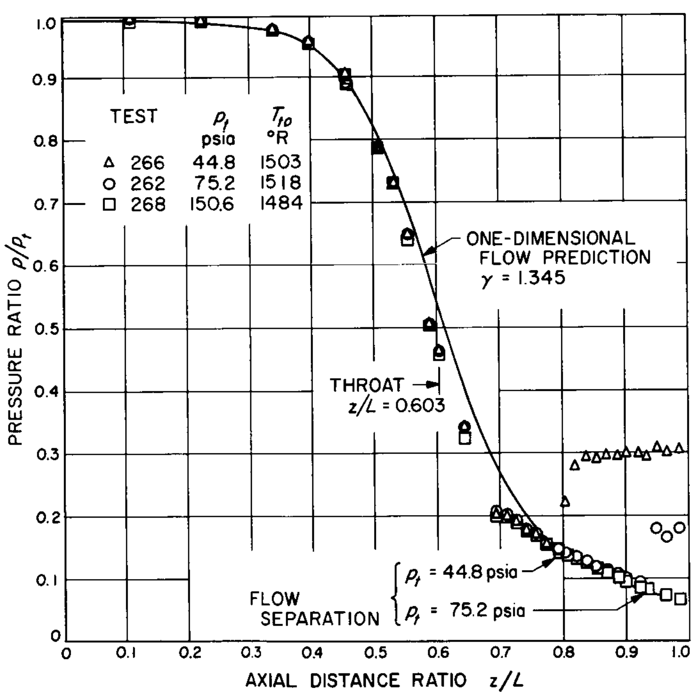

Fig. 6. Ratio of static to stagnation pressure along the nozzle

In Fig. 7, the ratio of the local mass flux $\rho_e u_e$, calculated from the measured wall static pressures, to that predicted from one-dimensional flow $\rho_1 u_1$, is shown at p_t = 75 psia for different stagnation temperatures and cooled approach lengths. For the tests shown, the maximum value of the mass flux $\rho_e u_e$ occurred at z/L = 0.58. This location corresponds to the intersection of the sonic line with the nozzle wall and is upstream of the geometric throat, which is located at z/L = 0.603. Just downstream of the throat there is a sharp dip in the mass-flux ratio, the reduction below that predicted from one-dimensional flow amounting to about 15%. There appears to be a slight trend toward mass-flux ratios increasing with stagnation temperature, especially near the nozzle exit. The effect of boundary-layer thickness at the nozzle inlet on the mass-flux ratio is negligible.

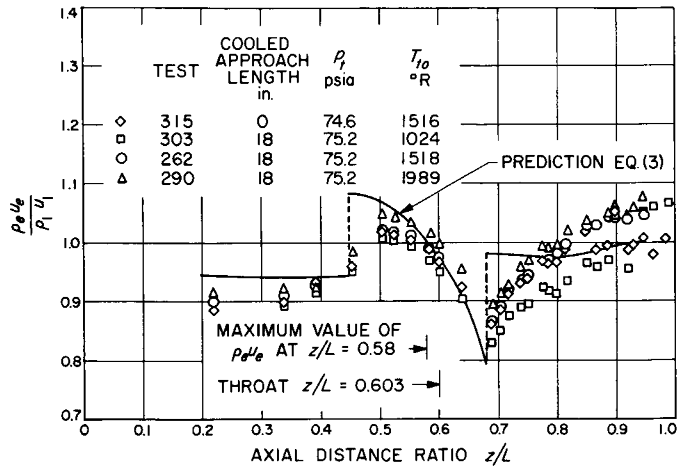

Fig. 7. Ratio of local to one-dimensional mass flux along the nozzle

Since the deviations from one-dimensional flow are significant in the throat region, it is of interest to determine to what extent the mass flux at the edge of the boundary layer is predictable. Oswatitsch and Rothstein (Ref. 9) considered isentropic, two-dimensional flow in a convergent-divergent nozzle. The wall boundary layer is neglected as is the requirement that the fluid velocity at the wall be exactly parallel to it. The final result of their analysis can be cast in the form of a ratio of the mass flux at the nozzle wall to that for one-dimensional flow

$$\frac{\rho_e u_e}{\rho_1 u_1} = \frac{\left\{1 - \frac{\gamma - 1}{2}\left(M_1 \frac{a_1}{a_0}\right)^2 \left(\frac{u_e}{u_1}\right)^2\right\}^{\frac{1}{\gamma-1}}}{\frac{\rho_1}{\rho_0}} \frac{u_e}{u_1} \tag{3}$$

where

$$\frac{u_e}{u_1} = \sqrt{\left\{1 + \frac{1}{2}\left[\frac{1}{2}\, r\, \frac{d^2r}{dz^2} + \frac{1}{4}\, \frac{\frac{du_1}{dz}}{u_1}\, r\, \frac{dr}{dz} - \left(\frac{dr}{dz}\right)^2\right]\right\}^2 + \left(\frac{dr}{dz}\right)^2}$$

The predicted mass-flux ratio is only a function of the nozzle configuration, with the subscript 1 denoting average quantities for one-dimensional flow. The prediction shown in Fig. 7 is in fair agreement with the data in the throat region. It also indicates the sonic line to be upstream of the throat. At the intersection of the conical sections of the nozzle with the throat curvature, there is a predicted discontinuity in the mass-flux ratio as indicated by the dashed lines. The prediction is not shown in the nozzle-entrance region, since there, restrictions on the magnitude of the nozzle radius and its derivatives implied in the analysis are not satisfied. Even in the throat region, these are marginal.

V. BOUNDARY LAYERS AT THE NOZZLE INLET

To indicate the nature of the boundary layer at the nozzle inlet with the 18-in. cooled approach length, the velocity ratio u/u_e, mass-flux ratio $\rho u/\rho_e u_e$, and stagnation-temperature distribution $(T_t - T_w)/(T_{te} - T_w)$ are shown in Fig. 8 for a stagnation temperature of 1500°R and a range of stagnation pressures from 45 to 254 psia. The profiles indicate that the boundary layers are turbulent over the range of stagnation pressures. A 1/7-power-law curve for negligible property variation across the boundary layer is shown for comparison. Values of the thicknesses δ^*, θ, and ϕ near the nozzle inlet were calculated by taking into account the mass, momentum, and energy defects for flow through a pipe of radius R.

$$\delta^*\left(R - \frac{\delta^*}{2}\right) = \int_0^\infty \left(1 - \frac{\rho u}{\rho_e u_e}\right)(R - y)\, dy \quad (4)$$

$$\theta\left(R - \frac{\theta}{2}\right) = \int_0^\infty \frac{\rho u}{\rho_e u_e}\left(1 - \frac{u}{u_e}\right)(R - y)\, dy \quad (5)$$

$$\phi\left(R - \frac{\phi}{2}\right) = \int_0^\infty \frac{\rho u}{\rho_e u_e}\left[1 - \left(\frac{T_t - T_w}{T_{te} - T_w}\right)\right](R - y)\, dy \quad (6)$$

In general, these thicknesses are about 5% lower than those obtained by assuming flow over a plane surface. The effect of increasing stagnation pressures is to decrease the displacement, momentum, and energy thicknesses.

In Fig. 9, the velocity profiles of Fig. 8 are shown in terms of $u^+ = u/(\sqrt{\tau_w/\rho_e})$ and $y^+ = (y\sqrt{\tau_w/\rho_e})/\nu_e$. The wall shear was determined by matching the profiles in

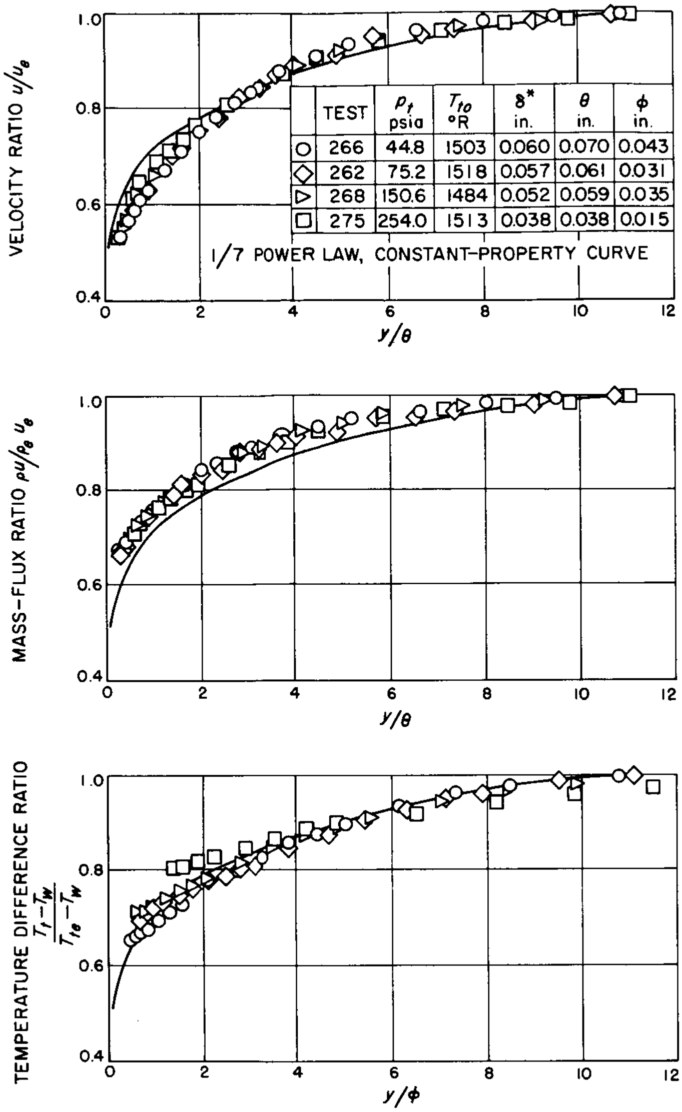

Fig. 8. Boundary-layer profiles 1.25 in. upstream of nozzle inlet with 18-in. cooled approach length

the wall vicinity to the "law of the wall," which was taken in the form

$$u^+ = 5.5 + 2.5 \ln y^+ \qquad \text{for } y^+ > 30 \tag{7}$$

In the wall vicinity, the "law of the wall" appears to be valid, and in the outer part of the boundary layer, the departure is typical of the "law of the wake" proposed by Coles (Ref. 10). Shown in two ways in Fig. 9 are the friction coefficients, $c_f/2 = \tau_w/(\rho_e u_e^2)$, predicted from the Blasius flat-plate relation

$$\frac{\tau_w}{\rho u_e^2} = \frac{0.0128}{\left(\dfrac{\rho u_e \theta}{\mu}\right)^{1/4}} \tag{8}$$

With properties ρ and μ evaluated at the free-stream temperature, the predictions exceed those deduced from matching to the "law of the wall" by about 20%. With properties evaluated at the film temperature, the predictions are about 55% higher. Also shown in the Figure are the friction coefficients predicted from the boundary layer analysis of Ref. 11, which is discussed in Section VII. These predictions are nearer those deduced from the "law of the wall," though they are still high.

At the other stagnation temperatures of 1030 and 2000°R, as well as with the shorter cooled approach lengths of 6 and 12 in., the boundary-layer profiles (not shown) were also turbulent. However, with no cooled approach length, the boundary layer appears to be in the transition region, as indicated by the velocity profiles shown in Fig. 10. These profiles lie between a turbulent and laminar one, as shown by the 1/7-power law and Blasius' laminar-flow profiles.

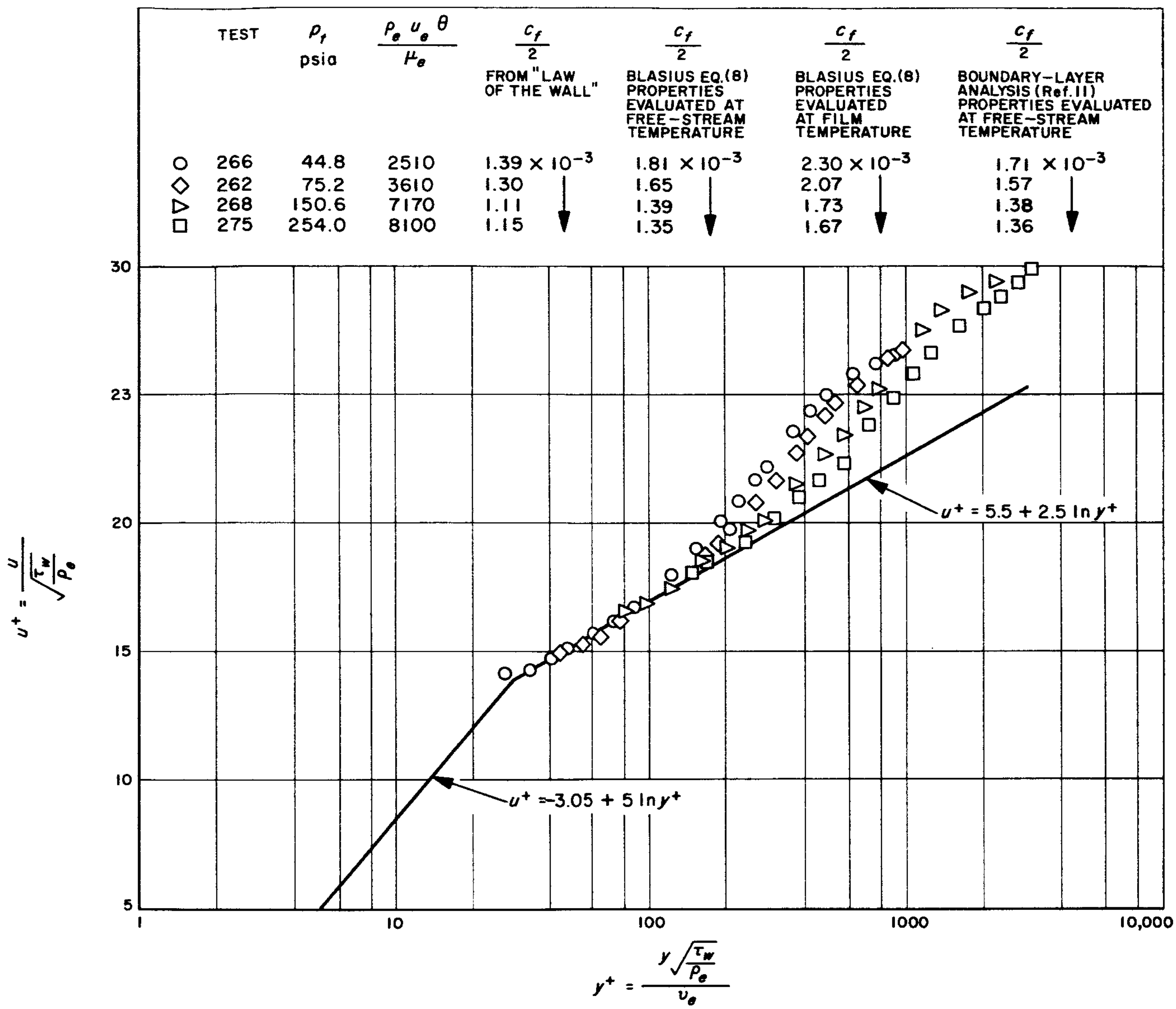

Fig. 9. Velocity distributions 1.25 in. upstream of nozzle inlet with 18-in. cooled approach length

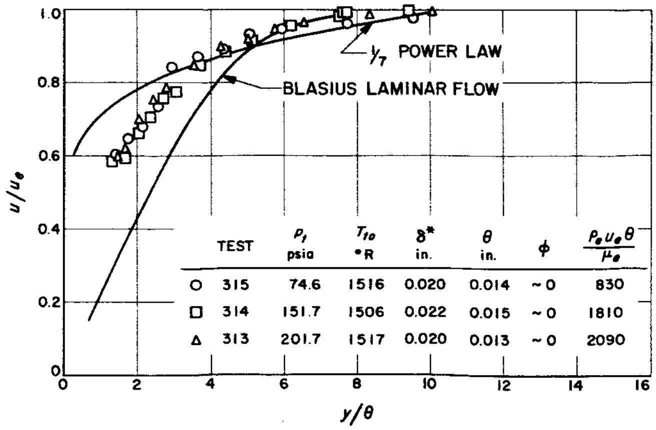

Fig. 10. Velocity profiles 1.25 in. upstream of nozzle inlet without cooled approach length

VI. HEAT-TRANSFER RESULTS

The variation of the heat-transfer coefficient along the nozzle with the 18-in. cooled approach length is shown in Fig. 11 for stagnation temperatures of about 1030, 1500, and 2000°R and a range of stagnation pressures from 30 to 254 psia. At the highest stagnation temperature, it was not possible to obtain data above a stagnation pressure of 125 psia because of temperature limitations on the wall-thermocouple insulating material. The curves in the Figure were faired through the data. It is evident that during a given test, circumferential variations in heat transfer did exist, as indicated by the symbols which are tagged alike. These indicate thermocouple plugs spaced within 55 deg of each other. A certain amount of consistency can be deduced by comparing data obtained from the same thermocouple plugs for different tests. The majority of the tests were duplicated and found reproducible to within $\pm 2\%$. It was not possible to explain these variations by nonuniformities in the flow based on measurements in the gas stream at the nozzle inlet. However, it is possible that nonuniformities could have existed in the boundary layer.

The heat-transfer coefficients in Fig. 11 increase, as expected, with increasing stagnation pressures as a result of larger mass fluxes; however, their variation with stagnation temperature at the different stagnation pressures is less clear, with the trends dependent on stagnation pressure. The maximum value of the heat-transfer coefficients occurs just upstream of the throat in the vicinity where the mass flux $\rho_e u_e$, as indicated in Fig. 7, is a maximum. A substantial decrease in heat transfer downstream of the point of flow separation which occurred at the low stagnation pressures is indicated by the tests at a stagnation pressure of 45 psia. At the lowest stagnation pressure, the data are not shown in this region, since there were large fluctuations in the wall-thermocouple readings.

To represent the heat-transfer results shown in Fig. 11 in terms of correlation parameters commonly used involves both the selection of a characteristic length and the temperature at which properties are evaluated. In Fig. 12 there are shown, in addition to the data of Fig. 11, data from many more tests at intermediate stagnation pressures presented in terms of the group, $St\,Pr^{0.6}$, and the Reynolds number based on the nozzle local diameter. Fluid properties were evaluated at the static temperature at the edge of the boundary layer, and the mass flux $\rho_e u_e$ was used to compute both the Stanton and Reynolds numbers. The variation of viscosity, specific heat, and Prandtl number with temperature for air was obtained from Ref. 12. Each of the plots in Fig. 12 indicates the heat-transfer data obtained at a single area ratio or axial station. Hence, in each of the plots, increasing Reynolds numbers $(\rho_e u_e D/\mu_e)$ at the different stagnation temperatures correspond directly to increasing stagnation pressures, since the nozzle diameter is constant.

Proceeding through the subsonic part of the nozzle (decreasing area ratios), there is a substantial reduction in heat transfer at the lower stagnation pressures below that typical of a turbulent boundary layer (Curve A) where the dependence of the heat-transfer coefficient on the mass flux is $h \alpha (\rho_e u_e)^{4/5}$. This reduction persists through the throat and into the supersonic region. It could actually continue to the exit of the nozzle; however, in these tests it was not possible to operate the nozzle without separation near the exit at low stagnation pressures. Measurements in separated regions are not shown. At the higher stagnation pressures (higher Reynolds numbers), above 75 psia, the heat transfer is typical of a turbulent boundary layer.

Other investigators have observed unexpected trends accompanying the acceleration of turbulent boundary layers. The trends shown in Fig. 12 are similar to the results of Ref. 1, which were obtained from rocket-engine tests over a similar range of stagnation pressures. The large positive slope of the experimental curves at area ratios near 1 was noted as well as the eventual decrease in slope with increasing stagnation pressure. This implies that for the rocket-engine tests, injection and combustion effects did not substantially alter the heat-transfer trends from those indicated in Fig. 12. In Ref. 13, a turbulent boundary layer at the entrance of a supersonic nozzle was found to undergo transition to a nearly laminar one at the nozzle exit. The stagnation pressure was 4.3 psia. When the stagnation pressure was increased to 14.2 psia, a turbulent boundary layer was found at the nozzle exit. No boundary-layer measurements were made within the nozzle. In Ref. 14, it was observed that heat-transfer trends of the type seen here at the low stagnation pressures existed under lower pressure-gradient conditions. There was departure from fully turbulent flow through the acceleration region as indicated by the linearity of the measured velocity profiles in the wall vicinity.

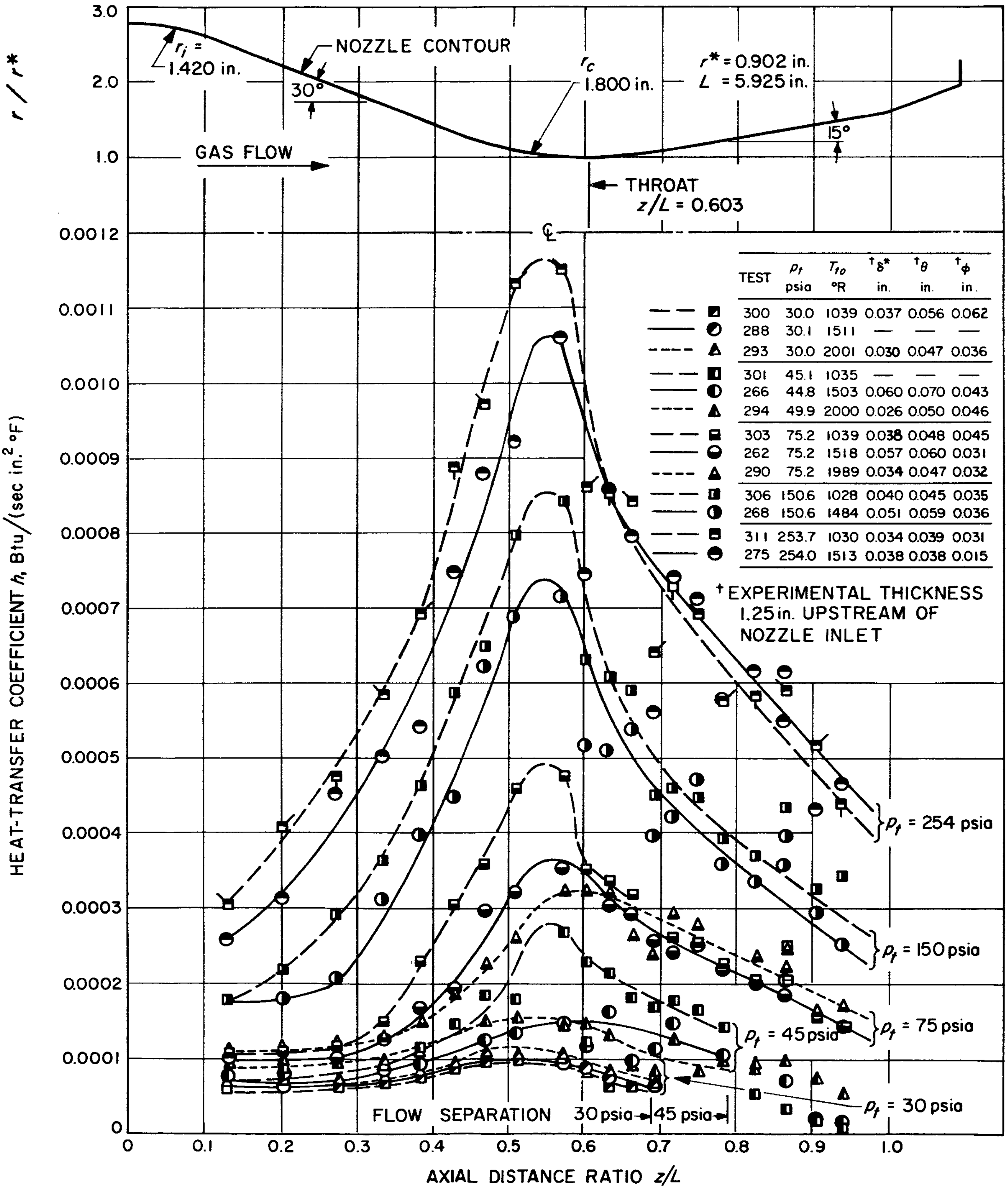

Fig. 11. Heat-transfer coefficient vs. axial distance ratio with 18-in. cooled approach length

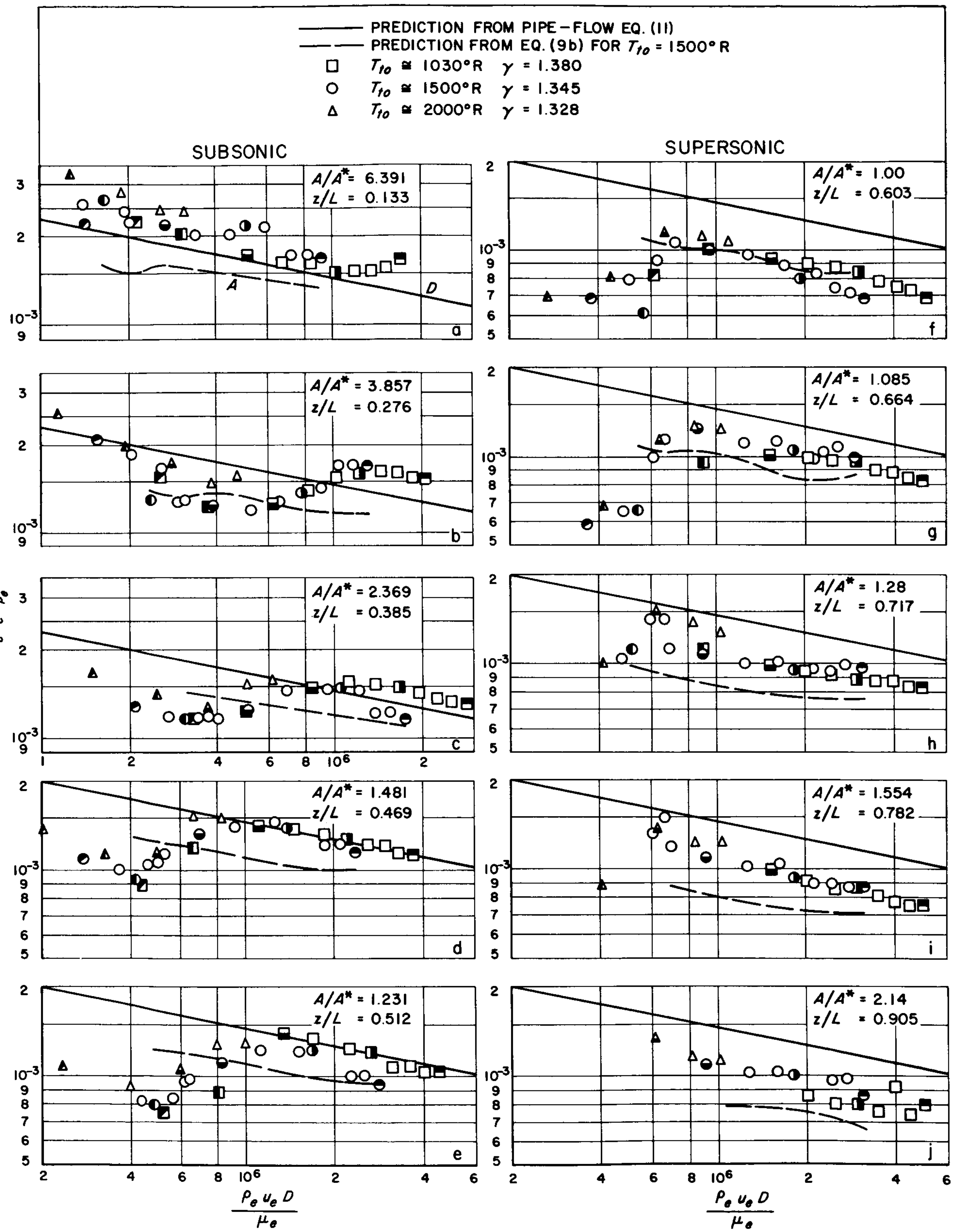

Fig. 12. Heat-transfer results at various subsonic and supersonic area ratios with 18-in. cooled approach length

From these observations, it seems logical to speculate that at the lower stagnation pressures, the boundary layer may have undergone transition from the turbulent profile at the nozzle inlet to a partially laminar profile under the influence of the large, favorable pressure gradient. The consequent decrease in eddy transport would reduce both the wall friction and heat transfer. In Section VIII, a parameter relating a predicted reduction in net production of turbulent kinetic energy to the low stagnation pressures is discussed.

To indicate the variation of the Stanton number with Reynolds number along the nozzle, a few of the tests from Fig. 11 are shown again in Fig. 13. To help identify the axial location in terms of the Reynolds number, the measuring station nearest the nozzle inlet is noted and the data points in the supersonic region are tagged. No additional information is shown in this Figure; however, the trends of conditions along the nozzle are more evident than in Fig. 11. Again, the data downstream of the nozzle-inlet region for the lowest stagnation pressure deviate furthest from the $(\rho_e u_e)^{4/5}$ dependency, which is shown as a reference curve.

The effect of varying nozzle-inlet boundary-layer thicknesses on the heat transfer is shown in Fig. 14, in particular for a stagnation temperature of 1500°R and a range of stagnation pressures from 75 to 200 psia. With no cooled approach length, for which the ratio of estimated boundary-layer thickness to nozzle-inlet radius is about 0.05, the heat-transfer coefficient is above the thicker layer results. This trend persists through the nozzle and

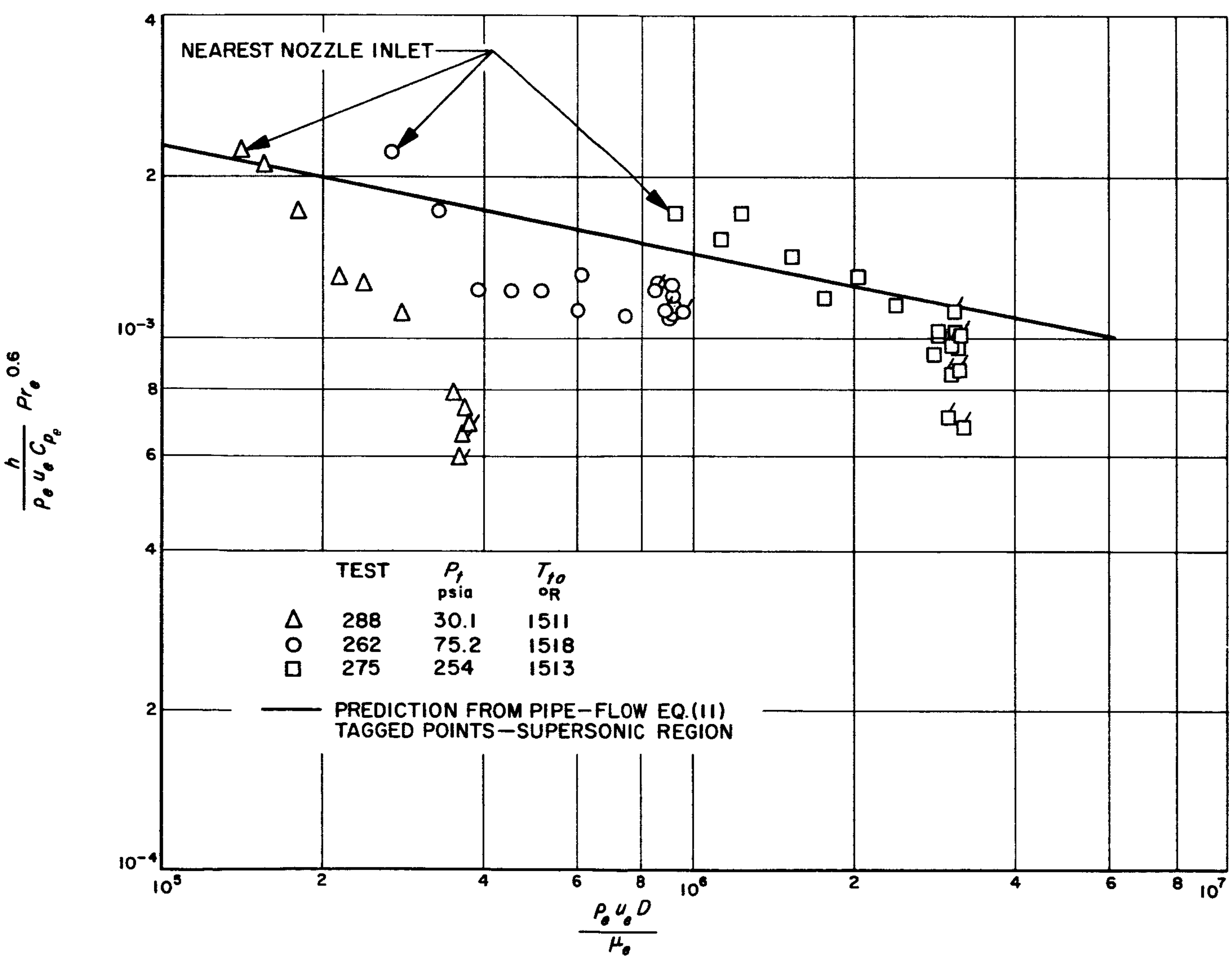

Fig. 13. Heat-transfer results along nozzle with 18-in. cooled approach length

extends into the supersonic region. Just upstream of the throat, where the heat-transfer coefficient is a maximum, the thinnest layer results exceed the thickest layer results obtained with the 18-in. cooled approach length by about 10%. Apparently, with no cooled approach length, transition from the boundary-layer profile shown in Fig. 10 to a turbulent one occurred upstream of the first heat-transfer measuring station.

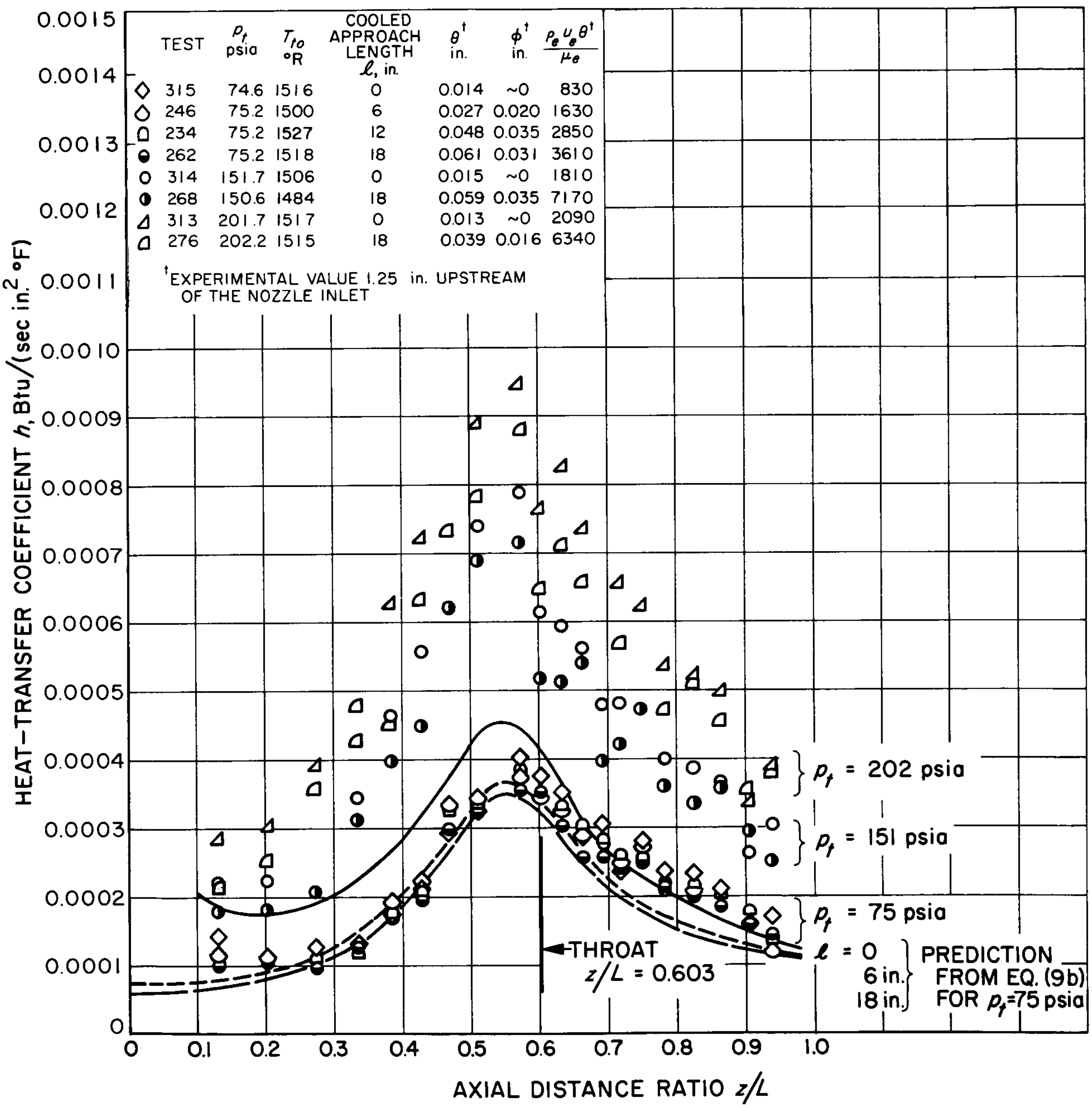

Fig. 14. Heat-transfer coefficients for various boundary-layer thicknesses at nozzle inlet vs. axial distance ratio

VII. COMPARISON OF HEAT-TRANSFER RESULTS WITH PREDICTIONS

Methods of predicting nozzle heat transfer consist either of boundary-layer analyses or, because of their simplicity, of those related to pipe flow. In the boundary-layer analyses (e.g., Refs. 15, 16), the integral forms of the momentum and energy equations are solved based on a number of assumptions, the most important of which is an assumed form of Reynolds analogy between heat transfer and wall friction. A limited amount of data (Refs. 14, 17, 18) for heat transfer to an accelerated, essentially incompressible, turbulent boundary layer where property variations were small has indicated that heat-transfer coefficients determined from the wall friction through one of the analogies known to apply for constant free-stream velocity were far in excess of actual values. However, since boundary-layer measurements were not made in the nozzle, an experimental check was not possible.

Another, more recent, boundary-layer prediction method in which various heat-transfer assumptions can be compared to experimental results is a modification of the turbulent boundary-layer analysis of Ref. 15. In the modified analysis, as in Ref. 15, the integral forms of the momentum and energy equations are solved simultaneously for θ and ϕ. The assumptions involve the specification of the heat-transfer and wall-friction coefficients, and the similarity of the boundary-layer velocity and stagnation-temperature profiles on a 1/7-power-law basis with respect to their individual thicknesses, which can be different from one another. The prediction yields both the flow and thermal characteristics when the nozzle configuration, wall temperature, and free-stream properties are specified. To initiate the prediction, a knowledge of θ and the ratio of thicknesses $\delta_{t/\delta}$ is required at one location which was taken at the boundary-layer measuring station 1.25 in. upstream of the nozzle inlet. A complete report on the computation procedure of the modified boundary-layer analysis, which is programmed for numerical solution on an IBM 7090 computer, is presented in Ref. 11.

The heat-transfer specification from the modified turbulent boundary-layer analysis (Ref. 11) is

$$\frac{h}{\rho_e u_e c_p} = K^* \frac{c_f^*}{2} \left(\frac{\phi}{\theta}\right)^n \qquad (9a)$$

where

$$K^* = \left\{\sqrt{\frac{c_f^*}{2}} \left[5\,Pr + 5 \ln (5\,Pr + 1) - 14 + \sqrt{\frac{2}{c_f^*}}\right]\right\}^{-1}$$

The factor K^* is similar to the Prandtl-number correction factor in the von Kármán analogy. The coefficient c_f^* is analogous to the wall friction coefficient c_f but with the momentum thickness dependence replaced by the energy thickness. The ratio $(\phi/\theta)^n$ is a factor included in the analysis. For the present results, at stagnation pressures above 75 psia, n was found to have a value near zero. The wall friction coefficient is predicted either from the Blasius flat-plate relation (Eq. 8), with properties ρ and μ evaluated at the film temperature, as was done in the earlier analysis (Ref. 15), or by taking the adiabatic wall friction coefficient (predicted from Cole's relation [Ref. 19] between the friction coefficient for a compressible and incompressible flow) with properties evaluated as in Ref. 11. This latter method is suggested by a limited amount of data for low-speed flow (Ref. 20), which indicate both the Stanton number and wall friction coefficient with properties evaluated at the free-stream temperature to be insensitive to severe wall cooling. Of note is that for a severely cooled wall, the friction coefficient predicted by the latter method is substantially below that predicted by evaluating properties at the film temperature.

Prediction of the heat-transfer coefficient from Eq. (9a) requires both the selection of n and the temperature at which properties are to be evaluated. With $n \simeq 0.1$, the prediction is approximately the same as that of Ref. 15. For comparison purposes, two limiting values of n are considered. These correspond to assuming a Stanton-number dependence only on the thermal characteristic ϕ; i.e., $n = 0$, for which Eq. (9a) becomes

$$\frac{h}{\rho_e u_e c_p} = K^* \frac{c_f^*}{2} \qquad (9b)$$

or to taking $n = 0.25$, for which Eq. (9a) becomes approximately the von Kármán analogy

$$\frac{h}{\rho_e u_e c_p} = K \frac{c_f}{2} \qquad (10)$$

where

$$K = \left\{\sqrt{\frac{c_f}{2}}\left[\,5\,Pr + 5\ln(5\,Pr + 1) - 14 + \sqrt{\frac{2}{c_f}}\,\right]\right\}^{-1}$$

Other analyses which assume a Stanton-number dependence on ϕ have been made in Refs. 17 and 21 and compared to experimental heat-transfer results for accelerated turbulent boundary-layer flows. In Ref. 17, the predictions exceeded the data by about 30% in part of the acceleration region, while in Ref. 21, the correspondence with the data was good.

The heat-transfer predictions shown in Fig. 15 as curve A are from Eq. (9b) for a stagnation temperature of 1500°R and a range of stagnation pressures from 45 to 254 psia, with the 18-in. cooled approach length. These predictions were made with properties evaluated as in Ref. 11 and conditions at the edge of the boundary layer determined from the wall static-pressure measurements. Shown as curve C in Fig. 15 is the prediction from Eq. (10), in which the friction coefficient $c_f/2$ was determined from the modified turbulent boundary-layer analysis. The reduction in the predicted heat-transfer coefficients provided by Eq. (9b) below the von Kármán analogy is due to the greater predicted thermal than velocity boundary-layer thicknesses through the nozzle. At the highest stagnation pressure, the predicted ratios of ϕ/θ as indicated in Fig. 16 are as large as 6 in the throat region. At the 75-psia stagnation pressure, the correspondence of the prediction from the modified turbulent boundary-layer analysis, Eq. (9b), with the data is good except near the nozzle exit. At the highest stagnation pressure of 254 psia, where the circumferential variation of the data is considerable, the correspondence with the averaged heat-transfer data is fair. The reproducibility of the data in Fig. 15 for 254 psia is indicated by the two sets of data shown by the open and shaded symbols. At the lowest stagnation pressure, $p_t = 44.8$ psia, the prediction exceeds the data by as much as 50% in the throat region. For the range of stagnation pressures, the predicted maximum value of the heat-transfer coefficient is just upstream of the throat, in agreement with the data.

The effect of temperature choice for property evaluation may be observed in Fig. 15 by comparing curves A and B. Curve B represents Eq. (9b) with properties evaluated at the film temperature T_f. In the throat region, it lies above the data but is in better agreement near the nozzle exit than curve A.

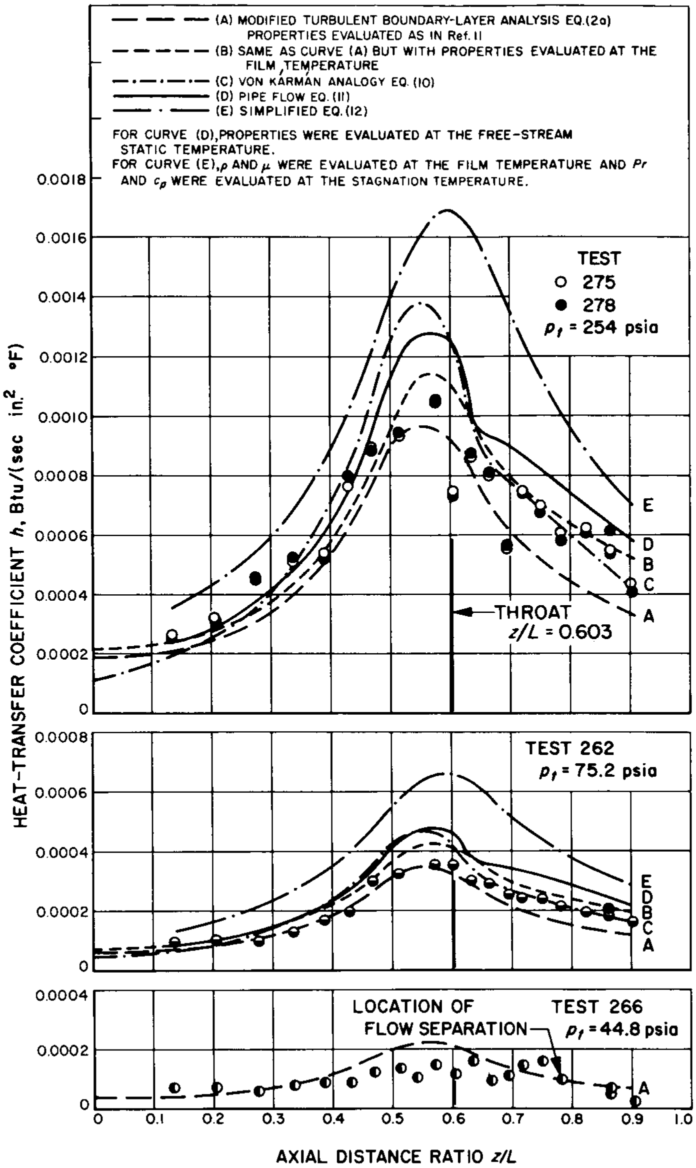

Fig. 15. Comparison of experimental heat-transfer coefficients with predictions at T_{to} = 1500°R with 18-in. cooled approach length

For comparison, the predictions from the following form of the pipe-flow equation for fully developed flow in which both the thermal and velocity boundary layer extend to the centerline and there is no significant pressure gradient are shown as curve D in Fig. 15.

$$St\,Pr^{0.6} = 0.023\,Re_D^{-0.2} \tag{11}$$

Also shown, as curve E in Fig. 15, is the equation of Ref. 22:

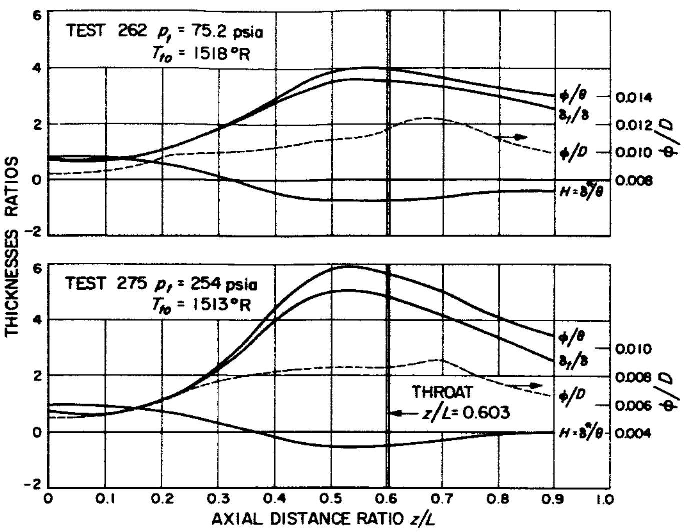

Fig. 16. Predicted thickness ratios along nozzle with 18-in. cooled approach length

$$h = \left[\frac{0.026}{(D^*)^{0.2}} \left(\frac{\mu^{0.2} c_p}{Pr^{0.6}}\right)_0 \left(\frac{p_o g_c}{c^*}\right)^{0.8} \left(\frac{D^*}{r_c}\right)^{0.1}\right] \left(\frac{A^*}{A}\right)^{0.9} \sigma \tag{12}$$

In the pipe-flow equation, all properties were evaluated at the free-stream static temperature, while in Eq. (12), the Prandtl number and specific heat were assumed constant at their stagnation temperature values and ρ and μ were evaluated at the film temperature. In Eq. (12), one-dimensional flow quantities were used, since two-dimensional effects are not taken into account in the derivation. If they were, the prediction would be nearer that of the pipe-flow equation. Two-dimensional values of local mass flux are 15% below the one-dimensional values just downstream of the nozzle throat, as seen in Fig. 7. The prediction from Eq. (12) exceeds the data by as much as 80% in the throat region. The pipe-flow prediction, Eq. (11), though in better agreement with the data, is still about 25% high at the throat.

From these observations, it appears that fair agreement with the data is provided at the higher stagnation pressures by the modified boundary-layer analysis taken in the form of Eq. (9b), with properties evaluated as in Ref. 11. These predictions are also shown, along with others, at the intermediate pressures of p_t = 60 and 150 psia for T_{to} = 1500°R, as curve A in Fig. 12. The predicted Stanton-number dependence on the mass flux is approximately that of the pipe-flow equation, which is shown as curve D. However, the prediction for all the axial locations cannot be approximated by an equation like the pipe-flow equation but with a lower coefficient because of the variation of the predicted value of ϕ relative to D. For a given run, ϕ decreases through the subsonic region, attaining a minimum near the throat, and then increases in the supersonic region, qualitatively similar but not in direct correspondence with the nozzle diameter. A few of these predicted ratios are shown in Fig. 16.

In Figs. 12c through 12i, the reduction in heat transfer at Reynolds numbers, Re_D, less than about 8×10^5 is not predictable from an analysis for a turbulent boundary layer, as indicated by the prediction from Eq. (9b) shown in Fig. 12 as curve A.

Predictions from Eq. (9b) (not shown) were also made at stagnation temperatures of 1030 and 2000°R, with the 18-in. cooled approach length. The magnitude of the decrease in the heat-transfer coefficient with increasing stagnation temperature at the higher stagnation pressures shown in Fig. 11 was not predictable. From Eq. (9b), the dependence of the heat-transfer coefficient on stagnation temperature at a given stagnation pressure is nearly $h \; \alpha \; T_{to}^{-0.28} \phi^{-0.2}$. However, the energy thickness at the nozzle inlet decreased with increasing stagnation temperature, such that the difference in predicted heat-transfer coefficients was substantially less than exhibited by the data.

The trend of higher heat-transfer coefficients through the nozzle with thinner boundary layers at the nozzle inlet is shown in Fig. 14 to be predictable from Eq. (9b). However, the magnitude of the predicted increase should probably be estimated from the 6- and 18-in. cooled approach length predictions. For the zero cooled approach length prediction, wall cooling was assumed to begin at the nozzle inlet. To require that the Stanton numbers remain finite there, the energy thickness was taken at a small value equal to 0.001 in.

VIII. SOME ADDITIONAL OBSERVATIONS OF THE FLOW AND THERMAL CHARACTERISTICS

In this Section, some features of the flow are shown which depend on the predicted flow and thermal characteristics obtained from the modified turbulent boundary-layer analysis (Ref. 11), with properties evaluated as in Ref. 11. In Fig. 16, the predicted ratios of ϕ/θ and δ_t/δ indicate the thicker predicted thermal than velocity boundary layers, especially in the throat region. Because of the cooled wall, the displacement thickness δ^* becomes negative upstream of the throat, as does $H = \delta^*/\theta$.

In Fig. 17, the predicted momentum thickness Reynolds numbers are a minimum a considerable distance upstream of the throat. At the lowest stagnation pressure, where the heat transfer is below that typical of a turbulent boundary layer, the minimum Reynolds number is 1500. Although this predicted value is probably different from the actual value, it is still considerably above the measured value of 600 found in Ref. 14, below which there was departure from fully turbulent flow. For the case of constant free-stream velocity, Preston (Ref. 23) proposed a value of 320 above which the flow could be considered fully turbulent; for accelerated flows he estimated that the limit might be lower.

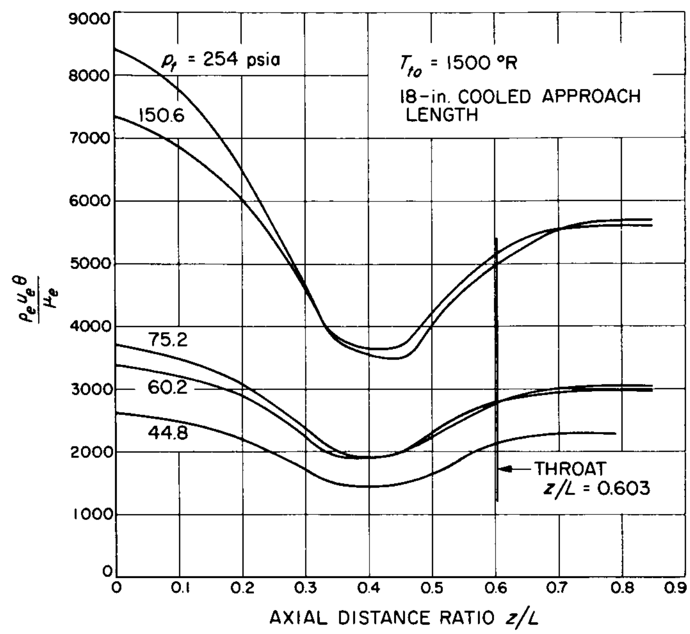

Fig. 17. Predicted momentum thickness Reynolds numbers along nozzle

To indicate the magnitude of the forces acting on the boundary layer through the nozzle, the ratio of the pressure forces which tend to accelerate the boundary-layer flow to the retardation wall shear forces is shown in Fig. 18 as

$$-\frac{\delta \dfrac{dp}{dx}}{\tau_w}$$

In this ratio the pressure gradient was numerically approximated from the wall static pressure measurements downstream of $z/L \simeq 0.3$. In the nozzle inlet section where the pressure gradient was difficult to obtain numerically, one-dimensional flow was assumed which provided an analytical relation for the pressure gradient. The ratio is largest in the convergent section before decreasing through the throat and divergent section. For comparison, the value of the ratio for fully developed flow in a circular pipe is shown to demonstrate the large flow accelerations in a nozzle.

To gain some knowledge of the mechanism which at the low stagnation pressures reduces the heat transfer below that typical of a fully turbulent boundary layer, reference is made to the boundary-layer turbulence-energy equation (e.g., Ref. 24). For simplicity, an incompressible plane flow is assumed for which the convection of turbulent kinetic energy by the mean flow is

$$u_j \frac{\partial \overline{\dfrac{q^2}{2}}}{\partial x_j} = \underbrace{-\overline{u'_i\, u'_j}\, \frac{\partial u_i}{\partial x_j}}_{\text{(a)}} \underbrace{- \frac{\partial}{\partial x_j} \overline{u'_j \left(\frac{p'}{\rho}\right.}}_{\text{(b)}} \underbrace{\overline{\left. + \frac{q^2}{2}\right)}}_{\text{(c)}} \underbrace{+ \nu \overline{u'_i \frac{\partial^2 u'_i}{\partial x_j^2}}}_{\text{(d)}} \qquad (13)$$

The terms represent the following:

(a) Production of turbulent kinetic energy by the working of the mean velocity gradients against the Reynolds stresses.

(b) Work done by the turbulence against the fluctuation pressure gradients.

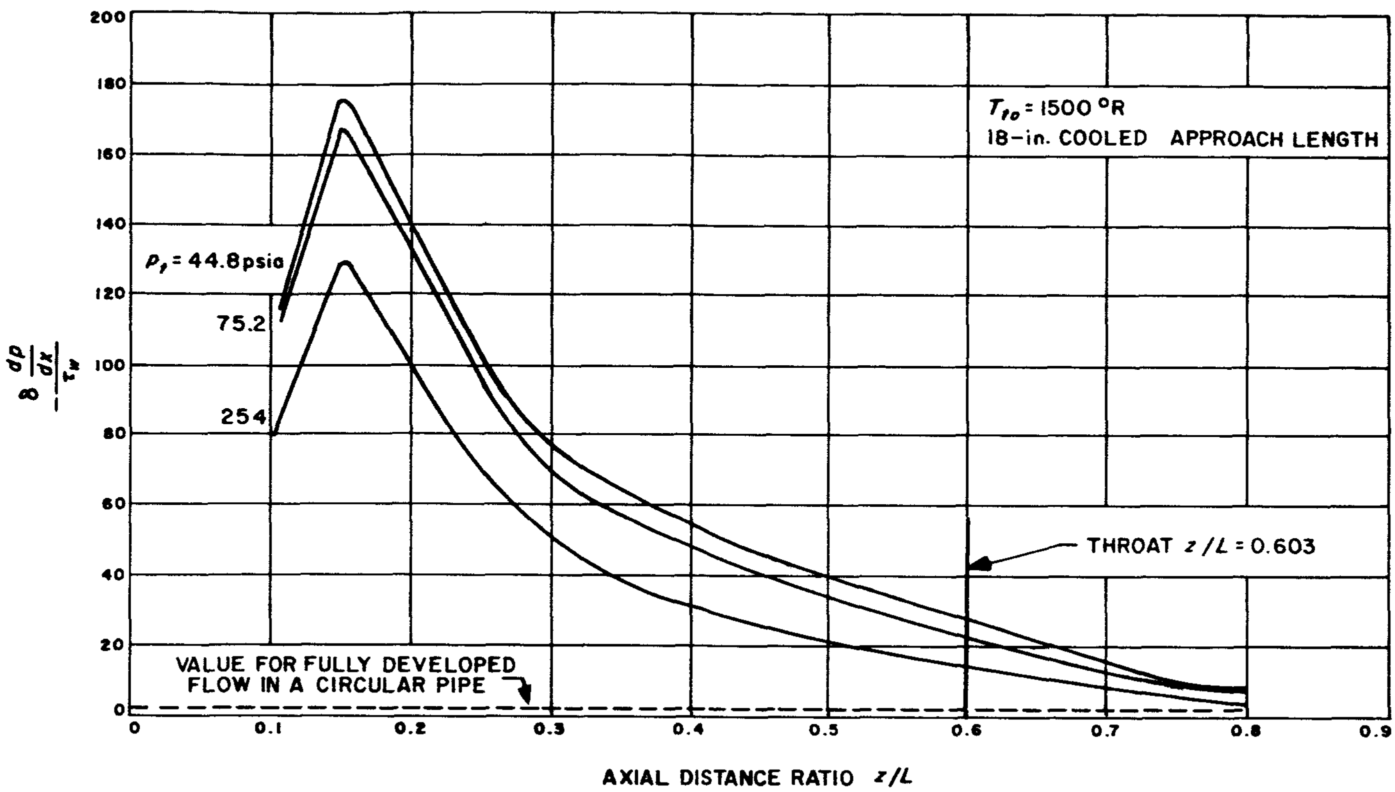

Fig. 18. Predicted ratio of pressure to wall shear forces acting on boundary layer along nozzle

(c) Convection of turbulent kinetic energy by the turbulence itself.

(d) Transfer of energy by the working of the turbulent viscous stresses.

For a two-dimensional flow with a pressure gradient, the significant terms from term (a) that lead to a production or decay of convected turbulent kinetic energy are

$$- \overline{u_i' \, u_j'} \frac{\partial u_i}{\partial x_j} = - \overline{u'v'} \frac{\partial u}{\partial y} - (\overline{u'^2} - \overline{v'^2}) \frac{\partial u}{\partial x} \tag{14}$$

The remaining terms (b), (c), and (d) in Eq. (13) are dependent on the turbulence produced. The first term in Eq. (14) is always positive and leads to a production of turbulent kinetic energy. However, with flow acceleration $\partial u/\partial x > 0$, the second term leads to a decay of turbulent kinetic energy provided that $\overline{u'^2} > \overline{v'^2}$. Thus, a measure of the importance of flow acceleration in reducing the net production of turbulent kinetic energy is given by a ratio of the two terms in Eq. (14):

$$\chi = \frac{(\overline{u'^2} - \overline{v'^2}) \dfrac{\partial u}{\partial x}}{- \overline{u'v'} \dfrac{\partial u}{\partial y}} \tag{15a}$$

To establish the variation of χ in the flow direction requires a knowledge of the turbulent quantities across the boundary layer. In the absence of turbulence measurements in accelerated flows, this estimate is restricted to the flat-plate measurements of Klebanoff (Ref. 25) at a momentum thickness Reynolds number of about 8×10^3. The production term $- \overline{u'v'} \, \partial u/\partial y$ is largest in the wall vicinity where $(y\sqrt{\tau_w/\rho_e})/\nu_e \simeq 30$. Using the "law of the wall," Eq. (7), the velocity gradient is

$$\frac{\partial u}{\partial y} = \frac{2.5}{30} \frac{\tau_w}{\rho_e \nu_e}$$

An average value of $(\overline{u'^2} - \overline{v'^2})/(-\overline{u'v'}) \simeq 1.8$ is taken from Klebanoff's data since this ratio did not vary appreciably across most of the boundary layer. Approximating the velocity gradient $\partial u/\partial x$ by its free-stream value du_e/dx and combining the other approximations gives

$$\chi \simeq \frac{22\nu_e \dfrac{du_e}{dx}}{\dfrac{\tau_w}{\rho_e}} \tag{15b}$$

Although the constant 22 is somewhat arbitrary, the essential feature is the dependence of χ on the group

$$\frac{\nu_e \dfrac{du_e}{dx}}{\dfrac{\tau_w}{\rho_e}}$$

The variation of χ along the nozzle is shown in Fig. 19 at $T_t = 1500°R$ for the range of stagnation pressures from 45 to 254 psia. With decreasing stagnation pressure, the increasing values of χ indicate the predicted reduced net production of turbulent kinetic energy. At the lowest stagnation pressure, χ attains a maximum value of 0.14. Actually, for the low stagnation pressures, the values of χ should exceed those shown, since the low heat transfer implies that the wall shear is below the predicted value. The variation of χ along the nozzle displays the same trend of being largest in the convergent section before diminishing through the throat and divergent section as the heat-transfer data at the low stagnation pressures which depart from those typical of a turbulent boundary

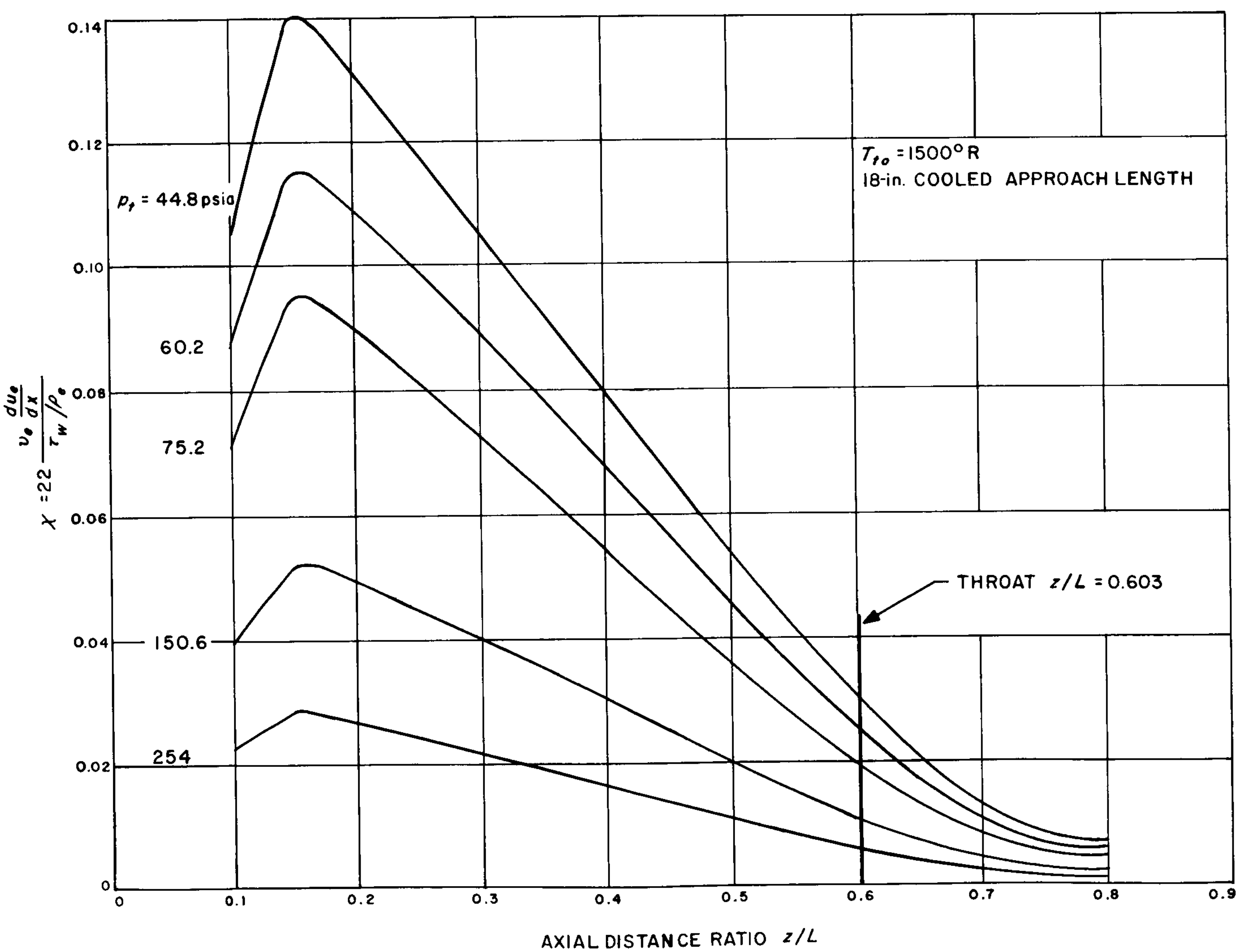

Fig. 19. Predicted effect of flow acceleration in reducing net production of turbulent kinetic energy at different stagnation pressures

layer observed in Fig. 12. The values of χ indicate when the turbulent shear stress $\overline{u'v'}$, which is related to the turbulent kinetic energy, is expected to be lower than that typical of a fully turbulent boundary layer. The transport of heat would also be reduced, since it depends on the level of turbulent transport.

IX. CONCLUSIONS

Experimental convective heat-transfer results have been presented for a turbulent boundary-layer flow through a cooled convergent–divergent nozzle. The scope of the investigation covered a wide range of stagnation pressures and temperatures as well as nozzle-inlet boundary-layer thicknesses. The experimental results indicated the following:

1. Heat-transfer coefficients increased with increasing stagnation pressure as a result of the larger mass fluxes, but only at stagnation pressures above about 75 psia were values typical of a turbulent boundary layer.
2. At low stagnation pressures, the heat-transfer coefficients were below that typical of a turbulent boundary layer even though the boundary layers at the nozzle inlet were turbulent.
3. The effect of stagnation temperature on heat transfer was less clear, with the trends dependent on stagnation pressure.
4. Heat-transfer coefficients were about 10% higher throughout the nozzle with the thinnest boundary layer at the nozzle inlet ($\delta/R \simeq 0.05$) than with the thickest inlet boundary layer ($\delta/R \simeq 0.25$).
5. The heat-transfer coefficient is a maximum upstream of the throat, where the mass flux, deduced from wall static pressure measurements, is largest. Deviations of the mass flux from that predicted for one-dimensional flow amounted to as much as 15% just downstream of the throat.
6. A substantial decrease in heat transfer existed downstream of the point of flow separation. Flow separation in the divergent portion of the nozzle occurred at the low stagnation pressures.

Various heat-transfer predictions were compared to the data. Fair agreement at the higher stagnation pressures is provided by a modification of the turbulent boundary-layer analysis of Ref. 15, in which the Stanton number is taken dependent on a Reynolds number based on a thickness characteristic of the thermal boundary layer. In this prediction, properties were evaluated as in Ref. 11. For the low stagnation pressures, where the turbulent boundary layer is thought to have undergone partial transition toward a laminar one, a parameter is found which is a measure of the importance of flow acceleration in reducing the transport of heat below that typical of a fully turbulent boundary layer.

More work is needed to gain some experimental knowledge of the flow and thermal boundary layers within a convergent–divergent nozzle and of the extent to which these are predictable by an analysis such as that of Ref. 11. To obtain this information, a conical nozzle of 10-deg half-angles of convergence and divergence has been constructed. This nozzle, which will be tested in the near future, is instrumented with boundary-layer probes and incorporates the calorimetric technique to obtain heat-transfer measurements.

NOMENCLATURE

a	speed of sound
A	local nozzle cross-sectional area
A^*	nozzle-throat area
c^*	characteristic velocity of $\rho_o A^* g_c/\dot{m}$
c_f	local wall friction coefficient, $c_f/2 = \tau_w/\rho_e u_e^2$
c_f^*	coefficient analogous to skin-friction coefficient, with momentum thickness dependence replaced by energy thickness
c_p	specific heat at constant pressure
D	nozzle diameter
D^*	nozzle-throat diameter
g_c	gravitational constant
h	convective heat-transfer coefficient
k	thermal conductivity
l	cooled approach length
L	axial length of nozzle = 5.925 in.
$\dot{m}$	mass flow rate
M	Mach number
p	static pressure
p_t	stagnation pressure
Pr	Prandtl number
q_w	wall heat flux
$q^2/2$	turbulent kinetic energy
r	nozzle radius
r^*	nozzle-throat radius
r_c	nozzle-throat radius of curvature
R	nozzle-inlet radius = 2.53 in.
Re_D	Reynolds number based on nozzle diameter, $\rho_e u_e D/\mu_e$
St	Stanton number, $h/\rho_e u_e c_{p_e}$
T	temperature
u	velocity component in x-direction
u^+	dimensionless velocity, $u/\sqrt{\tau_w/\rho_e}$
v	velocity component normal to wall
x	distance along wall in flow direction

NOMENCLATURE (Cont'd)

y distance normal to wall

y^+ dimensionless distance, $\dfrac{y\sqrt{\dfrac{\tau_w}{\rho_e}}}{\nu_e}$

z axial distance from nozzle inlet

γ specific-heat ratio

δ velocity boundary-layer thickness

δ_t stagnation-temperature boundary-layer thickness

δ^* displacement thickness

θ momentum thickness

μ viscosity

ν kinematic viscosity

ρ density

σ dimensionless property correction factor (defined in Ref. 22)

τ_w wall shear stress

ϕ energy thickness

χ parameter

Subscripts

$_a$ condition at radius which is less than r_b

$_{aw}$ adiabatic wall condition

$_b$ condition at radius which is greater than r_a

$_e$ condition at free-stream edge of boundary layer

$_f$ property evaluated at film temperature, $T_f = (T_w + T_e)/2$

$_{i,j}$ components in Cartesian coordinates

$_o$ upstream reservoir condition

$_t$ stagnation condition

$_w$ wall condition

$_1$ one-dimensional flow value

Superscripts

$'$ fluctuating component

$\overline{}$ time average

REFERENCES

1. Witte, A. B., and E. Y. Harper, *Experimental Investigation of Heat Transfer Rates in Rocket Thrust Chambers*, Technical Report No. 32-244, Jet Propulsion Laboratory, Pasadena, California, March 19, 1962. Also AIAA, Vol. 1, No. 2, 1963, pp. 443–51.

2. Saunders, O. A., and P. H. Calder, "Some Experiments on the Heat Transfer from a Gas Flowing Through a Convergent–Divergent Nozzle," *Proceedings of the 1951 Heat Transfer and Fluid Mechanics Institute*, Stanford University Press, 1951.

3. Ragsdale, W. C., and J. M. Smith, "Heat Transfer in Nozzles," *Chem. Engr. Sci.*, Vol. 11, 1960, p. 242–51.

4. Baron, J. R., and F. H. Durgin, *An Experimental Investigation of Heat Transfer at the Boundaries of Supersonic Nozzles*, Naval Supersonic Laboratory, Massachusetts Institute of Technology, WADC Technical Report 54-541, December 1954.

5. *Combined Bimonthly Summary No. 63, December 1, 1957 to February 1, 1958*, Jet Propulsion Laboratory, Pasadena, February 15, 1958, pp. 28–30. *Combined Bimonthly Summary No. 65, April 1, 1958 to June 1, 1958*, Jet Propulsion Laboratory, Pasadena, June 15, 1958, p. 32.

6. Kolozsi, J. J., *An Investigation of Heat Transfer Through the Turbulent Boundary Layer in an Axially Symmetric, Convergent–Divergent Nozzle*, Aerodynamic Lab., Ohio State University, TM-8, July 1958.

7. Livesey, J. L., "The Behavior of Transverse Cylindrical and Forward-Facing Pressure Probes in Transverse Total Pressure Gradients," *Journal of the Aeronautical Sciences*, Vol. 23, October 1956, pp. 949–55.

8. Seban, R. A., and D. Doughty, *Heat Transfer to Laminar and Turbulent Boundary Layers with Constant and Variable Free-Stream Velocity*, University of California, Institute of Engineering Research, Series 41, No. 13, August 1954.

9. Oswatitsch, K., and W. Rothstein, *Flow Pattern in a Converging–Diverging Nozzle*, NACA TM-1215, March 1949.

10. Coles, D., "The Law of the Wake in the Turbulent Boundary Layer," *Journal of Fluid Mechanics*, Vol. 1, 1956, pp. 191–226.

11. Elliott, D. G., D. R. Bartz, S. Silver, *Calculation of Turbulent Boundary-Layer Growth and Heat Transfer in Axi-Symmetric Nozzles*, Technical Report No. 32-387, Jet Propulsion Laboratory, Pasadena, February 15, 1963.

12. Keenan, J. H., and J. Kaye, *Gas Tables*, Wiley and Sons, Inc., New York, 1956.

13. Sergienko, A. A., and V. K. Gretsov, "Transition from a Turbulent into a Laminar Boundary Layer," *Soviet Physics—Doklady*, Vol. 4, No. 2, October 1959, pp. 275–76.

14. Back, L. H., *Heat Transfer to Turbulent Boundary Layers with a Variable Free-Stream Velocity*, Ph.D. Thesis, University of California, Berkeley, California, June 1962.

15. Bartz, D. R., "An Approximate Solution of Compressible Turbulent Boundary-Layer Development and Convective Heat Transfer in Convergent–Divergent Nozzles," *Transactions of the ASME*, Vol. 77, No. 8, 1955, pp. 1235–45.

16. Reshotko, E., and M. Tucker, *Approximate Calculation of the Compressible Turbulent Boundary Layer with Heat Transfer and Arbitrary Pressure Gradient*, NACA TN-4154, 1957.

REFERENCES (Cont'd)

17. Seban, R. A., and H. W. Chan, *Heat Transfer to Boundary Layers with Pressure Gradients,* University of California, Institute of Engineering Research, Series 41, No. 16, July 1957.

18. McCarthy, T. F., *Heat Transfer to Turbulent Boundary Layers with a Pressure Gradient,* Master's Thesis, University of Minnesota, August 1960.

19. Coles, D. E., *The Turbulent Boundary Layer in a Compressible Fluid,* Report No. P-2417, The Rand Corporation, Santa Monica, California, August 22, 1961.

20. Wolf, H., *The Experimental and Analytical Determination of the Heat Transfer Characteristics of Air and Carbon Dioxide in the Thermal Entrance Region of a Smooth Tube with Large Temperature Differences Between the Gas and the Tube Wall,* Ph.D. Thesis, Purdue University, Lafayette, Indiana, March 1958. Also *ASME Journal of Heat Transfer,* Vol. 81, November 1959, pp. 267–79.

21. Kutateladze, S. S., and A. I. Leontev, "Drag Law in a Turbulent Flow of a Compressible Gas and the Method of Calculating Friction and Heat Exchange," *Akademiya Nauk, Belorussk, S.S.R.,* Minsk, U.S.S.R., January 1961, pp. 1–23, 23–27, translated and issued by Technical Information and Library Services, Ministry of Aviation, December 1961.

22. Bartz, D. R., "A Simple Equation for Rapid Estimation of Rocket Nozzle Convective Heat-Transfer Coefficients," *Jet Propulsion,* Vol. 27, January 1957, pp. 49–51.

23. Preston, J. H., "The Minimum Reynolds Number for a Turbulent Boundary Layer and the Selection of a Transition Device," *Journal of Fluid Mechanics,* Vol. 3, Part 4. January 1958, pp. 373–84.

24. Hinze, J. O., *Turbulence,* p. 62, McGraw-Hill Book Company, Inc., New York, New York, 1959.

25. Klebanoff, P. S., *Characteristics of Turbulence in a Boundary Layer with Zero Pressure Gradient,* NACA TN-3178, 1954.

APPENDIX A

Construction and Calibration of Thermocouple Plugs

The thermocouples embedded in the 0.25-in.-diameter plugs were formed by welding the exposed ends of 0.005-in.-diameter fiberglass-insulated chromel and alumel wires to the bottoms of opposing radial holes, as shown in Fig. 3. The wires were injected into these holes by using a spring-loaded jig, and the junction weld was made on contact between the wire and the plug. The chromel and the alumel junctions were separated by approximately 0.0055 in. of plug material. The wires were then cemented into the grooves in the sides of the plugs with Technical G Copper Cement and calibrated. A finished plug is shown in Fig. A-1.

To provide good contact between surfaces when the plugs were pressed into the nozzle, both the surfaces of the plugs and the holes were finished to roughnesses less than 16 μin. An interference fit of 0.0005 in. between the plug and nozzle hole diameters was used. After the plugs were pressed into position flush with the outer surface of the nozzle, the inner ends were machined to match the contour of the nozzle. The locations at which the wires protruded from the outer ends of the plugs were sealed with Technical G Copper Cement, and a coat of Echo Bond 56-C conductive cement was applied over the plug and extended over the nozzle to exclude any possibility of water seepage into the plugs. The nozzle, after installation of plugs, is shown in Fig. A-2.

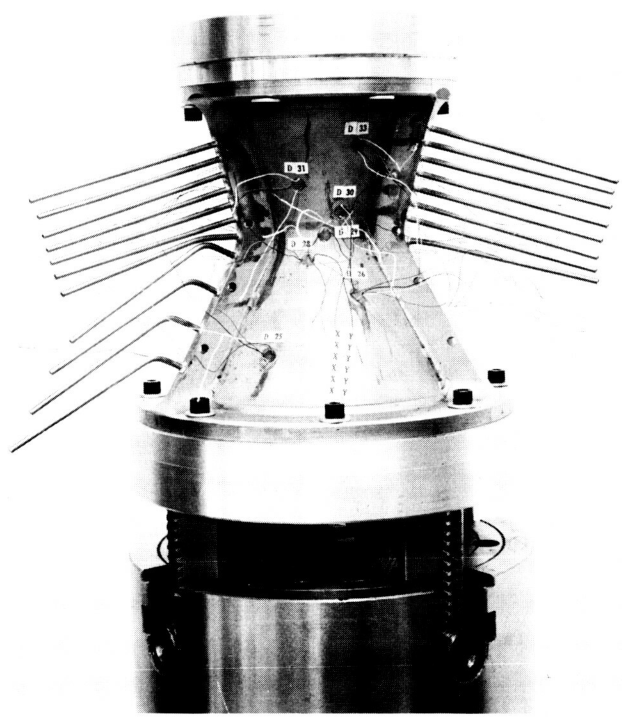

Fig. A-2. Nozzle after installation of thermocouple plugs

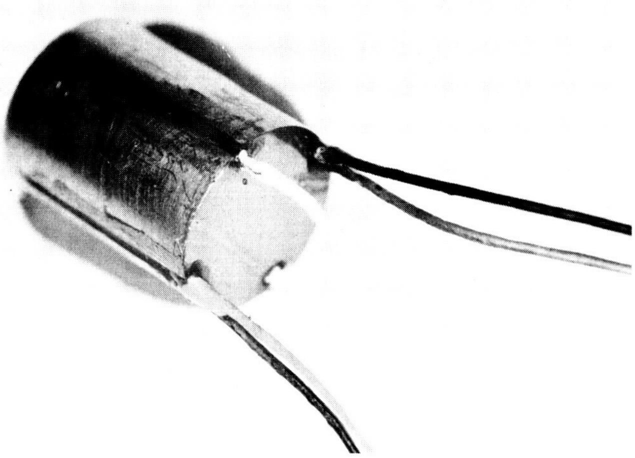

Fig. A-1. Thermocouple plug

For the calculation of the wall heat flux from Eq. (1), it is necessary to know precisely the distance between thermocouple weld junctions. Since the radial holes in the plugs were about three times the diameter of the bare end of the thermocouple wire, the exact location of the weld junction could not be obtained by physical measurement; thus, a Kelvin bridge circuit electrical calibrating technique was used as shown in Fig. A-3. This calibration was performed before the plugs were installed in the nozzle. A rod having the same diameter as a plug and of known electrical resistance R_R was connected to variable resistors R_b and R_d by wires with known resistances R_B and R_D. The plug with the thermocouples which were to be measured was held coaxially against one end of the rod. The contact resistance between rod and plug is represented by R_Y. A thermocouple wire of unknown resistance R_C leading to one of the junctions was con-

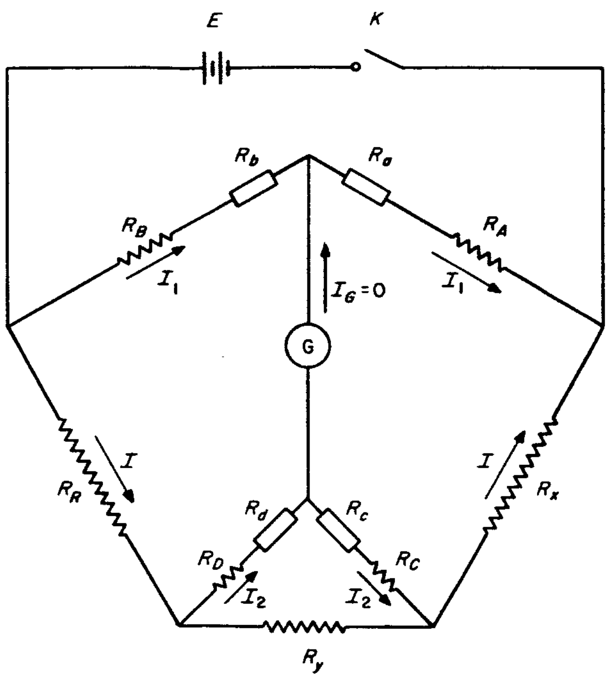

Fig. A-3. Kelvin bridge circuit used to determine thermocouple locations

nected to a variable resistor R_c and a galvanometer G. A thermocouple wire of the same material leading from another junction within the plug and represented by the unknown resistance R_A was connected to another variable resistor R_a, which was in turn connected to R_b and the other side of G. The resistance R_x represents the resistance of the plug between the junction wires R_C and R_A. The circuit assembly was completed with a battery E and a switch K. For the branch circuits with no current passing through G, Kirchkoff's second law may be applied, and the following equations may be written:

$$I_1 (R_A + R_a) = I_2 (R_C + R_c) + IR_x \qquad \text{(A-1)}$$

$$I_1 (R_B + R_b) = I_2 (R_D + R_d) + IR_R \qquad \text{(A-2)}$$

$$I_2 (R_C + R_c + R_D + R_d) = (I - I_2) R_y \qquad \text{(A-3)}$$

For $I_G = 0$,

$$\frac{R_A + R_a}{R_B + R_b} = \frac{R_C + R_c}{R_D + R_d} \qquad \text{(A-4)}$$

and the simultaneous solution of the above equations (A-1–A-4) yields

$$R_x = R_R \frac{R_A + R_a}{R_B + R_b} \qquad \text{(A-5)}$$

Therefore, by proper adjustment of the resistances of the decade boxes such that $I_G = 0$, R_x is independent of the unknown contact resistance R_y. Actually, it was not possible to make I_G exactly zero because of the limited sensitivity of the galvanometer; hence, R_y was made small in comparison to R_x. Incorporating the following equations using the electrical resistivity ρ,

$$R_x = \frac{\rho_x l_x}{A_x} \qquad \text{(A-6)}$$

$$R_R = \frac{\rho_R l_R}{A_R} \qquad \text{(A-7)}$$

where l_R is the known length of the rod. Since the diameters of the rod and plug are identical, $A_x = A_R$, the solution of Eqs. (A-5), (A-6), and (A-7) yields

$$l_x = \frac{R_A + R_a}{R_B + R_b} l_R \frac{\rho_R}{\rho_x} \qquad \text{(A-8)}$$

Equation (A-8) was used to determine the distance between the junctions formed by two wires of the same thermocouple material. The arithmetic average of distances between junctions formed by corresponding alumel and chromel wires was then used as the distance between two thermocouple junctions.

The distance between the nozzle gas-side wall and the inner thermocouple weld junction needed to calculate the wall temperature, however, could not be determined by the electrical technique and, consequently, had to be measured physically. The distance from the radial holes in which the inner thermocouple was welded to the inner surface of the plug was measured before injection of the wires. The length of the plug after installation and machining then made possible a simple calculation of the distance from wall to inner thermocouple with the assumption that the thermocouple wires were located on the centerlines of the holes.

The estimated maximum total error that could have occurred in reported experimental values of heat-transfer coefficient in the throat region at the higher stagnation pressures and temperatures is approximately ±8%. This error results from a ±1% error due to thermocouple locations determined by the Kelvin bridge measurements, a ±1½% error from inaccuracies in measurement of the temperatures within the nozzle wall, a ±5% uncertainty in the difference between stagnation temperature and gas-side walls temperature, and a ±½% error from additional miscellaneous sources. Under conditions for which the temperature differences between adjacent thermocouples were the smallest such as at low stagnation pressure and temperature near the nozzle inlet, the maximum total error could have been as much as ±21%. It should be noted, however, that these are considered to be maximum errors and that the accuracy of the reported results is probably much better.

APPENDIX B

Tabulated Data

Table B-1 presents the ranges of operating conditions in terms of stagnation pressure p_t, stagnation temperature T_{to}, and upstream cooled approach length l, for which wall static pressure and heat-transfer data tabulated in Tables B-2 and B-3, respectively, were obtained.

In Table B-2, experimental values of the wall static-to-stagnation pressure ratio p/p_t are tabulated as a function of both the nozzle axial distance-to-length ratio z/L and the nozzle-area to throat-area ratio A/A^* for a range of stagnation pressures from 45 to 150 psia. As mentioned previously, measurements at higher stagnation pressures were not obtained, because of manometer limitations. The symbol † denotes that flow separation existed at the indicated locations.

In Table B-3, a typical test entry includes cooled approach length l, stagnation pressure p_t, stagnation temperature T_{to}, mass flow rate $\dot{m}$, and thicknesses θ, δ^*, and ϕ at a location 1.25 in. upstream of the nozzle inlet.

Shown for each test are the experimental wall heat flux q_w and temperature T_w, along with the calculated heat-transfer coefficient h. The free-stream static temperature T_e and mass flux $\rho_e u_e$ at the edge of the boundary layer were calculated from the experimental static-to-stagnation pressure ratio p/p_t for isentropic flow (γ = const.) at the corresponding stagnation temperature value of γ for the products of combustion. For stagnation pressures above 150 psia and those few tests in Table B-2 for which pressure data were not obtained, values of p/p_t from tests below 150 psia were used, since p/p_t was found to be nearly invariant with stagnation pressure except in separated flow regions. Also included for each test are values of the Reynolds number per inch $(\rho_e u_e)/\mu_e$ and the Stanton number $h/\rho_e u_e c_{p_e}$. Since the methanol-to-air weight flow rate was small, the products of combustion could be treated approximately as air in the evaluation of viscosity, specific heat, and Prandtl number; these properties were obtained from Ref. 12.

In the separation region, only the directly measured wall heat fluxes and wall temperatures are shown in Table B-3. The heat transfer coefficients shown in Figs. 11 and 15 at a stagnation pressure of 45 psia were calculated in the separation region from

$$h = \frac{q_w}{T_{to} - T_w}$$

In this region the stagnation temperature T_{to} was used in computing h rather than the unknown adiabatic wall temperature T_{aw}.

Many of the tests tabulated were duplicated and found to be reproducible. These duplicate tests, however, are not included in the tabulations except at p_t = 254 psia and T_{to} = 1513°R, for which both tests 275 and 278 are shown.

Table B-1. Summary of tabulated tests, which appear in Tables B-2 and B-3 in the order shown

Test	p_t psia	T_{to} °R	l in.
319	35.9	1508	0
318	51.0	1509	↓
315	74.6	1516	↓
317	101.0	1510	↓
316	124.4	1505	↓
314	151.7	1506	↓
312	179.7	1467	↓
313	201.7	1517	↓
242	45.0	1490	6
245	60.2	1513	↓
246	75.2	1500	↓
237	45.2	1531	12
235	60.2	1545	↓
234	75.2	1527	↓
300	30.0	1039	18
301	45.1	1035	↓
303	75.2	1024	↓
304	100.8	1036	↓
305	125.6	1032	↓
306	150.6	1028	↓
308	175.8	1035	↓
309	201.7	1029	↓

Test	p_t psia	T_{to} °R	l in.
310	226.7	1032	18
311	253.7	1030	↓
288	30.1	1511	↓
287	40.2	1508	↓
266	44.8	1503	↓
281	50.1	1514	↓
280	55.1	1501	↓
263	60.2	1536	↓
262	75.2	1518	↓
269	100.2	1511	↓
267	134.8	1501	↓
268	150.6	1484	↓
271	175.0	1483	↓
273	201.0	1507	↓
277	225.7	1508	↓
278	250.7	1517	↓
275	253.7	1513	↓
293	30.0	2001	↓
294	49.9	2000	↓
290	75.2	1989	↓
296	101.2	2001	↓
298	125.8	2007	↓

Table B-2. Tabulation of static pressure data

Pressure tap number	Axial distance ratio z/L	Area ratio A/A^*	Static-to-stagnation pressure p/p_t for indicated test[a]										
			319 $p_t=35.9$ $T_{to}=1508$	318 $p_t=51.0$ $T_{to}=1509$	315 $p_t=74.6$ $T_{to}=1516$	317 $p_t=101.0$ $T_{to}=1510$	316 $p_t=124.4$ $T_{to}=1505$	314 $p_t=151.7$ $T_{to}=1506$	242 $p_t=45.0$ $T_{to}=1490$	245 $p_t=60.2$ $T_{to}=1513$	246 $p_t=75.2$ $T_{to}=1500$	237 $p_t=45.2$ $T_{to}=1531$	235 $p_t=60.2$ $T_{to}=1545$
1	0.107	7.001	—	0.997	0.997	0.997	0.997	—	0.997	0.996	0.997	—	—
2	0.222	4.691	—	0.991	0.991	0.991	0.991	—	0.991	0.990	0.991	—	—
3	0.3396	2.939	—	0.976	0.977	0.977	0.977	—	0.978	0.977	0.978	—	—
4	0.3401	2.924	—	0.977	0.977	0.977	0.977	—	0.978	0.977	0.979	0.979	0.979
5	0.395	2.255	—	0.957	0.958	0.958	0.958	—	0.960	0.958	0.958	0.961	0.960
6	0.455	1.631	—	0.908	0.909	0.908	0.908	—	0.911	0.910	0.910	0.912	0.912
7	0.460	1.561	—	0.899	0.901	0.901	0.900	—	0.905	0.901	0.902	0.904	0.903
8	0.506	1.235	—	0.787	0.789	0.789	0.788	—	0.792	0.790	0.789	0.788	0.788
9	0.529	1.135	—	0.727	0.730	0.728	0.728	—	0.732	0.730	0.730	0.732	0.734
10	0.554	1.054	—	0.643	0.647	0.644	0.644	—	0.653	0.650	0.650	0.652	0.650
11	0.587	1.0078	—	0.508	0.512	0.508	0.508	—	0.512	0.507	0.510	0.511	—
12	0.6018	1.0012	—	0.452	0.453	0.455	0.453	—	0.453	0.454	0.453	0.463	0.463
13	0.642	1.028	—	0.338	0.345	0.339	0.321	—	0.347	0.345	0.344	0.347	0.348
14	0.691	1.176	—	0.202	0.211	0.207	0.207	—	0.202	0.205	0.207	0.207	0.209
15	0.706	1.231	—	0.194	0.202	0.200	0.200	—	0.195	0.197	0.199	0.198	0.200
16	0.722	1.297	—	0.209	0.193	—	0.168	—	0.185	0.188	0.188	0.189	0.191
17	0.741	1.372	—	0.172	0.180	0.175	0.176	—	0.173	0.176	0.176	0.176	0.178
18	0.753	1.423	—	0.162	0.171	0.166	0.166	—	0.164	0.166	0.168	0.168	0.169
19	0.771	1.505	—	0.154	0.163	0.159	0.159	—	0.157	0.156	0.159	0.166	0.158
20	0.789	1.582	—	0.138	0.147	0.142	0.142	—	0.147	0.143	0.145	0.155	0.145
21	0.802	1.642	—	0.129	0.138	0.134	0.134	—	0.269†	0.143	0.145	0.206†	0.137
22	0.819	1.716	—	0.124	0.133	0.128	0.128	—	0.288	0.128	0.129	0.291	0.128
23	0.838	1.815	—	0.119	0.129	0.125	0.124	—	0.296	0.124	0.126	0.283	0.125
24	0.852	1.866	—	0.112	0.120	0.115	0.115	—	0.302	0.123	0.116	0.294	0.116
25	0.869	1.960	—	0.118†	0.105	0.107	0.106	—	0.301	0.115	0.108	0.298	0.107
26	0.887	2.049	—	0.148	0.099	0.100	0.100	—	0.304	0.165†	0.100	0.295	0.122†
27	0.900	2.112	—	0.215	0.103	0.100	0.097	—	0.304	0.212	0.094	0.300	0.194
28	0.921	2.210	—	0.220	0.085	0.087	0.087	—	0.305	0.226	0.087	0.301	0.222
29	0.932	2.283	—	0.217	0.082	0.084	0.084	—	0.307	0.228	0.083	0.301	0.225
30	0.949	2.379	—	0.230	0.078	0.080	0.079	—	0.306	0.230	0.083†	0.304	0.228
31	0.965	2.471	—	0.229	0.070	0.072	0.072	—	0.308	0.232	0.176	0.306	0.230
32	0.985	2.574	—	0.229	0.077†	0.068	0.068	—	0.309	0.234	0.183	0.307	0.231

[a]Stagnation pressure p_t in psia; stagnation temperature T_{to} in °R.

†Flow separation occurred at this location.

Table B-2 (continued).

Pressure tap number	Axial distance ratio z/L	Area ratio A/A^*	Static-to-stagnation pressure p/p_t for indicated test[a]										
			234 $p_t=75.2$ $T_{to}=1527$	300 $p_t=30.0$ $T_{to}=1039$	301 $p_t=45.1$ $T_{to}=1035$	303 $p_t=75.2$ $T_{to}=1024$	304 $p_t=100.8$ $T_{to}=1036$	305 $p_t=125.6$ $T_{to}=1032$	306 $p_t=150.6$ $T_{to}=1028$	288 $p_t=30.1$ $T_{to}=1511$	287 $p_t=40.2$ $T_{to}=1508$	266 $p_t=44.8$ $T_{to}=1503$	281 $p_t=50.1$ $T_{to}=1514$
1	0.107	7.001	—	0.995	0.996	0.996	0.996	—	0.997	0.996	0.996	0.996	0.995
2	0.222	4.691	—	0.990	0.991	0.991	0.991	—	0.991	0.991	0.991	0.991	0.991
3	0.3396	2.939	—	0.975	0.976	0.977	0.977	—	0.977	0.976	0.977	0.976	0.976
4	0.3401	2.924	0.979	0.975	0.976	0.976	0.976	—	0.976	0.976	0.977	0.976	0.976
5	0.395	2.255	0.960	0.955	0.956	0.957	0.956	—	0.957	0.957	0.958	0.958	0.957
6	0.455	1.631	0.912	0.904	0.907	0.906	0.906	—	0.907	0.907	0.908	0.907	0.908
7	0.460	1.561	0.903	0.899	0.898	0.900	0.898	—	0.898	0.899	0.899	0.899	0.900
8	0.506	1.235	0.788	0.787	0.786	0.786	0.785	—	0.784	0.787	0.788	0.791	0.788
9	0.529	1.135	0.732	0.725	0.724	0.724	0.723	—	0.723	0.727	0.730	0.731	0.729
10	0.554	1.054	0.652	0.639	0.638	0.642	0.640	—	0.640	0.643	0.645	0.650	0.647
11	0.587	1.0078	0.511	0.502	0.501	0.502	0.499	—	0.500	0.503	0.506	0.508	0.507
12	0.6018	1.0012	0.463	0.446	0.448	0.452	0.451	—	0.451	0.449	0.453	0.454	0.455
13	0.642	1.028	0.347	0.341	0.341	0.341	0.334	—	0.312	0.337	0.340	0.344	0.340
14	0.691	1.176	0.211	0.281†	0.200	0.203	0.203	—	0.203	0.244†	0.201	0.204	0.204
15	0.706	1.231	0.201	0.409	0.192	0.195	0.195	—	0.195	0.374	0.195	0.196	0.197
16	0.722	1.297	0.189	0.359	0.188	0.184	0.179	—	0.179	0.368	0.186	0.186	0.187
17	0.741	1.372	0.179	0.335	0.169	0.172	0.171	—	0.172	0.303	0.175	0.173	0.173
18	0.753	1.423	0.169	0.429	0.159	0.162	0.162	—	0.163	0.405	0.169	0.164	0.171
19	0.771	1.505	0.160	0.390	0.152	0.155	0.155	—	0.157	0.420	0.225†	0.158	0.157
20	0.789	1.582	0.146	0.367	0.217†	0.139	0.139	—	0.140	0.366	0.240	0.142	0.145
21	0.802	1.642	0.138	0.435	0.277	0.129	0.129	—	0.132	0.423	0.289	0.218†	0.139
22	0.819	1.716	0.130	0.421	0.286	0.124	0.124	—	0.125	0.446	0.316	0.280	0.129
23	0.838	1.815	0.126	0.398	0.284	0.121	0.120	—	0.121	0.410	0.289	0.293	0.219†
24	0.852	1.866	0.117	0.432	0.292	0.113	0.113	—	0.114	0.443	0.305	0.291	0.256
25	0.869	1.960	0.108	0.436	0.294	0.103	0.104	—	0.105	0.455	0.326	0.296	0.258
26	0.887	2.049	0.101	0.427	0.292	0.097	0.098	—	0.098	0.445	0.306	0.299	0.259
27	0.900	2.112	0.096	0.443	0.298	0.105	0.099	—	0.092	0.448	0.317	0.298	0.264
28	0.921	2.210	0.088	0.441	0.298	0.083	0.084	—	0.085	0.452	0.322	0.300	0.263
29	0.932	2.283	0.084	0.433	0.297	0.085†	0.081	—	0.082	0.473	0.318	0.296	0.264
30	0.949	2.379	0.081	0.443	0.300	0.173	0.077	—	0.078	0.452	0.328	0.309	0.267
31	0.965	2.471	0.168†	0.443	0.301	0.174	0.071	—	0.073	0.453	0.333	0.302	0.267
32	0.985	2.574	0.189	0.436	0.301	0.178	0.067	—	0.069	0.448	0.331	0.304	0.268

[a]Stagnation pressure p_t in psia; stagnation temperature T_{to} in °R.

†Flow separation occurred at this location.

Table B-2 (concluded).

Pressure tap number	Axial distance ratio x/L	Area ratio A/A^*	Static-to-stagnation pressure p/p_t for indicated test[a]										
			280 $p_t=55.1$ $T_{to}=1501$	263 $p_t=60.2$ $T_{to}=1536$	262 $p_t=75.2$ $T_{to}=1518$	269 $p_t=100.2$ $T_{to}=1511$	267 $p_t=134.8$ $T_{to}=1501$	268 $p_t=150.6$ $T_{to}=1484$	293 $p_t=30.0$ $T_{to}=2001$	294 $p_t=49.9$ $T_{to}=2000$	290 $p_t=75.2$ $T_{to}=1989$	296 $p_t=101.2$ $T_{to}=2001$	298 $p_t=125.8$ $T_{to}=2007$
1	0.107	7.001	—	0.996	0.996	0.996	0.996	0.997	0.997	0.996	0.997	0.996	0.997
2	0.222	4.691	0.991	0.991	0.991	0.991	0.991	0.991	0.992	0.991	0.991	0.991	0.992
3	0.3396	2.939	0.976	0.977	0.977	0.977	0.977	0.977	0.977	0.977	0.977	0.977	0.978
4	0.3401	2.924	0.976	0.977	0.977	0.977	0.977	0.977	0.977	0.977	0.977	0.977	0.977
5	0.395	2.255	0.961	0.957	0.958	0.958	0.957	0.958	0.958	0.957	0.958	0.958	0.958
6	0.455	1.631	0.908	0.908	0.910	0.908	0.908	0.908	0.909	0.909	0.909	0.909	0.910
7	0.460	1.561	0.900	0.900	0.901	0.900	0.899	0.900	0.901	0.901	0.900	0.901	0.901
8	0.506	1.235	0.789	0.788	0.789	0.788	0.788	0.788	0.791	0.795	0.791	0.792	0.791
9	0.529	1.135	0.730	0.728	0.731	0.729	0.728	0.728	0.731	0.735	0.732	0.732	0.732
10	0.554	1.054	0.646	0.637	0.638	0.645	0.648	0.647	0.644	0.648	0.649	0.647	0.649
11	0.587	1.0078	0.507	0.504	0.508	0.506	0.504	0.505	0.511	0.515	0.514	0.513	0.513
12	0.6018	1.0012	0.454	0.459	0.466	0.460	0.461	0.461	0.460	0.463	0.464	0.465	0.465
13	0.642	1.028	0.341	—	0.345	—	0.311	0.323	0.351	0.347	0.348	0.350	0.324
14	0.691	1.176	0.205	0.206	0.211	0.207	0.207	0.207	0.371†	0.210	0.214	0.215	0.215
15	0.706	1.231	0.198	0.198	0.203	0.199	0.199	0.199	0.331	0.202	0.204	0.207	0.207
16	0.722	1.297	0.188	0.188	0.194	0.189	0.190	0.190	0.407	0.193	0.189	0.193	0.190
17	0.741	1.372	0.174	0.175	0.180	0.176	0.176	0.176	0.407	0.180	0.181	0.183	0.182
18	0.753	1.423	0.171	0.166	0.171	0.167	0.167	0.167	0.381	0.170	0.172	0.174	0.173
19	0.771	1.505	0.158	0.157	—	0.158	0.159	0.159	0.425	0.162	0.162	0.165	0.165
20	0.789	1.582	0.145	0.142	0.148	0.144	0.144	0.145	0.419	0.145	0.146	0.148	0.149
21	0.802	1.642	0.138	0.134	0.140	0.134	0.136	0.132	0.407	0.136	0.138	0.139	0.139
22	0.819	1.716	0.129	0.127	0.133	0.129	0.128	0.128	0.432	0.135†	0.133	0.135	0.134
23	0.838	1.815	0.123	0.122	0.129	0.124	0.124	0.124	0.425	0.138	0.129	0.131	0.130
24	0.852	1.866	0.191†	0.114	0.120	0.116	0.116	0.116	0.431	0.130	0.118	0.121	0.121
25	0.869	1.960	0.205	0.105	0.111	0.107	0.107	0.108	0.443	0.229	0.120	0.112	0.111
26	0.887	2.049	0.236	0.116†	0.105	0.100	0.100	0.101	0.434	0.236	0.102	0.104	0.103
27	0.900	2.112	0.236	0.193	0.099	0.095	0.095	0.095	0.441	0.249	0.099	0.100	0.099
28	0.921	2.210	0.237	0.217	0.092	0.087	0.088	0.088	0.441	0.249	0.089	0.090	0.090
29	0.932	2.283	0.241	0.218	0.089	0.083	0.083	0.083	0.439	0.249	0.086	0.088	0.087
30	0.949	2.379	0.242	0.230	0.178†	—	—	—	0.447	0.257	0.083	0.084	0.083
31	0.965	2.471	0.243	0.223	0.166	0.074	0.073	0.074	0.449	0.260	0.081	0.077	0.077
32	0.985	2.574	0.244	0.225	0.179	0.067	0.069	0.069	0.444	0.262	0.166†	0.072	0.072

[a]Stagnation pressure p_t in psia; stagnation temperature T_{to} in °R.

†Flow separation occurred at this location.

Table B-3. Tabulation of heat-transfer data

z/L	q_w BTU/sec in.[2]	T_w °R	T_e °R	h $\frac{\text{BTU}}{\text{sec in.}^2\ °\text{F}}$	$\rho_e u_e$ $\frac{\text{lb}}{\text{sec in.}^2}$	$\frac{\rho_e u_e}{\mu_e}$ in.$^{-1}$	$St = \frac{h}{\rho_e u_e c_{p_e}}$
	Test 319. (l = 0 in., p_t = 35.9 psia, T_{t_o} = 1508°R, $\dot{m}$ = 1.212 lb/sec, θ = — in., δ^* = — in., ϕ = — in.)						
0.133	0.0773	690	1507	0.945 × 10^{-4}	0.0639	0.279 × 10^{5}	5.66 × 10^{-3}
0.204	—	—	1505	—	0.0854	0.400	—
0.276	0.0619	665	1502	0.735	0.110	0.536	2.58
0.336	—	—	1499	—	0.142	0.694	—
0.385	0.0792	663	1492	0.940	0.182	0.884	1.85
0.429	0.0858	658	1480	1.01	0.233	1.14	1.67
0.469	0.0911	665	1460	1.09	0.303	1.49	1.39
0.512	0.0989	669	1412	1.19	0.391	1.94	1.18
0.541	—	—	1370	—	0.428	2.19	—
0.573	0.0885	650	1300	1.06	0.455	2.38	0.899
0.603	0.0787	645	1230	0.944	0.452	2.44	0.816
0.634	0.0657	631	1155	0.782	0.425	2.39	0.728
0.664	0.0532	619	1080	0.632	0.391	2.26	0.647
0.693	0.0555	625	995	0.672	0.333	2.07	0.819
0.717	0.0463	628	†	†	†	†	†
0.750	0.0715	623	↓	↓	↓	↓	↓
0.782	0.0644	649	↓	↓	↓	↓	↓
0.825	0.0596	641	↓	↓	↓	↓	↓
0.864	0.0297	597	↓	↓	↓	↓	↓
0.864	0.0530	608	↓	↓	↓	↓	↓
0.905	0.0905	665	↓	↓	↓	↓	↓
0.938	0.0819	645	↓	↓	↓	↓	↓
	Test 318. (l = 0 in., p_t = 51.0 psia, T_{t_o} = 1509°R, $\dot{m}$ = 1.720 lb/sec, θ = — in., δ^* = — in., ϕ = — in.)						
0.133	0.0884	709	1508	1.11 × 10^{-4}	0.0903	0.395 × 10^{5}	4.68 × 10^{-3}
0.204	—	—	1505	—	0.122	0.568	—
0.276	0.0745	687	1503	0.906	0.156	0.762	2.23
0.336	—	—	1500	—	0.201	0.986	—
0.385	0.0918	686	1492	1.12	0.259	1.25	1.55
0.429	0.104	686	1480	1.27	0.331	1.62	1.48
0.469	0.117	702	1460	1.47	0.431	2.12	1.32
0.512	0.121	710	1412	1.53	0.556	2.75	1.06
0.541	—	—	1370	—	0.615	3.11	—
0.573	0.117	693	1300	1.47	0.646	3.39	0.879
0.603	0.143	718	1230	1.87	0.642	3.48	1.14
0.634	0.0971	678	1155	1.22	0.604	3.40	0.801
0.664	0.0757	660	1080	0.943	0.556	3.21	0.679
0.693	0.0992	686	995	1.29	0.472	2.95	1.11
0.717	0.0956	681	975	1.25	0.458	2.89	1.11
0.750	0.101	671	945	1.32	0.430	2.78	1.24
0.782	0.0875	691	905	1.18	0.396	2.67	1.22
0.825	0.0762	654	870	0.986	0.361	2.51	1.12
0.864	0.0755	650	†	†	†	†	†
0.864	0.110	665	↓	↓	↓	↓	↓
0.905	0.0711	642	↓	↓	↓	↓	↓
0.938	0.0453	603	↓	↓	↓	↓	↓

†Flow separation existed at this location.

Table B-3 (continued).

x/L	q_w BTU/sec in.^{2}	T_w °R	T_e °R	h $\frac{\text{BTU}}{\text{sec in.}^2\ \text{°F}}$	$\rho_e u_e$ $\frac{\text{lb}}{\text{sec in.}^2}$	$\frac{\rho_e u_e}{\mu_e}$ in.$^{-1}$	$St = \frac{h}{\rho_e u_e c_{p_e}}$
	Test 315. (l = 0 in., p_t = 74.6 psia, T_{t_o} = 1516°R, $\dot{m}$ = 2.538 lb/sec, θ = 0.014 in., δ^* = 0.020 in., $\phi \cong$ 0 in.)						
0.133	0.110	741	1515	1.42 × 10^{-4}	0.125	0.549 × 10^5	4.33 × 10^{-3}
0.204	—	—	1514	—	0.174	0.824	—
0.276	0.0995	729	1510	1.26	0.229	1.10	2.11
0.336	—	—	1505	—	0.299	1.43	—
0.385	0.131	747	1501	1.71	0.389	1.86	1.58
0.429	0.164	767	1489	2.20	0.504	2.41	1.69
0.469	0.200	825	1466	2.93	0.643	3.16	1.76
0.512	0.213	842	1420	3.21	0.844	4.07	1.47
0.541	—	—	1370	—	0.924	4.64	—
0.573	0.252	868	1302	4.03	0.962	5.04	1.62
0.603	0.235	861	1236	3.76	0.970	5.20	1.52
0.634	0.221	849	1155	3.52	0.910	5.11	1.53
0.664	0.189	826	1080	2.94	0.820	4.85	1.44
0.693	0.197	818	1005	3.07	0.722	4.47	1.72
0.717	0.191	807	988	2.95	0.702	4.38	1.71
0.750	0.187	778	960	2.79	0.660	4.24	1.67
0.782	0.157	777	930	2.36	0.622	4.07	1.55
0.825	0.159	755	885	2.35	0.566	3.83	1.70
0.864	0.142	757	850	2.11	0.521	3.59	1.67
0.864	0.170	740	850	2.46	0.521	3.59	1.94
0.905	0.115	720	815	1.64	0.465	3.34	1.46
0.938	0.125	682	792	1.70	0.424	3.08	1.68
	Test 317. (l = 0 in., p_t = 101.0 psia, T_{t_o} = 1510°R, $\dot{m}$ = 3.419 lb/sec, θ = 0.013 in., δ^* = 0.019 in., $\phi \cong$ 0 in.)						
0.133	0.123	783	1509	1.69 × 10^{-4}	0.174	0.736 × 10^5	3.73 × 10^{-3}
0.204	—	—	1507	—	0.236	1.10	—
0.276	0.124	777	1504	1.69	0.312	1.47	2.08
0.336	0.181	852	1501	2.75	0.403	1.92	2.64
0.385	0.186	836	1494	2.76	0.521	2.49	1.90
0.429	0.237	874	1480	3.75	0.666	3.21	2.16
0.469	0.262	929	1460	4.56	0.861	4.21	2.05
0.512	0.302	956	1410	5.56	1.12	5.47	1.91
0.541	—	—	1365	—	1.23	6.22	—
0.573	0.312	968	1300	6.01	1.29	6.76	1.80
0.603	0.271	941	1230	5.02	1.28	6.94	1.54
0.634	0.271	927	1150	4.96	1.21	6.82	1.62
0.664	0.240	903	1070	4.29	1.10	6.45	1.56
0.693	0.218	876	1000	3.76	0.952	5.95	1.60
0.717	0.227	866	980	3.90	0.916	5.80	1.73
0.750	0.221	831	950	3.62	0.868	5.61	1.65
0.782	0.184	831	920	3.05	0.812	5.37	1.53
0.825	0.188	802	880	3.00	0.743	5.05	1.66
0.864	0.171	807	850	2.78	0.680	4.74	1.68
0.864	0.200	787	850	3.15	0.680	4.74	1.90
0.905	0.135	761	810	2.05	0.618	4.46	1.37
0.938	0.156	719	785	2.26	0.576	4.15	1.62

Table B-3 (continued).

z/L	q_w BTU/sec in.^{2}	T_w °R	T_e °R	h $\frac{\text{BTU}}{\text{sec in.}^2\ \text{°F}}$	$\rho_e u_e$ $\frac{\text{lb}}{\text{sec in.}^2}$	$\frac{\rho_e u_e}{\mu_e}$ in.$^{-1}$	$St = \frac{h}{\rho_e u_e c_{p_e}}$
	Test 316. (l = 0 in., p_t = 124.4 psia, T_{t_o} = 1505°R, $\dot{m}$ = 4.224 lb/sec, θ = 0.014 in., δ^* = 0.020 in., $\phi \cong$ 0 in.)						
0.133	0.134	805	1504	1.91 × 10^{-4}	0.222	0.954 × 10^5	3.29 × 10^{-3}
0.204	—	—	1502	—	0.298	1.38	—
0.276	0.146	820	1499	2.14	0.375	1.83	2.19
0.336	0.192	902	1496	3.19	0.493	2.38	2.50
0.385	0.227	894	1490	3.74	0.653	3.10	2.05
0.429	0.271	925	1480	4.70	0.834	4.00	2.17
0.469	0.284	969	1455	5.36	1.07	5.24	1.94
0.512	0.318	992	1405	6.33	1.41	6.75	1.74
0.541	—	—	1360	—	1.53	7.71	—
0.573	0.329	992	1290	6.71	1.60	8.41	1.63
0.603	0.273	962	1220	5.32	1.57	8.60	1.33
0.634	0.268	945	1140	5.14	1.54	8.33	1.38
0.664	0.250	925	1060	4.70	1.33	7.88	1.42
0.693	0.233	900	1000	4.26	1.18	7.38	1.46
0.717	0.246	893	980	4.48	1.13	7.20	1.61
0.750	0.236	853	950	4.06	1.07	6.96	1.50
0.782	0.199	854	920	3.45	1.00	6.66	1.41
0.825	0.202	825	875	3.39	0.917	6.29	1.52
0.864	0.183	829	840	3.12	0.834	5.90	1.54
0.864	0.218	810	840	3.59	0.834	5.90	1.78
0.905	0.147	782	815	2.33	0.764	5.52	1.26
0.938	0.179	738	785	2.68	0.708	5.14	1.56
	Test 314. (l = 0 in., p_t = 151.7 psia, T_{t_o} = 1506°R, $\dot{m}$ = 5.182 lb/sec, θ = 0.015 in., δ^* = 0.022 in., $\phi \cong$ 0 in.)						
0.133	0.149	829	1505	2.21 × 10^{-4}	0.271	1.16 × 10^5	3.12 × 10^{-3}
0.204	0.153	824	1503	2.24	0.364	1.69	2.36
0.276	—	—	1500	—	0.457	2.24	—
0.336	0.190	951	1498	3.45	0.600	2.90	2.21
0.385	0.263	936	1490	4.64	0.796	3.77	2.08
0.429	0.299	965	1480	5.57	1.02	4.88	2.11
0.469	0.307	1009	1455	6.25	1.30	6.39	1.86
0.512	0.341	1034	1405	7.40	1.72	8.23	1.67
0.541	—	—	1360	—	1.86	9.40	—
0.573	0.352	1036	1290	7.89	1.95	10.3	1.57
0.603	0.293	1000	1220	6.15	1.91	10.5	1.26
0.634	0.288	982	1140	5.93	1.79	10.2	1.31
0.664	0.277	965	1060	5.62	1.63	9.60	1.39
0.693	0.248	931	1000	4.77	1.44	8.99	1.34
0.717	0.253	918	980	4.82	1.38	8.77	1.42
0.750	0.262	881	950	4.72	1.30	8.48	1.43
0.782	0.218	882	920	3.99	1.22	8.12	1.34
0.825	0.221	850	875	3.86	1.12	7.66	1.42
0.864	0.205	856	840	3.64	1.02	7.19	1.48
0.864	0.235	835	840	4.04	1.02	7.19	1.64
0.905	0.161	804	815	2.64	0.932	6.73	1.17
0.938	0.199	758	785	3.05	0.863	6.26	1.46

Table B-3 (continued).

x/L	q_w BTU/sec in.^{2}	T_w °R	T_e °R	h $\frac{\text{BTU}}{\text{sec in.}^2\ °\text{F}}$	$\rho_e u_e$ $\frac{\text{lb}}{\text{sec in.}^2}$	$\frac{\rho_e u_e}{\mu_e}$ in.$^{-1}$	$St = \frac{h}{\rho_e u_e c_{p_e}}$
	Test 312. (l = 0 in., p_t = 179.7 psia, T_{t_o} = 1467°R, $\dot{m}$ = 6.159 lb/sec, θ = 0.016 in., δ^* = 0.024 in., $\phi \cong$ 0 in.)						
0.133	0.163	858	1466	2.68 × 10^{-4}	0.321	1.38 × 10^5	3.20 × $^{-3}$
0.204	0.166	859	1464	2.73	0.431	2.00	2.43
0.276	0.200	908	1461	3.59	0.542	2.65	2.54
0.336	0.208	1006	1458	4.52	0.712	3.44	2.45
0.385	0.265	964	1452	5.29	0.942	4.47	2.01
0.429	0.321	1003	1443	6.96	1.20	5.78	2.23
0.469	0.321	1041	1418	7.63	1.54	7.56	1.91
0.512	0.352	1065	1369	8.99	2.04	9.75	1.71
0.541	—	—	1326	—	2.21	11.1	—
0.573	0.366	1063	1257	9.59	2.31	12.1	1.61
0.603	0.300	1026	1189	7.26	2.27	12.4	1.26
0.634	0.318	1026	1111	7.85	2.13	12.0	1.46
0.664	0.300	998	1033	7.08	1.93	11.4	1.48
0.693	0.250	954	975	5.46	1.71	10.6	1.30
0.717	0.276	951	955	6.06	1.63	10.4	1.50
0.750	0.279	907	926	5.67	1.55	10.0	1.45
0.782	0.231	904	897	4.72	1.45	9.62	1.34
0.825	0.238	873	853	4.64	1.32	9.08	1.44
0.864	0.216	883	819	4.34	1.20	8.54	1.48
0.864	0.249	861	819	4.79	1.20	8.54	1.64
0.905	0.183	828	794	3.34	1.10	7.97	1.25
0.938	0.208	782	765	3.52	1.02	7.40	1.42
	Test 313. (l = 0 in., p_t = 201.7 psia, T_{t_o} = 1517°R, $\dot{m}$ = 6.884 lb/sec, θ = 0.013 in., δ^* = 0.020 in., $\phi \cong$ 0 in.)						
0.133	0.179	886	1516	2.84 × 10^{-4}	0.360	1.55 × 10^5	3.02 × 10^{-3}
0.204	0.188	892	1514	3.02	0.484	2.24	2.39
0.276	0.225	940	1511	3.91	0.608	2.96	2.47
0.336	0.225	1044	1508	4.76	0.799	3.86	2.30
0.385	0.315	1010	1502	6.24	1.06	5.01	2.11
0.429	0.344	1038	1492	7.23	1.35	6.47	2.06
0.469	0.338	1080	1467	7.86	1.74	8.48	1.75
0.512	0.355	1105	1416	8.85	2.28	11.0	1.50
0.541	—	—	1371	—	2.48	12.5	—
0.573	0.373	1100	1300	9.46	2.59	13.6	1.42
0.603	0.321	1067	1230	7.64	2.54	13.9	1.18
0.634	0.347	1058	1149	8.25	2.39	13.5	1.37
0.664	0.320	1034	1068	7.34	2.16	12.8	1.37
0.693	0.280	996	1008	6.03	1.92	12.0	1.27
0.717	0.307	985	988	6.55	1.83	11.7	1.45
0.750	0.313	944	958	6.22	1.74	11.3	1.42
0.782	0.266	944	927	5.36	1.62	10.8	1.35
0.825	0.274	909	882	5.23	1.49	10.2	1.44
0.864	0.255	916	847	4.98	1.35	9.58	1.52
0.864	0.274	896	847	5.15	1.35	9.58	1.57
0.905	0.191	859	821	3.39	1.24	8.96	1.13
0.938	0.238	811	791	3.91	1.15	8.30	1.41

Table B-3 (continued).

z/L	q_w BTU/sec in.²	T_w °R	T_e °R	h BTU / sec in.² °F	$\rho_e u_e$ lb / sec in.²	$\rho_e u_e / \mu_e$ in.$^{-1}$	$St = \frac{h}{\rho_e u_e c_{p_e}}$
	Test 242. (l = 6 in., p_t = 45.0 psia, T_{to} = 1490°R, $\dot{m}$ = 1.549 lb/sec, θ = 0.023 in., δ^* = 0.018 in., ϕ = 0.018 in.)						
0.133	0.0707	626	1489	0.819×10^{-4}	0.0806	0.362×10^{5}	3.85×10^{-3}
0.204	0.0713	621	1487	0.821	0.111	0.530	2.80
0.276	0.0662	626	1484	0.767	0.141	0.680	2.09
0.336	—	—	1481	—	0.179	0.880	—
0.385	0.0873	629	1475	1.02	0.236	1.14	1.54
0.429	0.0838	624	1463	0.972	0.304	1.48	1.23
0.469	0.117	658	1445	1.42	0.392	1.94	1.40
0.512	0.128	673	1396	1.59	0.520	2.45	1.17
0.541	—	—	1346	—	0.564	2.86	—
0.573	0.113	656	1287	1.39	0.597	3.13	0.897
0.603	0.113	674	1227	1.44	0.592	3.22	0.948
0.634	0.155	697	1138	2.06	0.560	3.17	1.45
0.664	0.123	655	1059	1.57	0.515	2.99	1.22
0.693	0.109	661	980	1.41	0.437	2.75	1.30
0.717	0.124	664	970	1.63	0.422	2.67	1.56
0.750	0.132	647	940	1.70	0.401	2.59	1.68
0.782	0.108	643	911	1.40	0.376	2.48	1.52
0.825	0.0562	593	†	†	†	†	†
0.864	0.0460	583	↓	↓	↓	↓	↓
0.864	0.0204	552	↓	↓	↓	↓	↓
0.905	0.0397	568	↓	↓	↓	↓	↓
0.938	0.0104	533	↓	↓	↓	↓	↓
	Test 245. (l = 6 in., p_t = 60.2 psia, T_{to} = 1513°R, $\dot{m}$ = 2.042 lb/sec, θ = 0.028 in., δ^* = 0.024 in., ϕ = 0.021 in.)						
0.133	0.0838	654	1512	0.976×10^{-4}	0.118	0.516×10^{5}	3.13×10^{-3}
0.204	0.0846	645	1510	0.975	0.153	0.728	2.41
0.276	0.0793	654	1507	0.923	0.195	0.917	1.82
0.336	0.0880	668	1504	1.04	0.250	1.18	1.60
0.385	0.114	666	1498	1.35	0.320	1.13	1.51
0.429	0.119	672	1486	1.42	0.410	1.96	1.33
0.469	0.170	716	1460	2.15	0.521	2.55	1.59
0.512	0.167	734	1419	2.18	0.688	3.35	1.22
0.541	—	—	1370	—	0.750	3.78	—
0.573	0.206	747	1301	2.77	0.792	4.11	1.34
0.603	0.189	761	1232	2.62	0.785	4.24	1.30
0.634	0.197	753	1059	2.73	0.744	4.17	1.46
0.664	0.179	726	1025	2.43	0.674	3.94	1.45
0.693	0.169	734	1000	2.34	0.584	3.61	1.62
0.717	0.156	709	976	2.10	0.562	3.52	1.52
0.750	0.173	696	946	2.31	0.528	3.39	1.73
0.782	0.139	694	916	1.87	0.500	3.25	1.52
0.825	0.137	672	882	1.81	0.465	3.10	1.59
0.864	0.123	655	843	1.60	0.431	2.95	1.52
0.864	0.144	653	843	1.87	0.431	2.95	1.78
0.905	0.0809	615	†	†	†	†	†
0.938	0.0222	553	†	†	†	†	†

†Flow separation existed at this location.

Table B-3 (continued).

x/L	q_w BTU/sec in.^{2}	T_w °R	T_e °R	h $\frac{\text{BTU}}{\text{sec in.}^2\ \text{°F}}$	$\rho_e u_e$ $\frac{\text{lb}}{\text{sec in.}^2}$	$\frac{\rho_e u_e}{\mu_e}$ in.$^{-1}$	$St = \frac{h}{\rho_e u_e c_{p_e}}$
	Test 246. (l = 6 in., p_t = 75.2 psia, T_{t_0} = 1500°R, $\dot{m}$ = 2.567 lb/sec, θ = 0.027 in., δ^* = 0.221 in., ϕ = 0.020 in.)						
0.133	0.0960	669	1499	1.15 × 10^{-4}	0.132	0.590 × 10^5	3.30 × 10^{-3}
0.204	0.0960	659	1497	1.14	0.188	0.866	2.30
0.276	0.0942	674	1494	1.14	0.236	1.12	1.86
0.336	0.107	696	1491	1.33	0.298	1.41	1.72
0.385	0.151	708	1485	1.91	0.396	1.88	1.73
0.429	0.172	729	1473	2.24	0.507	2.45	1.70
0.469	0.239	781	1445	3.35	0.652	3.19	1.98
0.512	0.235	809	1405	3.45	0.868	4.23	1.53
0.541	—	—	1356	—	0.938	4.75	—
0.573	0.257	802	1288	3.81	0.986	5.16	1.49
0.603	0.228	812	1223	3.46	0.979	5.31	1.38
0.634	0.218	784	1143	3.21	0.924	5.21	1.37
0.664	0.205	758	1069	2.95	0.848	4.93	1.39
0.693	0.188	760	995	2.75	0.729	4.54	1.52
0.717	0.178	730	978	2.51	0.702	4.43	1.45
0.750	0.192	715	950	2.68	0.666	4.27	1.59
0.782	0.152	713	920	2.13	0.625	4.10	1.39
0.825	0.154	691	876	2.12	0.570	3.87	1.52
0.864	0.135	683	841	1.85	0.521	3.63	1.46
0.864	0.164	682	841	2.25	0.521	3.63	1.78
0.905	0.132	668	807	1.79	0.472	3.38	1.55
0.938	0.0954	611	†	†	†	†	†
	Test 237. (l = 12 in., p_t = 45.2 psia, T_{t_0} = 1531°R, $\dot{m}$ = 1.514 lb/sec, θ = 0.046 in., δ^* = 0.029 in., ϕ = 0.043 in.)						
0.133	0.0665	614	1530	0.726 × 10^{-4}	—	—	—
0.204	0.0661	609	1528	0.717	0.0868	0.395 × 10^5	3.11 × 10^{-3}
0.276	0.0665	620	1525	0.731	0.125	0.593	2.21
0.336	0.0680	621	1522	0.748	0.172	0.810	1.64
0.385	0.101	625	1516	1.11	0.226	1.07	1.86
0.429	0.0991	638	1504	1.12	0.288	1.54	1.47
0.469	0.114	637	1482	1.29	0.372	1.87	1.31
0.512	0.116	650	1431	1.33	0.514	2.50	0.985
0.541	—	—	1390	—	0.564	2.81	—
0.573	0.103	635	1319	1.17	0.595	3.09	0.760
0.603	0.0948	639	1248	1.10	0.592	3.16	0.721
0.634	—	—	1161	—	0.558	3.12	—
0.664	0.102	638	1075	1.20	0.514	2.95	0.921
0.693	0.0890	631	1019	1.06	0.443	2.70	0.949
0.717	0.129	657	988	1.60	0.427	2.64	1.50
0.750	0.117	631	963	1.41	0.403	2.55	1.41
0.782	0.0925	625	937	1.12	0.382	2.47	1.19
0.825	0.0727	592	†	†	†	†	†
0.864	0.0214	557	↓	↓	↓	↓	↓
0.864	0.0558	571	↓	↓	↓	↓	↓
0.905	0.0476	572	↓	↓	↓	↓	↓
0.938	0.0142	529	↓	↓	↓	↓	↓

†Flow separation existed at this location.

Table B-3 (continued).

z/L	q_w BTU/sec in.^{2}	T_w °R	T_e °R	h BTU/(sec in.^{2} °F)	$\rho_e u_e$ lb/(sec in.^{2})	$\rho_e u_e/\mu_e$ in.$^{-1}$	$St = \frac{h}{\rho_e u_e c_{p_e}}$
	Test 235. (l = 12 in., p_t = 60.2 psia, T_{t_0} = 1545°R, $\dot{m}$ = 2.007 lb/sec, θ = 0.050 in., δ^* = 0.032 in., ϕ = 0.044 in.)						
0.133	0.0790	625	1544	0.859 × 10^{-4}	—	—	—
0.204	0.0838	623	1542	0.911	0.132	0.580 × 10^{5}	2.60 × 10^{-3}
0.276	0.0836	640	1539	0.924	0.174	0.818	2.04
0.336	0.0868	640	1536	0.961	0.236	1.12	1.57
0.385	0.119	653	1530	1.34	0.313	1.45	1.53
0.429	0.126	665	1517	1.44	0.403	1.90	1.38
0.469	0.179	699	1492	2.13	0.528	2.51	1.56
0.512	0.177	718	1449	2.16	0.688	3.34	1.21
0.541	—	—	1399	—	0.750	3.73	—
0.573	0.203	727	1329	2.56	0.792	4.04	1.25
0.603	0.190	737	1258	2.45	0.785	4.19	1.22
0.634	0.213	749	1082	2.81	0.743	4.13	1.51
0.664	0.186	711	1047	2.36	0.674	3.89	1.41
0.693	0.170	717	1022	2.21	0.590	3.59	1.51
0.717	0.170	701	996	2.18	0.570	3.49	1.55
0.750	0.169	677	966	2.12	0.535	3.36	1.57
0.782	0.145	683	936	1.85	0.500	3.20	1.51
0.825	0.153	668	901	1.93	0.451	3.02	1.74
0.864	0.118	644	861	1.46	0.403	2.85	1.48
0.864	0.147	642	861	1.81	0.403	2.85	1.20
0.905	0.129	630	†	†	†	†	†
0.938	0.207	543	†	†	†	†	†
	Test 234. (l = 12 in., p_t = 75.2 psia, T_{t_0} = 1527°R, $\dot{m}$ = 2.555 lb/sec, θ = 0.048 in., δ^* = 0.037 in., ϕ = 0.035 in.)						
0.133	0.0902	642	1526	1.02 × 10^{-4}	—	—	—
0.204	0.0895	637	1524	1.01	0.156	0.648 × 10^{5}	2.44 × 10^{-3}
0.276	0.0975	661	1521	1.13	0.215	1.01	2.01
0.336	0.107	672	1518	1.26	0.285	1.34	1.70
0.385	0.150	687	1512	1.80	0.382	1.81	1.69
0.429	0.170	708	1500	2.08	0.493	2.37	1.63
0.469	0.248	764	1470	3.27	0.653	3.13	1.94
0.512	0.243	788	1430	3.34	0.861	4.17	1.49
0.541	—	—	1380	—	0.938	4.67	—
0.573	0.273	792	1311	3.83	0.972	5.11	1.52
0.603	0.241	798	1245	3.44	0.972	5.24	1.38
0.634	0.235	780	1163	3.32	0.924	5.14	1.42
0.664	0.224	749	1088	3.07	0.834	4.85	1.47
0.693	0.205	752	1012	2.85	0.736	4.49	1.56
0.717	0.193	726	995	2.62	0.702	4.38	1.51
0.750	0.194	700	967	2.57	0.660	4.22	1.54
0.782	0.163	703	937	2.18	0.618	4.03	1.44
0.825	0.164	683	891	2.17	0.562	3.79	1.58
0.864	0.141	672	856	1.84	0.521	3.57	1.45
0.864	0.159	666	856	2.06	0.521	3.57	1.62
0.905	0.138	660	821	1.78	0.472	3.45	1.55
0.938	0.112	611	798	1.37	0.437	3.11	1.29

†Flow separation existed at this location.

Table B-3 (continued).

z/L	q_w BTU/sec in.^{2}	T_w °R	T_e °R	h $\frac{\text{BTU}}{\text{sec in.}^2\ \text{°F}}$	$\rho_e u_e$ $\frac{\text{lb}}{\text{sec in.}^2}$	$\frac{\rho_e u_e}{\mu_e}$ in.$^{-1}$	$St = \frac{h}{\rho_e u_e c_{p_e}}$
	Test 300. (l = 18 in., p_t = 30.0 psia, T_{t_o} = 1039°R, $\dot{m}$ = 1.233 lb/sec, θ = 0.056 in., δ^* = 0.037 in., ϕ = 0.062 in.)						
0.133	0.0264	580	1038	0.576 × 10^{-4}	0.0798	0.470 × 10^5	2.89 × 10^{-3}
0.204	0.0282	580	1037	0.615	0.0958	0.567	2.57
0.276	0.0271	580	1035	0.592	0.120	0.732	1.99
0.336	0.0293	590	1033	0.655	0.156	0.935	1.69
0.385	0.0339	583	1028	0.746	0.201	1.21	1.49
0.429	0.0391	582	1021	0.863	0.256	1.57	1.35
0.469	0.0413	588	1005	0.926	0.324	2.02	1.15
0.512	0.0438	591	973	0.995	0.422	2.64	0.950
0.541	—	—	941	—	0.464	3.00	—
0.573	0.0415	580	896	0.938	0.486	3.29	0.785
0.603	0.0521	593	841	1.23	0.478	3.38	1.05
0.634	0.0273	571	799	0.619	0.453	3.34	0.560
0.664	0.0275	575	†	†	†	†	†
0.693	0.0312	584					
0.717	0.0427	588					
0.750	0.0771	606					
0.782	0.0645	610					
0.825	0.0241	576					
0.864	0.0567	619					
0.864	0.0531	590					
0.905	0.0529	609					
0.938	0.0335	568					
	Test 301. (l = 18 in., p_t = 45.1 psia, T_{t_o} = 1035°R, $\dot{m}$ = 1.888 lb/sec, θ = — in., δ^* = — in., ϕ = — in.)						
0.133	0.0321	593	1034	0.727 × 10^{-4}	0.111	0.672 × 10^5	2.62 × 10^{-3}
0.204	0.0346	594	1033	0.786	0.135	0.826	2.32
0.276	0.0305	595	1031	0.692	0.177	1.07	1.57
0.336	0.0368	611	1029	0.871	0.229	1.40	1.52
0.385	0.0487	607	1024	1.14	0.292	1.80	1.57
0.429	0.0621	611	1015	1.48	0.379	2.33	1.56
0.469	0.0735	631	1000	1.84	0.490	3.06	1.51
0.512	0.0698	636	967	1.79	0.642	4.02	1.12
0.541	—	—	937	—	0.703	4.57	—
0.573	0.101	645	893	2.69	0.734	4.99	1.49
0.603	0.0848	642	847	2.28	0.722	5.14	1.29
0.634	0.0809	632	792	2.15	0.684	5.08	1.29
0.664	0.0684	624	734	1.81	0.627	4.80	1.19
0.693	0.0633	620	678	1.69	0.540	4.45	1.30
0.717	0.0665	615	668	1.77	0.522	4.35	1.40
0.750	0.0634	602	648	1.65	0.490	4.22	1.40
0.782	0.0552	592	†	†	†	†	†
0.825	0.0268	567					
0.864	0.0138	555					
0.864	0.0142	543					
0.905	0.00784	538					
0.938	0.00390	528					

†Flow separation existed at this location.

Table B-3 (continued).

z/L	q_w BTU/sec in.^{2}	T_w °R	T_e °R	h $\frac{\text{BTU}}{\text{sec in.}^2\ \text{°F}}$	$\rho_e u_e$ $\frac{\text{lb}}{\text{sec in.}^2}$	$\frac{\rho_e u_e}{\mu_e}$ in.$^{-1}$	$St = \frac{h}{\rho_e u_e c_{p_e}}$
	Test 303. (l = 18 in., p_t = 75.2 psia, T_{t_0} = 1024°R, $\dot{m}$ = 3.142 lb/sec, θ = 0.048 in., δ^* = 0.038 in., ϕ = 0.045 in.)						
0.133	0.0424	618	1023	1.04 × 10^{-4}	0.188	1.14 × 10^5	2.23 × 10^{-3}
0.204	0.0425	623	1022	1.06	0.226	1.38	1.88
0.276	0.0459	632	1020	1.17	0.292	1.78	1.61
0.336	0.0544	661	1018	1.50	0.382	2.34	1.58
0.385	0.0829	665	1013	2.31	0.490	3.06	1.90
0.429	0.106	680	1006	3.09	0.649	3.94	1.95
0.469	0.115	701	992	3.60	0.816	5.13	1.77
0.512	0.139	715	956	4.60	1.06	6.78	1.75
0.541	—	—	925	—	1.16	7.60	—
0.573	0.142	711	882	4.77	1.22	8.36	1.59
0.603	0.110	699	834	3.53	1.21	8.62	1.19
0.634	0.106	683	782	3.37	1.14	8.52	1.22
0.664	0.100	679	729	3.20	1.04	8.10	1.27
0.693	0.0840	660	677	2.58	0.910	7.50	1.18
0.717	0.0866	651	662	2.63	0.875	7.36	1.25
0.750	0.0856	640	642	2.55	0.826	7.08	1.28
0.782	0.0758	639	624	2.27	0.770	6.77	1.23
0.825	0.0709	621	597	2.05	0.702	6.38	1.22
0.864	0.0693	628	573	2.06	0.642	6.03	1.34
0.864	0.0863	623	573	2.53	0.642	6.03	1.64
0.905	0.0553	600	551	1.53	0.590	5.73	1.08
0.938	0.0532	577	†	†	†	†	†
	Test 304. (l = 18 in., p_t = 100.8 psia, T_{t_0} = 1036°R, $\dot{m}$ = 4.207 lb/sec, θ = 0.047 in., δ^* = 0.038 in., ϕ = 0.044 in.)						
0.133	0.0524	643	1035	1.33 × 10^{-4}	0.253	1.49 × 10^5	2.11 × 10^{-3}
0.204	0.0537	650	1034	1.39	0.302	1.82	1.85
0.276	0.0624	668	1032	1.70	0.382	2.36	1.78
0.336	0.0746	708	1030	2.28	0.507	3.08	1.80
0.385	0.108	704	1025	3.27	0.660	4.02	1.99
0.429	0.133	721	1016	4.26	0.848	5.24	2.02
0.469	0.138	741	1002	4.72	1.09	6.79	1.74
0.512	0.166	754	972	6.06	1.43	8.95	1.71
0.541	—	—	940	—	1.55	10.1	—
0.573	0.171	750	893	6.32	1.63	11.0	1.58
0.603	0.132	726	848	4.58	1.62	11.4	1.15
0.634	0.132	719	792	4.54	1.52	11.3	1.23
0.664	0.121	714	738	4.15	1.38	10.7	1.24
0.693	0.0999	689	685	3.25	1.21	9.92	1.12
0.717	0.102	688	670	3.35	1.16	9.68	1.19
0.750	0.101	676	650	3.24	1.10	9.37	1.22
0.782	0.0868	672	630	2.79	1.04	9.02	1.12
0.825	0.0839	655	605	2.60	0.945	8.54	1.15
0.864	0.0870	668	582	2.84	0.865	8.07	1.37
0.864	0.0960	661	582	3.06	0.865	8.07	1.47
0.905	0.0672	637	558	2.01	0.792	7.59	1.06
0.938	0.0700	619	540	2.01	0.736	7.07	1.14

†Flow separation existed at this location.

Table B-3 (continued).

z/L	q_w BTU/sec in.^{2}	T_w °R	T_e °R	h $\frac{\text{BTU}}{\text{sec in.}^2\ °\text{F}}$	$\rho_e u_e$ $\frac{\text{lb}}{\text{sec in.}^2}$	$\frac{\rho_e u_e}{\mu_e}$ in.$^{-1}$	$St = \frac{h}{\rho_e u_e c_{p_e}}$
	Test 305. (l = 18 in., p_t = 125.6 psia, T_{to} = 1032°R, $\dot{m}$ = 5.053 lb/sec, θ = 0.045 in., δ^* = 0.039 in., ϕ = 0.039 in.)						
0.133	0.0592	653	1031	1.57 × 10^{-4}	0.307	1.85 × 10^5	2.05 × 10^{-3}
0.204	0.0659	666	1030	1.81	0.371	2.26	1.95
0.276	0.0802	689	1028	2.35	0.483	2.92	1.95
0.336	0.0937	732	1026	3.14	0.631	3.83	2.00
0.385	0.123	722	1022	4.01	0.822	5.02	1.96
0.429	0.150	736	1014	5.13	1.05	6.51	1.96
0.469	0.152	756	998	5.60	1.36	8.49	1.68
0.512	0.176	768	964	6.87	1.76	11.2	1.58
0.541	—	—	934	—	1.93	12.7	—
0.573	0.180	764	890	7.17	2.02	13.8	1.44
0.603	0.148	741	840	5.49	2.01	14.2	1.12
0.634	0.139	731	778	5.09	1.86	13.9	1.12
0.664	0.133	725	720	4.87	1.66	13.2	1.21
0.693	0.111	702	683	3.83	1.51	12.4	1.06
0.717	0.115	699	668	3.98	1.45	12.1	1.14
0.750	0.101	684	644	3.66	1.36	11.6	1.12
0.782	0.0968	681	627	3.25	1.22	11.2	1.06
0.825	0.0917	663	602	2.96	1.17	10.6	1.05
0.864	0.0905	674	579	3.05	1.08	10.0	1.18
0.864	0.115	670	579	3.81	1.08	10.0	1.47
0.905	0.0750	645	554	2.33	0.984	9.40	0.986
0.938	0.0836	625	537	2.46 ↓	0.926	8.80 ↓	1.11 ↓
	Test 306. (l = 18 in., p_t = 150.6 psia, T_{to} = 1028°R, $\dot{m}$ = 6.300 lb/sec, θ = 0.045 in., δ^* = 0.040 in., ϕ = 0.035 in.)						
0.133	0.0635	670	1027	1.78 × 10^{-4}	0.368	2.22 × 10^5	1.94 × 10^{-3}
0.204	0.0753	684	1026	2.19	0.444	2.71	1.98
0.276	0.0930	710	1024	2.93	0.580	3.50	2.03
0.336	0.0986	756	1022	3.64	0.757	4.60	1.93
0.385	0.132	742	1018	4.65	0.986	6.02	1.90
0.429	0.158	756	1010	5.88	1.21	7.80	1.87
0.469	0.160	777	994	6.52	1.63	10.2	1.61
0.512	0.185	788	960	7.96	2.11	13.5	1.52
0.541	—	—	930	—	2.31	15.2	—
0.573	0.190	786	887	8.42	2.42	16.7	1.42
0.603	0.156	760	837	6.31	2.41	17.1	1.07
0.634	0.152	752	775	6.10	2.24	16.7	1.12
0.664	0.147	746	717	5.91	1.99	15.8	1.23
0.693	0.121	721	680	4.52	1.81	14.8	1.04
0.717	0.123	717	665	4.61	1.74	14.5	1.10
0.750	0.124	705	642	4.49	1.63	14.0	1.14
0.782	0.108	702	625	3.94	1.53	13.4	1.07
0.825	0.105	685	600	3.70	1.40	12.7	1.10
0.864	0.106	701	577	3.99	1.29	12.0	1.29
0.864	0.120	691	577	4.35	1.29	12.0	1.40
0.905	0.0828	665	552	2.77	1.18	11.3	0.977
0.938	0.0929	642	535	2.92 ↓	1.11	10.5 ↓	1.09 ↓

Table B-3 (continued).

z/L	q_w BTU/sec in.^{2}	T_w °R	T_e °R	h $\frac{\text{BTU}}{\text{sec in.}^2\ \text{°F}}$	$\rho_e u_e$ $\frac{\text{lb}}{\text{sec in.}^2}$	$\frac{\rho_e u_e}{\mu_e}$ in.$^{-1}$	$St = \frac{h}{\rho_e u_e c_{p_e}}$
	Test 308. (l = 18 in., p_t = 175.8 psia, T_{t_0} = 1035°R, $\dot{m}$ = 7.728 lb/sec, θ = 0.041 in., δ^* = 0.033 in., ϕ = 0.037 in.)						
0.133	0.0731	686	1034	2.10 × 10^{-4}	0.430	2.59 × 10^5	1.96 × 10^{-3}
0.204	0.0897	706	1033	2.73	0.519	3.16	2.11
0.276	0.105	732	1031	3.49	0.676	4.09	2.07
0.336	0.107	776	1029	4.16	0.883	5.37	1.89
0.385	0.143	760	1025	5.22	1.15	7.03	1.82
0.429	0.153	768	1017	5.77	1.48	9.10	1.57
0.469	0.171	794	1001	7.24	1.90	11.9	1.54
0.512	0.187	801	967	8.26	2.46	15.7	1.35
0.541	—	—	936	—	2.70	17.7	—
0.573	0.201	801	893	9.26	2.83	19.3	1.33
0.603	0.162	775	843	6.80	2.81	19.9	0.991
0.634	0.165	769	780	6.90	2.61	19.5	1.09
0.664	0.154	760	722	6.38	2.33	18.4	1.14
0.693	0.131	735	685	5.05	2.11	17.3	0.993
0.717	0.138	731	670	5.32	2.03	16.9	1.09
0.750	0.138	715	646	5.08	1.91	16.3	1.11
0.782	0.116	712	629	4.29	1.78	15.6	1.00
0.825	0.120	695	604	4.28	1.64	14.8	1.09
0.864	0.113	708	581	4.25	1.51	14.0	1.17
0.864	0.133	701	581	4.89	1.51	14.0	1.35
0.905	0.0904	673	556	3.04	1.38	13.2	0.921
0.938	0.0966	648	539	3.03	1.30	12.3	0.974
	Test 309. (l = 18 in., p_t = 201.7 psia, T_{t_0} = 1029°R, $\dot{m}$ = 8.567 lb/sec, θ = 0.038 in., δ^* = 0.035 in., ϕ = 0.029 in.)						
0.133	0.0786	702	1028	2.41 × 10^{-4}	0.493	2.96 × 10^5	1.96 × 10^{-3}
0.204	0.0990	725	1027	3.26	0.595	3.63	2.20
0.276	0.110	750	1025	3.96	0.776	4.68	2.05
0.336	0.113	795	1023	4.85	1.01	6.14	1.92
0.385	0.144	775	1019	5.71	1.32	8.08	1.74
0.429	0.177	791	1011	7.50	1.69	10.4	1.78
0.469	0.177	809	995	8.22	2.17	13.6	1.52
0.512	0.197	816	961	9.59	2.83	18.0	1.37
0.541	—	—	931	—	3.10	20.3	—
0.573	0.206	813	881	10.3	3.24	22.1	1.30
0.603	0.168	786	838	7.54	3.22	22.8	0.957
0.634	0.166	780	776	7.42	2.99	22.3	1.02
0.664	0.160	774	718	7.19	2.67	21.1	1.12
0.693	0.133	746	681	5.46	2.42	19.8	0.937
0.717	0.144	748	666	6.08	2.33	19.4	1.08
0.750	0.142	730	643	5.67	2.19	18.7	1.08
0.782	0.119	724	626	4.70	2.04	17.9	0.956
0.825	0.122	708	601	4.63	1.88	17.0	1.03
0.864	0.121	723	578	4.95	1.73	16.0	1.19
0.864	0.143	719	578	5.71	1.73	16.0	1.38
0.905	0.117	694	553	4.32	1.58	15.1	1.14
0.938	0.106	662	536	3.55	1.49	14.1	0.995

Table B-3 (continued).

z/L	q_w BTU/sec in.^{2}	T_w °R	T_e °R	h BTU/sec in.^{2} °F	$\rho_e u_e$ lb/sec in.^{2}	$\rho_e u_e / \mu_e$ in.$^{-1}$	$St = h / \rho_e u_e c_{p_e}$
	Test 310. (l = 18 in., p_t = 226.7 psia, T_{t_o} = 1032°R, $\dot{m}$ = 9.516 lb/sec, θ = 0.038 in., δ^* = 0.031 in., ϕ = 0.035 in.)						
0.133	0.0872	716	1031	2.77 × 10^{-4}	0.554	3.34 × 10^5	2.00 × 10^{-3}
0.204	0.106	739	1030	3.65	0.668	4.10	2.19
0.276	0.115	764	1028	4.30	0.875	5.28	1.97
0.336	0.117	808	1026	5.23	1.14	6.91	1.84
0.385	0.152	789	1022	6.32	1.49	9.05	1.71
0.429	0.185	804	1014	8.20	1.90	11.7	1.73
0.469	0.180	822	998	8.76	2.45	15.3	1.44
0.512	0.203	829	964	10.4	3.18	20.2	1.32
0.541	—	—	934	—	3.48	22.8	—
0.573	0.209	828	890	11.2	3.65	24.9	1.25
0.603	0.173	800	840	8.24	3.62	25.7	0.932
0.634	0.172	795	778	8.20	3.37	25.1	1.00
0.664	0.164	788	720	7.79	3.00	23.7	1.07
0.693	0.138	760	683	5.93	2.71	22.3	0.905
0.717	0.148	760	668	6.51	2.61	21.8	1.03
0.750	0.147	743	644	6.14	2.46	21.0	1.04
0.782	0.125	737	627	5.17	2.30	20.2	0.934
0.825	0.131	723	602	5.21	2.11	19.1	1.03
0.864	0.125	737	579	5.34	1.95	18.0	1.14
0.864	0.152	730	579	6.30	1.95	18.0	1.35
0.905	0.103	701	554	3.85	1.78	17.0	0.902
0.938	0.121	675	537	4.18	1.67	15.8	1.04
	Test 311. (l = 18 in., p_t = 253.7 psia, T_{t_o} = 1030°R, $\dot{m}$ = 10.411 lb/sec, θ = 0.039 in., δ^* = 0.034 in., ϕ = 0.031 in.)						
0.133	0.0985	732	1029	3.30 × 10^{-4}	0.619	3.73 × 10^5	2.14 × 10^{-3}
0.204	0.113	754	1028	4.08	0.750	4.57	2.18
0.276	0.120	777	1026	4.76	0.979	5.90	1.95
0.336	0.123	819	1024	5.86	1.28	7.74	1.84
0.385	0.156	803	1020	6.91	1.66	10.1	1.67
0.429	0.188	816	1012	8.90	2.12	13.1	1.68
0.469	0.187	834	996	9.71	2.73	17.1	1.43
0.512	0.207	841	962	11.4	3.55	22.6	1.29
0.541	—	—	932	—	3.89	25.5	—
0.573	0.209	833	889	11.5	4.08	27.8	1.15
0.603	0.173	809	839	8.63	4.05	28.7	0.871
0.634	0.172	802	777	8.51	3.76	28.1	0.931
0.664	0.169	797	719	8.42	3.35	26.6	1.04
0.693	0.141	771	682	6.43	3.04	25.0	0.877
0.717	0.154	776	667	7.30	2.92	24.4	1.04
0.750	0.155	758	643	6.93	2.75	23.5	1.05
0.782	0.130	752	626	5.77	2.57	22.6	0.935
0.825	0.137	738	601	5.84	2.36	21.4	1.03
0.864	0.130	749	578	5.93	2.17	20.2	1.14
0.864	0.163	745	578	7.28	2.17	20.2	1.39
0.905	0.115	718	553	4.64	1.99	19.0	0.973
0.938	0.121	688	536	4.38	1.87	17.7	0.977

Table B-3 (continued).

x/L	q_w BTU/sec in.^{2}	T_w °R	T_e °R	h $\frac{\text{BTU}}{\text{sec in.}^2\ \text{°F}}$	$\rho_e u_e$ $\frac{\text{lb}}{\text{sec in.}^2}$	$\frac{\rho_e u_e}{\mu_e}$ in.$^{-1}$	$St = \frac{h}{\rho_e u_e c_{p_e}}$
	Test 288. (l = 18 in., p_t = 30.1 psia, T_{t_o} = 1511°R, $\dot{m}$ = 1.009 lb/sec, θ = — in., δ^* = — in., ϕ = — in.)						
0.133	—	—	—	—	—	—	—
0.204	0.0509	622	1508	0.572×10^{-4}	0.0764	0.350×10^{5}	2.87×10^{-3}
0.276	0.0569	640	1506	0.654	0.0930	0.438	2.70
0.336	0.0595	650	1502	0.692	0.123	0.578	2.20
0.385	0.0637	630	1496	0.725	0.156	0.758	1.66
0.429	0.0750	635	1485	0.860	0.204	0.972	1.63
0.469	0.0811	644	1465	0.943	0.259	1.28	1.41
0.512	—	—	1415	—	0.337	1.65	—
0.541	—	—	1370	—	0.371	1.87	—
0.573	0.0800	634	1310	0.937	0.386	2.02	0.938
0.603	0.0733	625	1235	0.856	0.382	2.07	0.876
0.634	0.0648	624	1165	0.763	0.361	2.02	0.833
0.664	0.0532	624	1100	0.634	0.337	1.95	0.750
0.693	0.0531	625	†	†	†	†	†
0.717	0.0460	602					
0.750	0.0742	602					
0.782	0.0267	715					
0.825	0.0199	725					
0.864	0.0150	701					
0.864	—	581					
0.905	0.0543	671					
0.938	0.0229	548					
	Test 287. (l = 18 in., p_t = 40.2 psia, T_{t_o} = 1508°R, $\dot{m}$ = 1.357 lb/sec, θ = — in., δ^* = — in., ϕ = — in.)						
0.133	0.0634	651	1507	0.739×10^{-4}	0.0858	0.307×10^{5}	3.39×10^{-3}
0.204	0.0584	636	1505	0.669	0.102	0.410	2.51
0.276	0.0670	656	1502	0.786	0.125	0.576	2.67
0.336	0.0664	668	1499	0.792	0.160	0.771	1.91
0.385	0.0739	643	1493	0.856	0.208	0.992	1.47
0.429	0.0910	654	1480	1.064	0.268	1.28	1.53
0.469	0.0990	665	1460	1.182	0.345	1.69	1.32
0.512	0.104	666	1410	1.251	0.455	2.20	1.06
0.541	—	—	1370	—	0.495	2.49	—
0.573	0.103	660	1305	1.251	0.514	2.72	0.942
0.603	0.110	659	1240	1.338	0.514	2.79	1.02
0.634	0.0849	648	1160	1.031	0.489	2.75	0.834
0.664	0.0755	639	1070	0.918	0.445	2.58	0.828
0.693	0.0587	625	1000	0.710	0.385	2.36	0.746
0.717	0.0956	662	975	1.219	0.368	2.32	1.35
0.750	0.0730	635	950	0.907	0.351	2.24	1.02
0.782	0.0813	639	†	†	†	†	†
0.825	0.0814	631					
0.864	0.0532	609					
0.864	0.0772	621					
0.905	0.0694	617					
0.938	0.0204	548					

†Flow separation existed at this location.

Table B-3 (continued).

x/L	q_w BTU/sec in.^{2}	T_w °R	T_e °R	h $\frac{\text{BTU}}{\text{sec in.}^2\ \text{°F}}$	$\rho_e u_e$ $\frac{\text{lb}}{\text{sec in.}^2}$	$\frac{\rho_e u_e}{\mu_e}$ in.$^{-1}$	$St = \frac{h}{\rho_e u_e c_{p_e}}$
	Test 266. (l = 18 in., p_t = 44.8 psia, T_{t_0} = 1503°R, $\dot{m}$ = 1.555 lb/sec, θ = 0.070 in., δ^* = 0.060 in., ϕ = 0.043 in.)						
0.133	0.0652	636	1502	0.752 × 10^{-4}	0.0834	0.362 × 10^5	3.45 × 10^{-3}
0.204	0.0653	631	1500	0.749	0.109	0.493	2.63
0.276	0.0544	630	1497	0.623	0.142	0.678	1.68
0.336	0.0688	658	1494	0.816	0.182	0.884	1.73
0.385	0.0803	639	1490	0.932	0.234	1.12	1.42
0.429	0.0778	636	1480	0.901	0.304	1.48	1.14
0.469	0.104	659	1455	1.24	0.390	1.91	1.22
0.512	0.109	673	1405	1.33	0.503	2.45	1.03
0.541	—	—	1365	—	0.554	2.81	—
0.573	0.120	668	1295	1.49	0.580	3.02	0.990
0.603	0.0930	660	1225	1.14	0.576	3.13	0.779
0.634	0.128	678	1140	1.62	0.548	3.08	1.17
0.664	0.0804	638	1055	0.981	0.465	2.87	0.848
0.693	0.0894	653	1000	1.13	0.430	2.62	1.06
0.717	0.113	672	970	1.47	0.413	2.53	1.43
0.750	0.127	663	945	1.65	0.389	2.43	1.72
0.782	0.0821	642	920	1.04	0.368	2.33	1.14
0.825	—	—	†	†	†	†	†
0.864	0.0574	606					
0.864	0.0420	581					
0.905	0.0250	565					
0.938	0.0143	540					
	Test 281. (l = 18 in., p_t = 50.1 psia, T_{t_0} = 1514°R, $\dot{m}$ = 1.693 lb/sec, θ = — in., δ^* = — in., ϕ = — in.)						
0.133	0.0716	662	1513	0.841 × 10^{-4}	0.0972	0.428 × 10^5	3.31 × 10^{-3}
0.204	0.0695	650	1511	0.805	0.118	0.580	2.61
0.276	0.0763	671	1508	0.905	0.153	0.740	2.28
0.336	0.0761	683	1505	0.918	0.201	0.964	1.76
0.385	0.0868	661	1499	1.02	0.257	1.25	1.42
0.429	0.108	682	1487	1.30	0.330	1.63	1.51
0.469	0.123	699	1464	1.53	0.420	2.14	1.40
0.512	0.129	709	1425	1.62	0.579	2.81	1.08
0.541	—	—	1385	—	0.625	3.16	—
0.573	0.165	731	1320	2.17	0.649	3.40	1.29
0.603	0.158	720	1240	2.07	0.646	3.49	1.25
0.634	0.157	737	1165	2.12	0.618	3.44	1.35
0.664	0.131	708	1075	1.73	0.528	3.25	1.31
0.693	0.104	688	1000	1.35	0.486	2.98	1.13
0.717	0.155	729	980	2.14	0.465	2.92	1.86
0.750	0.148	708	955	2.01	0.437	2.83	1.82
0.782	0.131	694	925	1.76	0.410	2.72	1.75
0.825	0.124	675	†	†	†	†	†
0.864	0.0433	625					
0.864	0.0658	615					
0.905	0.0165	565					
0.938	0.0146	551					

†Flow separation existed at this location.

Table B-3 (continued).

z/L	q_w BTU/sec in.²	T_w °R	T_e °R	h $\frac{\text{BTU}}{\text{sec in.}^2\ °\text{F}}$	$\rho_e u_e$ $\frac{\text{lb}}{\text{sec in.}^2}$	$\frac{\rho_e u_e}{\mu_e}$ in.$^{-1}$	$St = \frac{h}{\rho_e u_e c_{p_e}}$
	Test 280. (l = 18 in., p_t = 55.1 psia, T_{t_o} = 1501°R, $\dot{m}$ = 1.869 lb/sec, θ = — in., δ^* = — in., ϕ = — in.)						
0.133	0.0743	669	1500	0.894×10^{-4}	—	—	—
0.204	0.0761	661	1499	0.907 ↓	0.197	0.651×10^{5}	1.77×10^{-3}
0.276	0.0749	673	1495	0.906	0.205	0.833 ↓	1.69 ↓
0.336	0.0818	694	1492	1.02	0.233	1.08	1.69
0.385	0.0916	670	1486	1.11	0.272	1.35	1.46
0.429	0.113	689	1474	1.40	0.336	1.75	1.61
0.469	0.141	720	1451	1.82	0.501	2.32	1.40
0.512	0.154	734	1405	2.03	0.636	3.05	1.23
0.541	—	—	1370	—	0.684	3.47	—
0.573	0.193	763	1290	2.71	0.715	3.79	1.46
0.603	—	—	1220	—	0.715	3.89	—
0.634	0.164	752	1140	2.30	0.681	3.83	1.35
0.664	0.158	740	1080	2.21	0.622	3.61	1.43
0.693	0.125	713	1000	1.71	0.538	3.32	1.29
0.717	0.161	740	980	2.30	0.516	3.24	1.82
0.750	0.175	734	960	2.50	0.486	3.13	2.03
0.782	0.150	718	930	2.12	0.457	2.99	1.90
0.825	0.136	693	890	1.87	0.417	2.86	1.83
0.864	0.123	681	†	†	†	†	†
0.864	0.143	663	↓	↓	↓	↓	↓
0.905	0.178	575	↓	↓	↓	↓	↓
0.938	0.141	558	↓	↓	↓	↓	↓
	Test 263. (l = 18 in., p_t = 60.2 psia, T_{t_o} = 1536°R, $\dot{m}$ = 2.133 lb/sec, θ = 0.070 in., δ^* = 0.059 in., ϕ = 0.043 in.)						
0.133	0.0751	654	1535	0.852×10^{-4}	0.111	0.450×10^{5}	2.93×10^{-3}
0.204	0.0765	652	1533	0.866 ↓	0.139	0.654 ↓	2.39 ↓
0.276	0.0689	654	1530	0.783	0.181	0.889	1.66
0.336	0.0814	684	1527	0.957	0.236	1.12	1.56
0.385	0.105	675	1521	1.23	0.312	1.46	1.41
0.429	0.109	676	1509	1.27	0.403	1.90	1.21
0.469	0.160	721	1482	1.98	0.521	2.44	1.47
0.512	0.164	745	1440	2.10	0.667	3.22	1.21
0.541	—	—	1390	—	0.729	3.65	—
0.573	0.201	759	1320	2.68	0.771	3.98	1.34
0.603	0.198	774	1250	2.71	0.764	4.06	1.39
0.634	0.189	758	1075	2.55	0.639	3.79	1.60
0.664	0.163	730	1040	2.16	0.594	3.59	1.46
0.693	0.159	743	1015	2.17	0.571	3.48	1.54
0.717	0.156	725	990	2.09	0.549	3.40	1.55
0.750	0.160	705	960	2.10	0.521	3.25	1.60
0.782	0.139	707	930	1.85	0.486	3.12	1.55
0.825	0.133	674	895	1.72	0.444	2.92	1.58
0.864	0.114	672	855	1.47	0.406	2.77	1.49
0.864	0.159	672	855	2.05	0.406	2.77	2.06
0.905	0.116	644	†	†	†	†	†
0.938	0.0316	566	†	†	†	†	†

†Flow separation existed at this location.

Table B-3 (continued).

z/L	q_w BTU/sec in.^{2}	T_w °R	T_e °R	h BTU / sec in.^{2} °F	$\rho_e u_e$ lb / sec in.^{2}	$\rho_e u_e / \mu_e$ in.$^{-1}$	$St = \frac{h}{\rho_e u_e c_{p_e}}$
	Test 262. (l = 18 in., p_t = 75.2 psia, T_{t_o} = 1518°R, $\dot{m}$ = 2.557 lb/sec, θ = 0.060 in., δ^* = 0.057 in., ϕ = 0.031 in.)						
0.133	0.0834	674	1517	0.989 × 10^{-4}	0.136	0.597 × 10^5	2.87 × 10^{-3}
0.204	0.0864	674	1515	1.03	0.174	0.822	2.26
0.276	0.0801	682	1512	0.959	0.229	1.10	1.61
0.336	0.102	719	1509	1.28	0.305	1.45	1.61
0.385	0.134	718	1503	1.68	0.396	1.86	1.52
0.429	0.151	734	1490	1.94	0.500	2.43	1.49
0.469	0.216	792	1460	2.99	0.666	3.21	1.73
0.512	0.220	823	1410	3.21	0.860	4.18	1.44
0.541	—	—	1370	—	0.938	4.72	—
0.573	0.262	756	1300	3.55	0.980	5.10	1.40
0.603	0.231	833	1230	3.52	0.968	5.24	1.42
0.634	0.206	799	1170	3.03	0.764	4.67	1.58
0.664	0.200	783	1090	2.91	0.732	4.50	1.60
0.693	0.176	777	1015	2.57	0.732	4.50	1.42
0.717	0.169	754	990	2.41	0.705	4.40	1.39
0.750	0.179	728	960	2.49	0.663	4.28	1.48
0.782	0.154	731	930	2.16	0.628	4.10	1.41
0.825	0.144	704	900	1.98	0.576	3.87	1.40
0.864	0.134	707	865	1.86	0.531	3.63	1.44
0.864	0.152	692	865	2.06	0.531	3.75	1.58
0.905	0.120	682	830	1.61	0.486	3.54	1.36
0.938	0.110	639	†	†	†	†	†
	Test 269. (l = 18 in., p_t = 100.2 psia, T_{t_o} = 1511°R, $\dot{m}$ = 3.435 lb/sec, θ = 0.066 in., δ^* = 0.055 in., ϕ = 0.045 in.)						
0.133	0.105	701	1510	1.29 × 10^{-4}	0.183	0.790 × 10^5	2.70 × 10^{-3}
0.204	0.100	693	1509	1.23	0.236	1.11	1.99
0.276	0.106	714	1505	1.33	0.312	1.47	1.63
0.336	0.126	780	1503	1.73	0.403	1.90	1.66
0.385	0.187	781	1496	2.57	0.521	2.49	1.76
0.429	0.204	799	1485	2.88	0.670	3.11	1.66
0.469	0.267	865	1460	4.18	0.868	4.21	1.86
0.512	0.292	896	1415	4.83	1.13	5.48	1.65
0.541	—	—	1370	—	1.24	6.23	—
0.573	0.312	899	1310	5.29	1.30	6.78	1.57
0.603	0.250	872	1240	4.10	1.28	6.96	1.25
0.634	0.241	845	1160	3.84	1.22	6.84	1.25
0.664	0.243	837	1080	3.87	1.10	6.47	1.40
0.693	0.205	814	1000	3.20	0.965	5.98	1.34
0.717	0.207	794	985	3.16	0.931	5.82	1.38
0.750	0.218	777	960	3.25	0.875	5.63	1.46
0.782	0.185	769	925	2.77	0.812	5.38	1.39
0.825	0.180	737	885	2.61	0.743	5.08	1.44
0.864	0.166	746	855	2.45	0.688	4.78	1.47
0.864	0.202	735	855	2.94	0.688	4.78	1.76
0.905	0.154	718	815	2.20	0.625	4.46	1.45
0.938	0.140	670	785	1.88	0.570	4.13	1.36

†Flow separation existed at this location.

Table B-3 (continued).

x/L	q_w BTU/sec in.^{2}	T_w °R	T_e °R	h BTU/sec in.^{2} °F	$\rho_e u_e$ lb/sec in.^{2}	$\rho_e u_e / \mu_e$ in.$^{-1}$	$St = \frac{h}{\rho_e u_e c_{p_e}}$
	Test 267. (l = 18 in., p_t = 134.8 psia, T_{to} = 1501°R, $\dot{m}$ = 4.606 lb/sec, θ = 0.060 in., δ^* = 0.054 in., ϕ = 0.036 in.)						
0.133	0.129	736	1500	1.69 × 10^{-4}	0.243	0.986 × 10^5	2.67 × 10^{-3}
0.204	0.124	734	1499	1.61	0.313	1.32	1.98
0.276	0.134	768	1495	1.83	0.417	1.86	1.69
0.336	0.173	854	1492	2.68	0.552	2.57	1.87
0.385	0.231	843	1486	3.53	0.716	3.40	1.79
0.429	0.250	869	1475	3.98	0.917	4.45	1.67
0.469	0.321	931	1454	5.69	1.16	5.76	1.89
0.512	0.331	956	1409	6.21	1.53	7.53	1.57
0.541	—	—	1362	—	1.67	8.48	—
0.573	0.356	953	1300	6.79	1.74	9.18	1.51
0.603	0.277	920	1225	5.03	1.73	9.42	1.14
0.634	0.274	891	1135	4.78	1.65	9.12	1.15
0.664	0.286	886	1055	5.03	1.40	8.55	1.45
0.693	0.228	852	1000	3.84	1.29	8.04	1.20
0.717	0.238	840	980	3.98	1.24	7.88	1.31
0.750	0.258	818	950	4.19	1.16	7.62	1.43
0.782	0.212	806	920	3.42	1.09	7.31	1.28
0.825	0.213	773	885	3.30	1.00	6.88	1.35
0.864	0.202	790	850	3.24	0.924	6.46	1.44
0.864	0.240	777	850	3.77	0.924	6.36	1.69
0.905	0.176	743	820	2.65	0.840	6.06	1.30
0.938	0.169	696	790	2.39	0.778	5.66	1.27
	Test 268. (l = 18 in., p_t = 150.6 psia, T_{to} = 1484°R, $\dot{m}$ = 5.158 lb/sec, θ = 0.059 in., δ^* = 0.051 in., ϕ = 0.036 in.)						
0.133	0.131	754	1483	1.79 × 10^{-4}	0.242	1.12 × 10^5	2.82 × 10^{-3}
0.204	0.132	751	1481	1.80	0.316	1.59	2.22
0.276	0.144	789	1478	2.08	0.441	2.23	1.80
0.336	0.186	880	1475	3.13	0.601	2.97	2.03
0.385	0.245	866	1470	3.98	0.782	3.79	1.82
0.429	0.266	888	1457	4.49	1.01	4.85	1.71
0.469	0.326	954	1434	6.23	1.32	6.38	1.82
0.512	0.345	974	1385	6.90	1.68	8.40	1.58
0.541	—	—	1345	—	1.85	9.54	—
0.573	0.361	959	1285	7.18	1.94	10.3	1.42
0.603	0.279	915	1210	5.17	1.94	10.6	1.04
0.634	0.286	891	1120	5.14	1.81	10.3	1.13
0.664	0.295	891	1045	5.40	1.60	9.80	1.36
0.693	0.231	850	990	3.98	1.46	9.11	1.11
0.717	0.241	849	965	4.21	1.40	8.91	1.23
0.750	0.277	830	930	4.73	1.32	8.60	1.42
0.782	0.215	814	900	3.60	1.24	8.22	1.19
0.825	0.209	778	870	3.35	1.14	7.76	1.21
0.864	0.213	804	835	3.58	1.04	7.30	1.42
0.864	0.242	787	835	3.97	1.04	7.30	1.57
0.905	0.189	752	805	2.95	0.958	6.83	1.27
0.938	0.171	707	780	2.52	0.982	6.31	1.18

Table B-3 (continued).

z/L	q_w BTU/sec in.^{2}	T_w °R	T_e °R	h $\frac{\text{BTU}}{\text{sec in.}^2\ \text{°F}}$	$\rho_e u_e$ $\frac{\text{lb}}{\text{sec in.}^2}$	$\frac{\rho_e u_e}{\mu_e}$ in.$^{-1}$	$St = \frac{h}{\rho_e u_e c_{p_e}}$
	Test 271. (l = 18 in., p_t = 175.0 psia, T_{t_o} = 1483°R, $\dot{m}$ = 6.011 lb/sec, θ = — in., δ^* = —in., ϕ = — in.)						
0.133	0.146	777	1482	2.07×10^{-4}	0.282	1.30×10^{5}	2.81×10^{-3}
0.204	0.154	777	1480	2.18	0.363	1.94	2.31
0.276	0.166	819	1477	2.50	0.515	2.59	1.87
0.336	0.219	918	1474	3.89	0.693	3.45	2.17
0.385	0.262	896	1468	4.47	0.910	4.39	1.77
0.429	0.298	928	1456	5.41	1.17	5.63	1.79
0.469	—	—	1434	—	—	—	—
0.512	—	—	1385	—	—	—	—
0.541	—	—	1345	—	—	—	—
0.573	—	—	1285	—	—	—	—
0.603	0.309	956	1210	6.20	2.26	12.3	1.08
0.634	0.301	938	1120	5.93	2.10	12.0	1.12
0.664	0.315	941	1045	6.37	2.01	11.3	1.27
0.693	0.249	890	990	4.63	1.70	10.6	1.10
0.717	0.267	887	965	5.00	1.63	10.3	1.25
0.750	0.300	872	935	5.51	1.49	9.95	1.47
0.782	0.224	847	900	3.98	1.43	9.49	1.14
0.825	0.220	805	870	3.68	1.32	8.96	1.14
0.864	0.226	839	835	4.06	1.22	8.46	1.38
0.864	0.271	826	835	4.74	1.22	8.46	1.61
0.905	—	—	805	—	—	—	—
0.938	—	—	780	—	—	—	—
	Test 273. (l = 18 in., p_t = 201.0 psia, T_{t_o} = 1507°R, $\dot{m}$ = 6.871 lb/sec, θ = 0.034 in., δ^* = 0.032 in., ϕ = 0.017 in.)						
0.133	0.154	801	1506	2.18×10^{-4}	0.372	1.62×10^{5}	2.25×10^{-3}
0.204	0.172	824	1504	2.53	0.486	2.20	1.99
0.276	0.221	904	1501	3.67	0.635	3.03	2.22
0.336	0.241	957	1498	4.39	0.812	3.95	2.08
0.385	0.274	921	1492	4.69	1.05	4.99	1.59
0.429	0.349	995	1482	6.87	1.35	6.60	1.96
0.469	0.371	1024	1459	7.80	1.74	8.54	1.73
0.512	0.374	1038	1409	8.17	2.25	11.0	1.40
0.541	—	—	1369	—	2.47	12.5	—
0.573	0.416	1048	1298	9.54	2.59	13.5	1.42
0.603	0.328	995	1228	6.78	2.57	14.0	1.03
0.634	0.358	1015	1143	7.87	2.45	13.8	1.28
0.664	0.330	975	1058	6.80	2.08	12.8	1.32
0.693	0.258	917	1003	4.84	1.92	11.7	1.01
0.717	0.313	943	973	6.25	1.85	11.3	1.37
0.750	0.314	899	948	5.82	1.74	10.9	1.33
0.782	0.254	890	924	4.68	1.67	11.0	1.14
0.825	0.270	875	894	4.91	1.54	10.4	1.30
0.864	0.240	869	859	4.36	1.43	9.73	1.27
0.864	0.283	851	859	4.98	1.43	9.73	1.42
0.905	0.210	808	825	3.45	1.31	9.26	1.09
0.938	0.236	775	800	3.73	1.20	8.74	1.28

Table B-3 (continued).

z/L	q_w BTU/sec in.^{2}	T_w °R	T_e °R	h BTU / sec in.^{2} °F	$\rho_e u_e$ lb / sec in.^{2}	$\rho_e u_e / \mu_e$ in.$^{-1}$	$St = \frac{h}{\rho_e u_e c_{p_e}}$
	Test 277. (l = 18 in., p_t = 225.7 psia, T_{t_0} = 1508°R, $\dot{m}$ = 7.775 lb/sec, θ = 0.039 in., δ^* = 0.038 in., ϕ = 0.018 in.)						
0.133	0.162	818	1507	2.35 × 10^{-4}	0.398	1.80 × 10^5	2.27 × 10^{-3}
0.204	0.185	841	1505	2.77	0.534	2.59	1.99
0.276	0.236	924	1502	4.04	0.698	3.32	2.23
0.336	0.254	991	1499	4.92	0.921	4.36	2.06
0.385	0.288	926	1492	4.96	1.19	5.59	1.49
0.429	0.358	1010	1480	7.25	1.51	7.31	1.85
0.469	0.387	1041	1450	8.39	2.01	9.69	1.61
0.512	0.402	1040	1401	8.80	2.60	12.6	1.30
0.541	—	—	1361	—	2.82	14.2	—
0.573	0.425	1066	1291	10.1	2.95	15.4	1.32
0.603	0.344	982	1222	6.93	2.92	15.8	0.930
0.634	0.372	1025	1162	8.35	2.30	14.1	1.44
0.664	0.358	992	1083	7.65	2.21	13.7	1.39
0.693	0.277	920	1008	5.21	2.21	13.6	0.956
0.717	0.323	960	983	6.65	2.12	13.3	1.27
0.750	0.334	923	954	6.49	2.00	12.9	1.28
0.782	0.271	905	924	5.14	1.90	12.3	1.11
0.825	0.295	898	894	5.61	1.74	11.7	1.32
0.864	0.263	895	859	5.01	1.60	10.9	1.28
0.864	0.307	876	859	5.65	1.60	10.9	1.44
0.905	0.233	833	825	4.01	1.47	10.3	1.13
0.938	0.256	794	800	4.16	1.35	9.59	1.27
	Test 278. (l = 18 in., p_t = 250.7 psia, T_{t_0} = 1517°R, $\dot{m}$ = 8.641 lb/sec, θ = 0.036 in., δ^* = 0.036 in., ϕ = 0.016 in.)						
0.133	0.169	840	1516	2.50 × 10^{-4}	0.442	2.00 × 10^5	2.17 × 10^{-3}
0.204	0.204	871	1514	3.15	0.593	2.75	2.04
0.276	0.255	954	1511	4.53	0.771	3.69	2.26
0.336	0.258	1014	1508	5.15	1.02	4.84	1.94
0.385	0.296	946	1502	5.20	1.33	6.22	1.40
0.429	0.376	1035	1490	7.87	1.67	8.13	1.81
0.469	0.393	1063	1460	8.77	2.24	10.8	1.51
0.512	0.419	1065	1410	9.32	2.88	14.0	1.24
0.541	—	—	1370	—	3.14	15.9	—
0.573	0.435	1085	1300	10.6	3.28	17.1	1.25
0.603	0.354	1004	1230	7.32	3.25	17.5	0.881
0.634	0.379	1045	1170	8.73	2.56	15.6	1.36
0.664	0.366	1017	1090	8.08	2.45	15.3	1.32
0.693	0.292	940	1015	5.61	2.45	15.1	0.924
0.717	0.347	985	990	7.38	2.36	14.8	1.27
0.750	0.351	942	960	6.94	2.22	14.3	1.24
0.782	0.287	925	930	5.56	2.10	13.7	1.08
0.825	0.309	917	900	5.98	1.93	13.0	1.27
0.864	0.273	916	865	5.31	1.78	12.2	1.23
0.864	0.325	899	865	6.12	1.78	12.2	1.41
0.905	0.231	847	830	4.01	1.63	11.4	1.02
0.938	0.272	814	805	4.49	1.50	10.7	1.23

Table B-3 (continued).

z/L	q_w BTU/sec in.²	T_w °R	T_e °R	h $\frac{\text{BTU}}{\text{sec in.}^2\ °\text{F}}$	$\rho_e u_e$ $\frac{\text{lb}}{\text{sec in.}^2}$	$\frac{\rho_e u_e}{\mu_e}$ in.$^{-1}$	$St = \frac{h}{\rho_e u_e c_{p_e}}$
	Test 275. (l = 18 in., p_t = 253.7 psia, T_{to} = 1513°R, $\dot{m}$ = 9.165 lb/sec, θ = 0.038 in., δ^* = 0.038 in., ϕ = 0.015 in.)						
0.133	0.174	839	1512	2.58 × 10^{-4}	0.447	2.02 × 10^5	2.21 × 10^{-3}
0.204	0.202	872	1510	3.15	0.600	2.78	2.01
0.276	0.255	951	1507	4.53	0.779	3.73	2.23
0.336	0.254	1006	1504	5.03	1.04	4.90	1.87
0.385	0.303	953	1498	5.44	1.34	6.30	1.44
0.429	0.356	1033	1486	7.48	1.69	8.22	1.70
0.469	0.388	1066	1456	8.80	2.26	10.9	1.50
0.512	0.402	1068	1406	9.24	2.92	14.2	1.21
0.541	—	—	1366	—	3.17	16.0	—
0.573	0.427	1088	1297	10.6	3.32	17.3	1.24
0.603	0.350	1014	1227	7.44	3.28	17.8	0.887
0.634	0.365	1052	1167	8.62	2.59	15.8	1.32
0.664	0.357	1018	1087	7.96	2.48	15.4	1.29
0.693	0.288	943	1012	5.61	2.48	15.2	0.912
0.717	0.342	989	987	7.41	2.39	14.9	1.26
0.750	0.354	948	957	7.14	2.25	14.5	1.26
0.782	0.292	934	928	5.80	2.12	13.9	1.11
0.825	0.313	923	898	6.17	1.95	13.1	1.29
0.864	0.278	921	863	5.51	1.80	12.3	1.26
0.864	0.323	900	863	6.15	1.80	12.3	1.40
0.905	0.245	855	828	4.34	1.65	11.6	1.08
0.938	0.276	823	803	4.67	1.51	10.8	1.27
	Test 293. (l = 18 in., p_t = 30.0 psia, T_{to} = 2001°R, $\dot{m}$ = 0.836 lb/sec, θ = 0.047 in., δ^* = 0.030 in., ϕ = 0.036 in.)						
0.133	0.0888	694	1999	0.679 × 10^{-4}	0.0451	0.165 × 10^5	5.43 × 10^{-3}
0.204	0.0869	688	1997	0.662	0.0590	0.239	4.05
0.276	0.0940	705	1993	0.725	0.0799	0.322	3.28
0.336	0.0960	722	1989	0.751	0.102	0.417	2.66
0.385	0.101	688	1981	0.774	0.132	0.540	2.12
0.429	0.123	699	1965	0.944	0.169	0.700	2.02
0.469	0.137	710	1935	1.07	0.219	0.912	1.76
0.512	0.137	706	1875	1.07	0.285	1.18	1.37
0.541	—	—	1815	—	0.313	1.34	—
0.573	0.134	700	1730	1.05	0.330	1.45	1.18
0.603	0.0992	673	1635	0.769	0.324	1.48	0.884
0.634	0.103	682	1545	0.813	0.305	1.44	1.00
0.664	0.0802	657	†	†	†	†	†
0.693	0.0835	660					
0.717	0.123	701					
0.750	0.101	673					
0.782	—	—					
0.825	0.109	717					
0.864	0.115	673					
0.864	0.149	672					
0.905	0.0554	658					
0.938	0.105	670					

†Flow separation existed at this location.

Table B-3 (continued).

x/L	q_w BTU/sec in.^{2}	T_w °R	T_e °R	h $\frac{\text{BTU}}{\text{sec in.}^2\ \text{°F}}$	$\rho_e u_e$ $\frac{\text{lb}}{\text{sec in.}^2}$	$\frac{\rho_e u_e}{\mu_e}$ in.$^{-1}$	$St = \frac{h}{\rho_e u_e c_{p_e}}$
	Test 294. (l = 18 in., p_t = 49.9 psia, T_{t_0} = 2000°R, $\dot{m}$ = 1.411 lb/sec, θ = 0.050 in., δ^* = 0.026 in., ϕ = 0.046 in.)						
0.133	0.116	746	1998	0.926 × 10^{-4}	0.0785	0.279 × 10^5	4.26 × 10^{-3}
0.204	0.118	742	1996	0.938	0.101	0.417	3.36
0.276	0.116	747	1992	0.924	0.132	0.550	2.53
0.336	0.117	779	1988	0.962	0.170	0.701	2.04
0.385	0.136	739	1980	1.08	0.219	0.898	1.78
0.429	0.165	753	1965	1.33	0.283	1.15	1.70
0.469	0.179	772	1940	1.46	0.367	1.50	1.44
0.512	0.183	778	1875	1.52	0.470	1.97	1.17
0.541	—	—	1815	—	0.517	2.21	—
0.573	0.179	759	1730	1.48	0.526	2.39	1.04
0.603	0.175	760	1635	1.46	0.522	2.43	1.04
0.634	0.146	742	1545	1.20	0.508	2.37	0.891
0.664	0.117	708	1440	0.948	0.460	2.22	0.785
0.693	0.102	704	1335	0.829	0.404	2.04	0.791
0.717	0.150	748	1310	1.28	0.389	2.00	1.27
0.750	0.103	677	1270	0.833	0.368	1.93	0.881
0.782	0.114	725	1225	0.968	0.340	1.82	1.11
0.825	0.106	683	†	†	†	†	†
0.864	0.117	689	↓	↓	↓	↓	↓
0.864	0.0495	682	↓	↓	↓	↓	↓
0.905	0.0872	661	↓	↓	↓	↓	↓
0.938	0.0665	628	↓	↓	↓	↓	↓
	Test 290. (l = 18 in., p_t = 75.2 psia, T_{t_0} = 1989°R, $\dot{m}$ = 2.162 lb/sec, θ = 0.048 in., δ^* = 0.034 in., ϕ = 0.032 in.)						
0.133	0.134	784	1987	1.10 × 10^{-4}	0.111	0.412 × 10^5	3.61 × 10^{-3}
0.204	0.139	781	1985	1.15	0.153	0.605	2.71
0.276	0.142	800	1981	1.19	0.194	0.799	2.21
0.336	0.148	837	1977	1.28	0.253	1.06	1.83
0.385	0.177	800	1969	1.49	0.330	1.35	1.63
0.429	0.213	838	1953	1.86	0.423	1.70	1.59
0.469	0.248	897	1925	2.27	0.556	2.30	1.48
0.512	0.278	918	1863	2.63	0.715	2.97	1.34
0.541	—	—	1805	—	0.781	3.34	—
0.573	0.326	953	1722	3.24	0.822	3.63	1.45
0.603	0.325	946	1630	3.23	0.816	3.71	1.48
0.634	0.311	960	1520	3.17	0.771	3.63	1.55
0.664	0.270	912	1420	2.66	0.698	3.40	1.46
0.693	0.245	888	1330	2.38	0.614	3.13	1.50
0.717	0.286	931	1300	2.93	0.590	3.03	1.92
0.750	0.283	884	1255	2.78	0.555	2.92	1.95
0.782	0.234	875	1220	2.30	0.520	2.79	1.73
0.825	0.242	856	1175	2.36	0.472	2.63	1.97
0.864	0.227	864	1130	2.24	0.434	2.47	2.04
0.864	0.256	837	1130	2.46	0.434	2.47	2.24
0.905	0.182	785	1085	1.68	0.396	2.31	1.69
0.938	0.191	750	1055	1.71	0.365	2.14	1.88

†Flow separation existed at this location.

Table B-3 (concluded).

x/L	q_w BTU/sec in.²	T_w °R	T_e °R	h $\frac{\text{BTU}}{\text{sec in.}^2\ \text{°F}}$	$\rho_e u_e$ $\frac{\text{lb}}{\text{sec in.}^2}$	$\frac{\rho_e u_e}{\mu_e}$ in.$^{-1}$	$St = \frac{h}{\rho_e u_e c_{p_e}}$
	Test 296. (l = 18 in., p_t = 101.2 psia, T_{t_o} = 2001°R, m = 2.973 lb/sec, θ = 0.049 in., δ^* = 0.029 in., ϕ = 0.044 in.)						
0.133	0.161	825	1999	1.37 × 10^{-4}	0.156	0.570 × 10^5	3.16 × 10^{-3}
0.204	0.169	820	1997	1.43	0.205	0.826	2.53
0.276	0.164	827	1993	1.39	0.267	1.09	1.88
0.336	0.180	895	1989	1.63	0.344	1.40	1.71
0.385	0.259	902	1981	2.37	0.441	1.82	1.94
0.429	0.298	938	1965	2.81	0.566	2.34	1.79
0.469	0.379	1038	1940	3.96	0.740	3.06	1.94
0.512	0.394	1069	1880	4.29	0.958	3.98	1.63
0.541	—	—	1820	—	1.05	4.47	—
0.573	0.443	1101	1735	5.08	1.10	4.84	1.70
0.603	0.379	1062	1645	4.20	1.09	4.94	1.43
0.634	0.389	1062	1545	4.36	1.04	4.83	1.59
0.664	0.360	1026	1435	3.94	0.938	4.54	1.60
0.693	0.312	977	1340	3.27	0.826	4.17	1.53
0.717	0.339	984	1310	3.62	0.799	4.06	1.76
0.750	0.339	941	1275	3.49	0.757	3.92	1.79
0.782	0.275	927	1240	2.82	0.708	3.76	1.55
0.825	0.271	886	1190	2.69	0.642	3.55	1.65
0.864	0.251	903	1145	2.55	0.590	3.32	1.70
0.864	0.299	881	1145	2.97	0.590	3.32	1.99
0.905	0.211	822	1097	1.99	0.535	3.10	1.48
0.938	0.225	778	1060	2.05	0.500	2.87	1.64
	Test 298. (l = 18 in., p_t = 126 psia, T_{t_o} = 2007°R, m = 3.635 lb/sec, θ = 0.052 in., δ^* = 0.036 in., ϕ = 0.040 in.)						
0.133	0.184	850	2005	1.59 × 10^{-4}	0.184	0.683 × 10^5	3.12 × 10^{-3}
0.204	0.187	851	2003	1.62	0.248	1.00	2.36
0.276	0.206	872	1999	1.81	0.326	1.33	2.01
0.336	0.226	953	1995	2.15	0.424	1.73	1.83
0.385	0.320	968	1985	3.09	0.552	2.23	2.02
0.429	0.382	1032	1970	3.94	0.712	2.91	2.00
0.469	0.423	1116	1940	4.79	0.917	3.78	1.89
0.512	0.458	1156	1880	5.47	1.20	4.95	1.66
0.541	—	—	1820	—	1.30	5.55	—
0.573	0.491	1166	1735	6.05	1.37	6.01	1.63
0.603	0.424	1118	1640	4.98	1.36	6.13	1.37
0.634	0.411	1111	1525	4.85	1.26	5.91	1.46
0.664	0.409	1082	1415	4.73	1.15	5.55	1.57
0.693	0.347	1027	1340	3.82	1.02	5.20	1.44
0.717	0.375	1027	1310	4.17	0.986	5.02	1.64
0.750	0.383	986	1275	4.12	0.934	4.86	1.71
0.782	0.325	981	1240	3.50	0.878	4.65	1.56
0.825	0.319	932	1185	3.30	0.806	4.33	1.61
0.864	0.304	959	1140	3.25	0.736	4.09	1.75
0.864	0.356	940	1140	3.74	0.736	4.09	2.01
0.905	0.244	867	1095	2.40	0.667	3.83	1.43
0.938	0.259	809	1060	2.42	0.618	3.56	1.57

ACKNOWLEDGMENT

The authors express their gratitude to Donald R. Bartz, who initiated the project, designed the nozzle, and developed the method for accurately locating the thermocouple positions. Appreciation is extended to Kenton MacDavid for the installation of the thermocouples and calibration of the thermocouple plugs; Rod MacLean, who followed construction, installed and performed initial tests on the nozzle; Arthur Giggar for constructing boundary layer probes; Joe Godley and others for their significant contributions to the success of the project.